REGULATION OF MOUSE EMBRYONIC AND EXTRAEMBRYONIC MORPHOGENESIS BY ZFP568 AND TRIM28

A Dissertation

Presented to the Faculty of the Graduate School

of Cornell University

In Partial Fulfillment of the Requirements for the Degree of

Doctor of Philosophy

by

Maho Shibata

January 2011

REGULATION OF MOUSE EMBRYONIC AND EXTRAEMBRYONIC MORPHOGENESIS BY ZFP568 AND TRIM28

Maho Shibata, Ph. D.

Cornell University 2011

In mammals, extraembryonic tissues are critical for sustaining embryonic life inside the uterus, providing nourishment and secreting factors to maintain pregnancy. However, our understanding of the genes controlling the morphogenesis of these tissues is still limited. *chato,* an ENU allele disrupting the mouse Kruppel-associated box (KRAB) zinc finger protein ZFP568, causes unique defects in the morphogenesis of extraembryonic tissues including yolk sac ruffling, incomplete formation of a yolk sac vascular plexus, and failure to form a normal placenta. Most *chato* embryos have an expanded chorionic ectoderm that, in extreme cases, prevents the closure of the ectoplacental cavity. Interestingly, I found that the severity of yolk sac defects in *chato* embryos correlated with trophoblast malformations, suggesting that all extraembryonic defects in *chato* mutants have a common developmental origin. To address the requirements of *Zfp568* in different extraembryonic lineages, I analyzed chimeric embryos generated by both tetraploid complementation assays and by the use of a reversible allele of *Zfp568* in combination with Cre lines. My results indicate that ZFP568 is required in the extraembryonic mesoderm to regulate the morphogenesis of the yolk sac and placenta, and support a previously undescribed role of the extraembryonic mesoderm in the morphogenesis of extraembryonic tissues.

Characterization and positional cloning of *chatwo,* another ENU-induced mutation that causes similar morphogenetic defects to those of *Zfp568* mutants, has

shed light on the molecular mechanisms utilized by ZFP568 to control morphogenesis. *chatwo* creates a hypomorphic mutation in TRIM28, a RBCC-bromo domain protein that recruits chromatin modifying enzymes and binds to KRAB zinc finger proteins. Results from genetic interaction studies, and analysis of *Trim28* mosaic embryos suggest that TRIM28 is required as a cofactor of ZFP568 in embryonic tissues to regulate embryo morphogenesis. Despite the fact that over 300 KRAB zinc finger proteins are found in genomes of tetrapod vertebrates, reasons for the rapid expansion of the KRAB zinc finger family remain unknown. My findings suggest that some KRAB zinc finger proteins, including ZFP568, may have evolved specialized functions for the control of early embryonic development in the mouse.

BIOGRAPHICAL SKETCH

Maho Shibata, daughter of Yoriyuki and Noriko Shibata was born in Nagano, Japan in 1982. She and her younger sister Waka spent much of their childhoods outside of Japan, attending elementary school in Greensboro, North Carolina, and middle school in Australia. After graduating from Shibuya Makuhari High School in Chiba, Japan in 2001, Maho moved to Charlottesville, Virginia to study at the University of Virginia. At the University of Virginia, she was strongly influenced by Professor Claire Cronmiller, who taught her Genetics course. In her third year of undergraduate studies, Maho joined Claire's lab to start an independent research project where she studied the role of epigenetic regulation during oogenesis in *Drosophila*. It was there that she developed an interest in both Genetics and Developmental Biology. After receiving a Bachelor of Science and graduating with highest distinction from the University of Virginia in 2005, she moved to Ithaca, NY in August 2005 and enrolled in the graduate program in the Field of Genetics and Development at Cornell University. In 2006, Maho joined Maria Garcia-Garcia's lab as her first graduate student. Maho has been conducting research in the Garcia lab for the past four years.

To my parents,

Yoriyuki and Noriko Shibata

ACKNOWLEDGMENTS

There are many people I would like to thank, for without their support, this thesis would not have been possible. I would first like to thank my advisor, Maria Garcia-Garcia, for being a wonderful mentor and patient teacher. I feel incredibly fortunate to have been a graduate student in her lab, and appreciate the guidance she has given me. Maria has taught me to be creative, and challenged me to think critically. I thank members of my committee, Ken Kemphues and Paul Soloway for all their time and help, and Teresa Gunn for being a part of my committee early on. I also thank Mariana Wolfner and Doina Tumbar, for advising me during my rotations.

Members of the Garcia lab, especially Kristin Blauvelt and Christina Cota, have provided me with many helpful suggestions and discussions. I would also like to thank former lab members Maegan Harden, Zhihong Lin and Andrew Recknagel, and members of the Tumbar lab, for treating me as a labmate. I thank Ke-Yu Deng from the Cornell Core Transgenic Mouse Facility for her help with mouse embryo culture and embryo transfers, Wei Wang and Jacob Kresovich from the Cornell Microarray Facility, Sylvia Allen and the Cornell Center for Animal Resources and Education for their support in the mouseroom and our collaborators Tim Bestor and Mathieu Boulard.

I am truly grateful for the support I have received from my friends and family. I would like to thank Heather Flores and SaraH Zanders for their friendship, and Karen Osorio, for being both a great friend and mentor. To my fiancé Wayne Kelley, I cannot thank you enough for your support and understanding. And lastly, I would like to thank my parents, for all the opportunities they have given me.

TABLE OF CONTENTS

LIST OF FIGURES

LIST OF TABLES

LIST OF ABBREVIATIONS

4N: Tetraploid

BMP: Bone morphogenetic protein

cDNA: Complementary DNA

ChIP: Chromatin Immunoprecipitation

C-terminus: Carboxy-terminus

DNA: Deoxyribonucleic acid

DAPI: 4',6-diamidino-2-phenylindole

DIG: Digoxigenin

E: Embryonic day

ENU: N-ethyl-N-nitrosourea

ES cells: Embryonic stem cells

fl: Flox

FLP: Flippase recombination enzyme

FN: Fibronectin

GFP: Green fluorescent protein

H3K9: Histone H3 lysine 9

H3K27: Histone H3 lysine 27

ICR: Imprinting control region

KRAB: Kruppel-associated box

N-terminus: Amino-terminus

PHD: Plant homeodomain

PCR: Polymerase chain reaction

qRT-PCR: Quantitative reverse transcription polymerase chain reaction

RBCC: Ring finger, B-box and coiled coil

rGT: Reversible gene trap

RNA: Ribonucleic acid

RT-PCR: Reverse transcription polymerase chain reaction

SNP: Single-nucleotide polymorphism

TE: Trophectoderm

TUNEL: Terminal deoxynucleotidyl transferase dUTP nick end labeling

TGFβ: Transforming growth factor beta

TRIM: Tripartite motif

VE: Visceral endoderm

VEGF: Vascular endothelial growth factor

wt: Wild type

X-gal: 5-bromo-4-chloro-3-indolyl-beta-D-galacto-pyranoside

YAP: Yes-associated protein

ZFP/ZNF: Zinc finger protein

CHAPTER 1

INTRODUCTION

A. Extraembryonic tissues

Introduction to embryonic development in amniote vertebrates

The amniote egg, thought to have evolved approximately 255 million years ago, allowed embryonic development to occur on land (Figure 1.1, Gilbert and Singer, 2010). For this, amniote eggs contain extraembryonic tissues that are critical for supporting the development of the embryo. Four extraembryonic tissues, the amnion, chorion, allantois and yolk sac, protect the developing embryo from dessication, provide nutrients, and allow for gas exchange and waste disposal. Although these extraembryonic tissues can be found in all amniote eggs, different organisms have developed additional extraembryonic structures to account for their diverse strategies to support embryonic development. Amniotes such as reptiles and birds lay shelled eggs, and development of the embryo occurs externally. The blastoderm develops on top of an abundant yolk, and the yolk sac provides nutrition to the embryo by digesting the yolk and transporting the resulting nutrients through blood vessels. The amnion retains amniotic fluid and prevents dehydration of the embryo, while the chorion allows for gas exchange through the eggshell, and the allantois functions to store waste (Figure 1.2).

In drastic contrast, most mammalian amniotes nurture their embryos internally in the female uterus throughout gestation. In order to obtain the nutrients and fluids required to survive in the uterine compartment, many mammalian embryos have developed additional extraembryonic tissues.

Embryonic development in mammals

Mammals are a class of vertebrates characterized by features such as mammary glands for nourishing their young, and hair or fur. There are approximately 5000 species of mammals, which can be further subdivided into three taxa: monotremes, marsupials

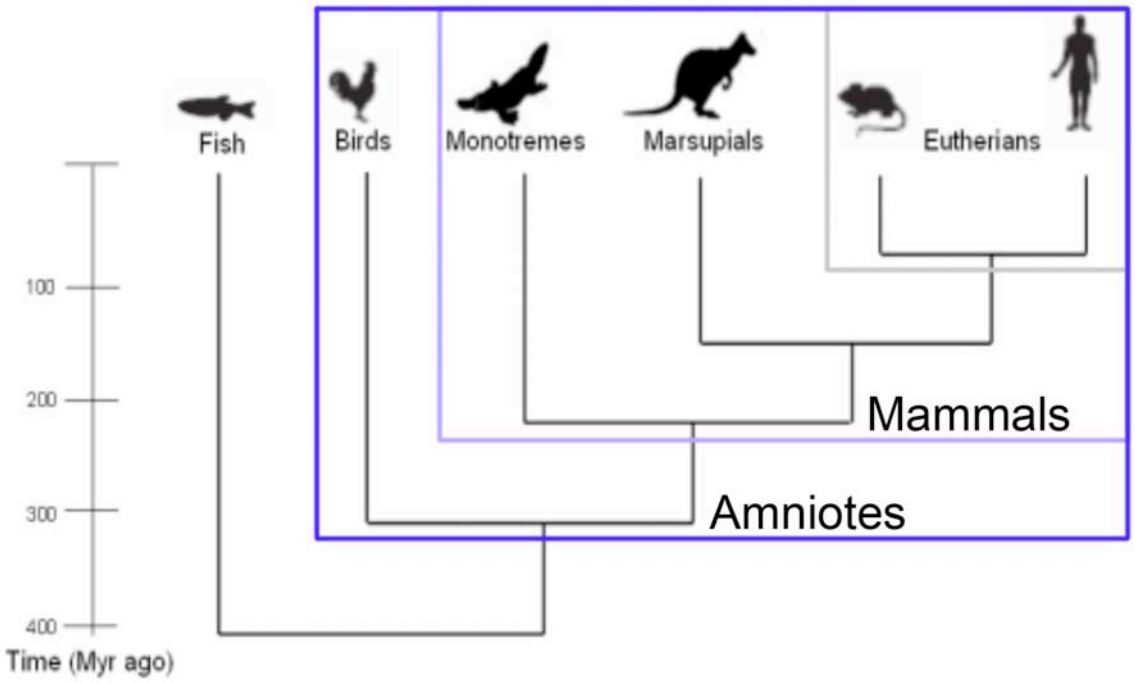

Figure 1.1. Phylogenetic tree of vertebrates. Extraembryonic tissues are conserved in amniotes (birds, reptiles and mammals), which evolved approximately 255 million years ago. In eutherians, or placental mammals, embryonic development occurs internally. Figure adapted from http://www.sanger.ac.uk.

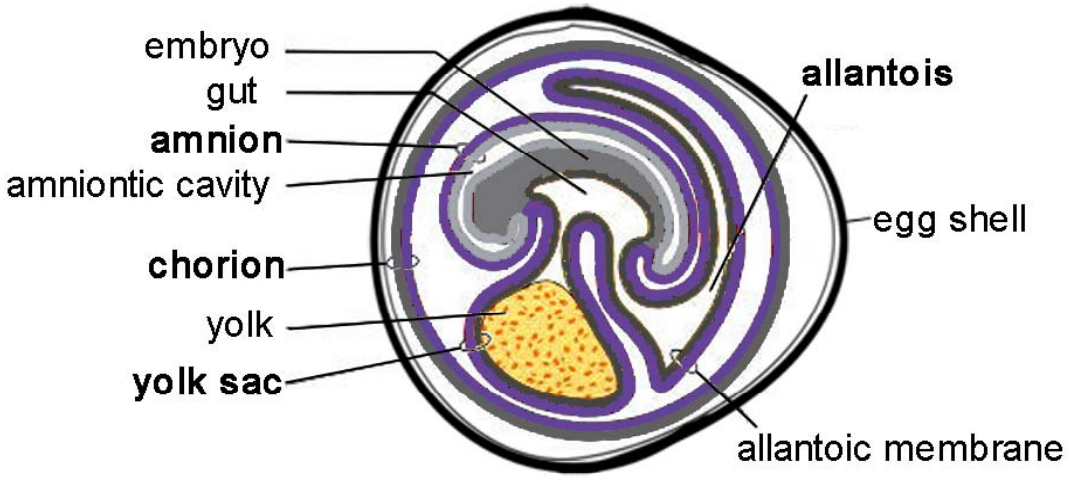

Figure 1.2. Illustration of a chick amniote egg. Four extraembryonic tissues, the amnion, chorion, allantois and yolk sac, protect the developing chick embryo from dessication, provide nutrients, and allow for gas exchange and waste disposal. Note the presence of an egg shell and yolk. Figure adapted from Gilbert and Singer, 2010.

and eutheria (Figure 1.1). Although monoteremes, including the platypus and echidnas, lay shelled eggs, marsupials and eutheria have evolved placentas that allow for development of the embryo inside the uterus of the mother. Marsupials such as koalas and kangaroos give birth to partially developed offspring that continue to develop in a special pouch in the mother's body. In eutheria, the placental mammals, embryonic development occurs internally within the mother's uterus. In addition to providing oxygen and nutrients to the developing embryo and eliminating waste, extraembryonic tissues of placental mammals also prevent immunological rejection of the embryo by the mother (Gilbert and Singer, 2010).

Development of extraembryonic tissues in the mouse

Mus musculus, or the house mouse, has developed as the main model organism for studying mammalian embryonic development. Its main advantages are its relatively short gestation time (21 days) and large litter sizes. Although embryonic development in the mouse is not identical to development in all other placental mammals, including humans, studies using the mouse as a model organism have expanded our understanding of the genes and molecular pathways required for embryonic development.

After fertilization in the oviduct, the mouse embryo undergoes several rounds of cleavages, forming a hollow blastocyst at embryonic day (E) 3.5. The trophectoderm cells surrounding the preimplantation blastocyst are the first cells to be specified, and these cells allow the mouse embryo to implant into the uterus at E4.5 (Figure 1.3A, blue). The trophectoderm cells furthest from the inner cell mass of the blastocyst differentiate into trophoblast giant cells, which no longer divide but continue to replicate DNA (Watson and Cross, 2005). These trophoblast giant cells secrete molecules including extracellular matrix proteins, cell adhesion molecules and

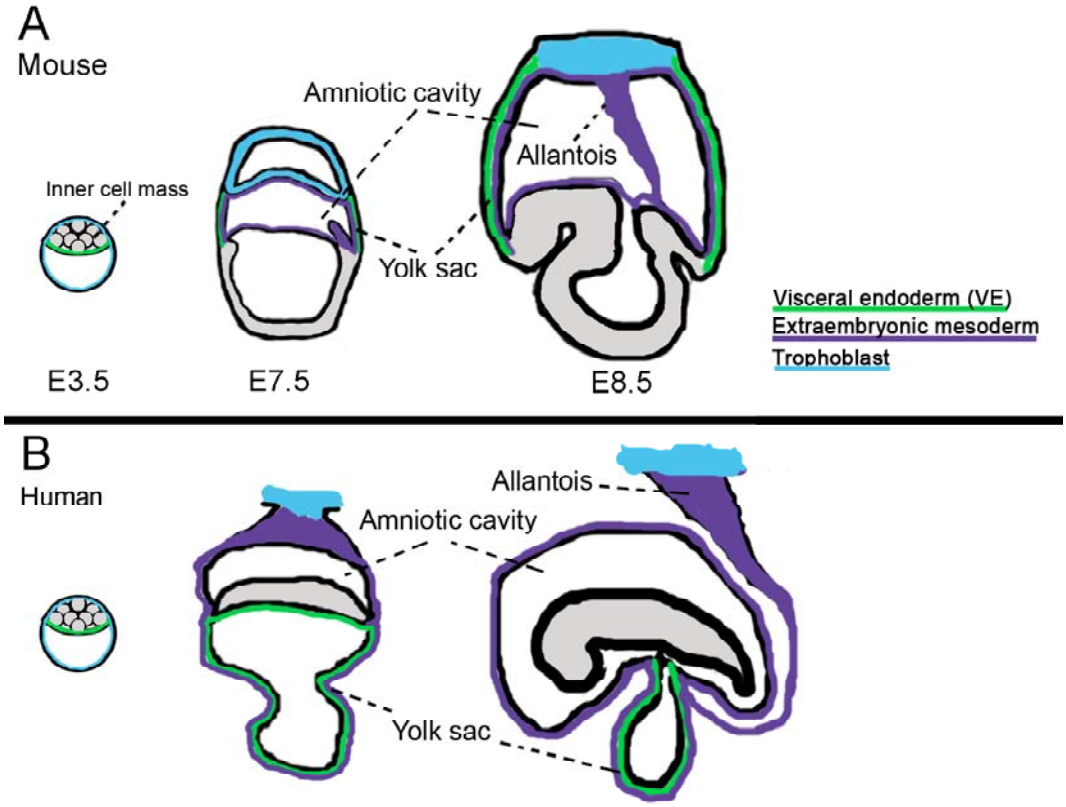

Figure 1.3. Illustration of early embryonic development in the mouse and human. **(A)** Illustration of three stages of mouse embryonic development, embryonic day (E) 3.5, E7.5 and E8.5. The major extraembryonic cell types, visceral endoderm (green), extraembryonic mesoderm (purple) and trophoblast cells (blue) are colored. **(B)** Illustration of comparative stages of human embryonic development. Extraembryonic cell types are represented in the same colors as in A. Note the differences in the location of the yolk sac cell types, and the position of the yolk sac with respect to the embryo. Embryos are not drawn to scale.

hormones important for pregnancy and embryonic development (Hu and Cross, 2010). Trophectoderm cells closer to the inner cell mass will form ectoplacental cone and extraembryonic ectoderm cells, which will form part of the placenta later in development (Figure 1.4, Watson and Cross, 2005).

The inner cell mass cells of the blastocyst will give rise to visceral endoderm (VE) cells of the yolk sac (Figure 1.3A, green), parietal endoderm cells and epiblast cells, the precursors for the embryo (Tam and Loebel, 2007). Following implantation, the epiblast cells grow and develop, forming a cup-shaped embryo (Figure 1.3A, gray).

An additional extraembryonic cell type, the extraembryonic mesoderm, arises from the posterior primitive streak and migrates into the extraembryonic region at E6.5 (Figure 1.3A, purple, Figure 1.4). The extraembryonic mesoderm cells that line the inner layer of the yolk sac in the mouse will serve as the site of initial hematopoiesis and vascular network formation. Extraembryonic mesoderm cells also line the amnion, which separates the embryo from the exocoelomic cavity. At approximately E8.5, the mouse embryo becomes enclosed by the amnion as it rotates and undergoes a process called embryonic turning.

In addition to contributing to the yolk sac and amnion, extraembryonic mesoderm cells are important for the formation of the chorion, a layer of extraembryonic ectoderm cells lined by extraembryonic mesoderm cells (Figure 1.4). The chorion expands and unites with the ectoplacental cone at approximately E8.5. For proper development of the placenta, the allantois, another extraembryonic mesoderm derived structure that extends from the primitive streak, must also connect with the chorion (Inman and Downs, 2007). After establishment of a chorio-allantoic connection, the chorion undergoes villous branching, transforming the flat chorionic plate. Blood vessels derived from the allantois penetrate the newly formed villous

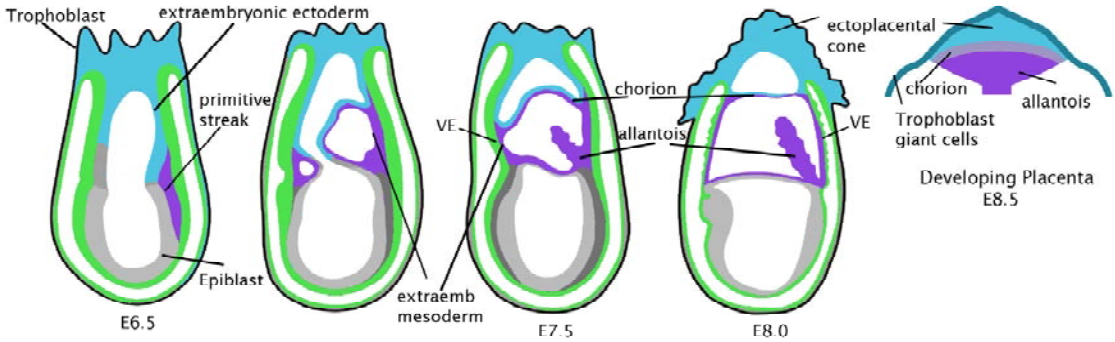

Figure 1.4. Layer organization in mouse development. Development of the amnion, chorion, allantois and placenta occur through coordinated rearrangements of multiple cell types. The major extraembryonic cell types, visceral endoderm (VE, green), extraembryonic mesoderm (extraemb mesoderm, purple) and trophoblast cells (blue) are colored. Extraembryonic mesoderm cells migrate into the extraembryonic region from the primitive streak. Modified from http://genex.hgu.mrc.ac.uk/Atlas/intro.html and Rossant and Cross, 2001.

folds, forming a structure called the labyrinth, where transfer of nutrients and gases between the maternal and fetal blood in the placenta will occur (Watson and Cross, 2005). The allantois will differentiate into the blood vessels of the umbilical cord, which will form a vascular bridge between the fetus and its mother (Inman and Downs, 2007).

Proper development of the placenta and yolk sac requires the correct specification, differentiation, and morphogenesis of trophoblast, visceral endoderm and extraembryonic mesoderm cells. Defects in any one of these cell types can disrupt extraembryonic development and result in embryonic lethality, as the placenta and yolk sac are essential for the growth and survival of the mouse embryo.

Comparisons of extraembryonic development in mouse and humans

In most eutherians including humans and mice, the early stages of embryogenesis are similar (O'Farrell et al., 2004). However, not all aspects of extraembryonic development are conserved. The egg cylinder shape of the rodent embryo, in which the epiblast develops in a cup shape, is thought to have evolved to allow for the birth of larger litters, as it reduces the volume of the embryo (Eakin and Behringer, 2004). In contrast to the cup shaped epiblasts found in rodents, most mammalian embryos develop in a planar form (Eakin and Behringer, 2004). The relative organization of extraembryonic tissues differs between mouse embryos, where the extraembryonic mesoderm lines the interior of the yolk sac (Figure 1.3A), and human embryos where extraembryonic mesoderm cells form the outer layer of the yolk sac (compare purple extraembryonic mesoderm cells in Figure 1.3A and 1.3B).

An additional notable difference between mouse and human embryos lies in the origin of the mesoderm cells of the yolk sac. In mice, extraembryonic mesoderm

cells migrate from the primitive streak to the extraembryonic region. In contrast, the extraembryonic mesoderm in human embryos is thought to initially arise from the yolk sac endoderm, prior to the formation of the primitive streak (Bianchi et al., 1993; Eakin and Behringer, 2004). These differences suggest that rodents have evolved specific mechanisms for controlling extraembryonic development.

Despite these differences, functions of many extraembryonic tissues, including the yolk sac, are conserved in mice and humans. In both organisms, the yolk sac is the first hematopoietic organ, and is also involved in the synthesis of growth factors (Freyer and Renfree, 2008). Mouse mutations that disrupt yolk sac development lead to embryonic lethality. In humans, abnormalities in the yolk sac can be detected in seventy percent of first trimester miscarriages (Freyer and Renfree, 2008). Although few studies have focused on defects in yolk sac development in humans, it is clear that the yolk sac is essential for proper embryonic development (Freyer and Renfree, 2008).

The structures of the mouse and human placentas are also slightly different, though many functions of cell types may be well conserved. For example, the trophoblast giant cells that form the outer layer of the mouse placenta behave similarly to human cytotrophoblast cells and allow for implantion of the embryo in the uterus (Rossant and Cross, 2001). In addition, the labyrinth layer of the mouse placenta, which forms after a chorio-allantoic connection is established, has similar functions to the chorionic villi in human placentas, allowing for nutrient and gas exchange between the mother and the fetus (Rossant and Cross, 2001). Thus, it is hoped that an increased understanding of extraembryonic development in mice will be useful for understanding human placental and yolk sac development.

Regulation of extraembryonic development in the mouse

The analysis of mouse mutants that cause abnormal extraembryonic development has revealed information about the genetic mechanisms controlling the development of extraembryonic tissues. The list of genes relevant for extraembryonic tissue development continues to grow, highlighting the complexity of events involved in the development of these tissues. Mutations affecting extraembryonic development can affect different aspects of extraembryonic development including trophoblast lineage specification, maintenance or differentiation, the development of the chorion or allantois, or yolk sac functions (Rossant and Cross, 2001).

Defects in the establishment of a chorio-allantoic connection, required for placental development are one of the most common causes of mid-gestation embryonic lethality, and can arise from abnormalities in either the chorion or the allantois (Rossant and Cross, 2001). Over 25 genes have been identified to be involved in regulating the proper growth, elongation, or attachment of the allantois to the chorion (Inman and Downs, 2007). This list includes genes such as *Brachyury* (*T*), involved in embryonic patterning, as well as genes such as *Vascular cell-adhesion molecule 1* (*Vcam1*) and *integrin α4* (*Itga4*), which encode cell adhesion molecules (Rossant and Cross, 2001; Inman and Downs, 2007).

Many single gene mutations affecting the development of the yolk sac have also been identified. In wild type embryos, the formation of a vascular network that provides a structure for delivering oxygen and nutrients to the growing embryo first occurs in the yolk sac. *Flk-1* positive hemangioblast precursors arise in the primitive streak and migrate to the yolk sac region, giving rise to both blood and endothelial cells (Coultas et al., 2005). By E8.25, these cells form blood islands at the proximal yolk sac as blood cells are surrounded by endothelial cells (Ferkowicz and Yoder, 2005). Eventually, through migration, reorganization and changes in the shape of

endothelial cells, these blood islands develop into a network of evenly spaced blood vessels, called the primary capillary plexus (Drake and Fleming, 2000; Ferkowicz and Yoder, 2005). Defects in signaling between the yolk sac VE and extraembryonic mesoderm layers, abnormalities in extracellular matrix components, and/or defects in endothelial cells, can all affect vasculogenesis. Many genes, including *Flk1, Retinoic acid*, *Transforming growth factor β (TGFβ)*, *Vascular endothelial growth factor A (VEGFA), Indian Hedgehog* and *Fibronectin* are required for proper vascular remodeling (Argraves and Christopher J Drake, 2005; Bohnsack et al., 2004; George et al., 1993; Goumans et al., 1999).

Mutations in single genes can often cause defects in more than one extraembryonic cell type. The analysis of chimeric embryos in which extraembryonic mesoderm cells are of one cell type and VE and trophoblast cells are of another, has allowed for the identification of the tissue specific requirements for some genes (Tam and Rossant, 2003).

One established method for creating chimeric embryos is the tetraploid complementation assay (Nagy, 2003). This technique involves the aggregation of tetraploid (4N) embryos of one genotype with embryonic stem (ES) cells of another genotype. Tetraploid embryos are created by electrofusion of wild type diploid 2-cell stage embryos (E1.5) (Nagy, 2003). Blastocysts formed from the ES cell-tetraploid embryo aggregates are then transferred to surrogate mothers. As ES cells behave like epiblast cells, whereas tetraploid cells develop normal trophoblast and visceral endoderm, resulting chimeric embryos will have embryonic lineages including the extraembryonic mesoderm derived from the ES cells, and extraembryonic VE and trophoblast lineages derived from the tetraploid embryos (Tam and Rossant, 2003).

Lineage specific conditional knockouts provide an alternative strategy to ES cell-tetraploid chimeras for studying the requirement of a gene within specific cell

types. Although the analysis of conditional knockouts are only possible when a conditional allele and an appropriate Cre line are available, an advantage to generating conditional knockouts is that large numbers of mosaic embryos can be created without physical manipulations (Tallquist and Soriano, 2000).

Studies of chimeric embryos have expanded our understanding of many mouse genes during extraembryonic development in the mouse. These studies have also shown that defects in one cell type can affect adjacent extraembryonic structures, highlighting the interdependence of the visceral endoderm, extraembryonic mesoderm and trophoblast during morphogenesis of extraembryonic tissues.

Genes controlling morphogenesis of mouse extraembryonic tissues

Several mutations have been identified to severely disrupt morphogenesis of extraembryonic tissues, all of which lead to embryonic arrest prior to E9.5. Most of the genes and pathways described below are important for the morphogenesis of more than one extraembryonic cell type, although tissue specific requirements have not been identified for many. Interestingly, some of these mutations affecting morphogenesis of extraembryonic tissues disrupt signaling pathways conserved from flies to mammals, whereas other mutations may affect genes unique to amniotes or even rodents.

Fibronectin

Fibronectin is a highly conserved component of the extracellular matrix, and is important for cell migration and adhesion of cells to the extracellular matrix. In extraembryonic tissues, Fibronectin is detected in the yolk sac, (between the VE and extraembryonic layers), in blood islands, and in the amnion (between the embryonic ectoderm and extraembryonic mesoderm layers) (George et al., 1993).

In homozygous embryos null for *Fibronectin*, extraembryonic mesoderm and VE layers are separated, and mutants fail to develop yolk sac vasculature (George et al., 1993). *Fibronectin* mutants are embryonic lethal, and display additional defects in embryonic tissues including a shortened anterior-posterior axis, a kinked neural tube, a reduction of head and trunk mesoderm, and failure to initiate embryonic turning (George et al., 1993).

The major receptor for Fibronectin is α5β1 integrin. Mouse mutants for *α5 integrin* arrest at approximately E9.5 and display defects similar to, although slightly milder than *Fibronectin* mutants (Yang et al., 1993). Consistent with its role as the Fibronectin receptor, *α5 integrin* mutants also cause separation between the VE and extraembryonic layers of the yolk sac, and defects in vasculogenesis (Yang et al., 1993).

TGFβ superfamily

Components of the Transforming growth factor β (TGFβ) superfamily signaling pathway are conserved across metazoans, and are important for many processes during embryonic development (Huminiecki et al., 2009). The TGFβ superfamily ligands include TGFβ and Bone morphogeneic proteins (BMPs). The ligands signal through type I and type II serine/threonine kinase receptors that phosphorylate and activate receptor-regulated SMADs (SMADs 1, 2, 3, 5, 8) (Wu and Hill, 2009). These SMADs then dimerize with a common SMAD, SMAD4, and become translocated to the nucleus where they function to regulate transcription. SMADs activate or repress transcription through recruitment of histone acetytransferases, histone deacetylases and chromatin remodeling complexes (Ross and Hill, 2008).

Several members of the TGFβ superfamily signaling pathway are essential for the development of extraembryonic tissues. *Bmp4*^{tm1blh} embryos, in which *Bmp4* has

been knocked out, display a variable phenotype and arrest between E6.5 and E9.5 (Winnier et al., 1995). Most *Bmp4*^{tm1blh} embryos arrest at the egg cylinder stage, but embryos that develop further display defects including blebbing of the yolk sac membrane, a reduction of blood islands in the yolk sac, and a failure to develop an allantoic bud (Winnier et al., 1995; Lawson et al., 1999). Analysis of *Bmp4* expression patterns and chimeric embryos created using wild type ES cells with embryos homozygous mutant for *Bmp4* have indicated a requirement for *Bmp4* in the extraembryonic chorionic ectoderm for proper development of the posterior primitive streak, from which extraembryonic mesoderm cells arise (Lawson et al., 1999). BMP signaling also appears to be important for allantois development, as a subset of *Bmp8b* mutants fail to develop an allantoic bud, and some *Bmp2* mutants display a short allantois that fails to contact the chorion (Inman and Downs, 2007).

Chimeric embryos in which a dominant negative kinase deficient TGFβ type II receptor is overexpressed in the extraembryonic mesoderm display defects in yolk sac vasculogenesis and blistering of the yolk sac at E9.5. Levels of Fibronectin are also reduced in yolk sacs of these chimeric embryos, indicating that TGFβ signaling is required for proper production of Fibronectin in the yolk sac (Goumans et al., 1999).

Smad1 mutants are lethal at E10.5, displaying extraembryonic defects including a ruffling and overgrowth of the posterior VE of the yolk sac and a folding of the chorion (Tremblay et al., 2001). *Smad5* mutants are embryonic lethal at approximately E9.5 to E11.5 with defects in yolk sac vasculature and gut development (Chang et al., 1999). Altogether, analyses of mutants affecting TGFβ superfamily signaling have identified important roles for this signaling pathway in yolk sac, allantois and chorion development.

Hippo-Yap

The Hippo-Yap signaling pathway is a highly conserved kinase signaling cascade which has been well studied in *Drosophila* for its role in cell growth. In recent years, work in the mouse has reveal roles for this pathway in organ size control and tumorigenesis (Zhao et al., 2010). Interestingly, proper Hippo-Yap signaling is also required for yolk sac and placental development.

Yes-associated protein 1 (YAP1, also known as YAP65) is a transcriptional coactivator protein with multiple protein-protein interaction domains. Embryos homozygous for a targeted mutation in *Yap1* arrest at E8.5 with defects including abnormal rippling of the yolk sac (Morin-Kensicki et al., 2006). *Yap1* mutants fail to form a yolk sac primitive vascular plexus, and although an elongated allantois is formed, chorio-allantoic union does not occur (Morin-Kensicki et al., 2006). *Yap1* embryos display a shortened and widened embryonic axis, and although yolk sac vasculogeneis is affected, allantoic or embryonic vasculogenesis is not, suggesting that differences exist in vessel formation in the yolk sac, the embryo and the allantois (Morin-Kensicki et al., 2006). *Yap1* is expressed ubiquitously, though at high levels in the extraembryonic mesoderm at E7.5 (Morin-Kensicki et al., 2006). Tissue specific requirements for *Yap1* during embryogenesis are currently unknown.

YAP1 activity is mediated by co-activator DNA binding proteins, TEAD1 and TEAD2, during embryonic development (Sawada et al., 2008). Mouse and human genomes contain four *Tead* (transcriptional enhancer factor 1) genes. Homozygous *Tead1* mutants are lethal at E11.5, and *Tead2* mice appear normal (Sawada et al., 2008). However, double homozygous mutants for *Tead1* and *Tead2* ($Tead1^{-/-}$ $Tead2^{-/-}$) arrest prior to by E8.5, with defects strongly resembling *Yap1* mutants. *Tead1* and *Tead2* also genetically interact with *Yap1*. Although PECAM positive cells are specified in $Tead1^{-/-}$ $Tead2^{-/-}$ yolk sacs, an organized vascular network fails to form

(Sawada et al., 2008). *Tead1*$^{-/-}$ *Tead2*$^{-/-}$ embryos also display a slight reduction in cell proliferation across all germ layers along with a slight increase in apoptosis, suggesting that Hippo-Yap signaling may function in regulating cell proliferation and survival (Sawada et al., 2008).

It is possible that Hippo-Yap signaling may have additional roles in addition to regulating cell proliferation and survival during embryonic development. In mouse ES cells, YAP has been found to interact with SMAD1 and inhibit neuronal differentiation, suggesting a cross-talk between the YAP and TGFβ superfamily signaling pathways (Alarcón et al., 2009; Zhao et al., 2010). Whether such cross talk is important for development of extraembryonic tissues remains to be determined.

Hand1

Mutants for a basic helix-loop-helix transcription factor HAND1 also display severe extraembryonic morphogenesis defects. *Hand1* mutants arrest at E8.5 and display a ruffling of the VE layer of the yolk sac and defects in yolk sac vasculogenesis (Firulli et al., 1998; Riley et al., 1998; Morikawa, 2004). In *Hand1* mutant yolk sacs, the migration and recruitment of smooth muscle cells to the endothelial cell network, which is required for maturation of blood vessels, is affected (Morikawa and Cserjesi, 2004). Abnormalities in chorionic fusion have also been reported for these mutants (Firulli et al., 1998). In addition, *Hand1* is required for the differentiation of the trophoblast giant cells, and *Hand1* mutant embryos have embryonic defects including a crooked neural tube, and fail to undergo embryonic turning (Riley et al., 1998). Embryos with defects including hemorrhagic yolk sacs resembling *Hand1* mutants were obtained when chimeric embryos were generated using *Hand1* null ES cells and wild type embryos, suggesting a requirement for *Hand1* in the extraembryonic mesoderm for proper yolk sac development (Riley, 2000).

In addition to *Hand1*, the HAND subclass of helix-loop-helix transcription factors contains another closely related family member, *Hand2* (Firulli, 2003). Although *Hand* genes can be found in genomes from flies to humans, *Hand1* orthologs are found in chick and Xenopus, but not in zebrafish (Angelo et al., 2000; Yelon et al., 2000). Furthermore, *Hand1* expression has been detected in the trophoblast in all eutherians examined (Riley et al., 1998) suggesting that some functions of *Hand1* may be specific to and conserved in eutherians. However, *Hand1* expression is not detected in the extraembryonic mesoderm components in human embryos (Knöfler et al., 2002), suggesting that functions of *Hand1* in the extraembryonic mesoderm in the mouse are not conserved in humans.

Recent studies of the zebrafish *Hand2* gene have provided mechanistic insight into how *Hand2* may affect morphogenesis. During looping morphogenesis of the gut, *Hand2* is involved in remodeling the extracellular matrix, and does so by controlling the activity of matrix metalloproteinases to affect laminin deposition (Yin et al., 2010). Studies in zebrafish have also identified a role for *Hand2* in the regulation of *Fibronectin1* expression during heart morphogenesis (Garavito-Aguilar et al., 2010). It is unknown whether *Hand1* or *Hand2* may also regulate remodeling of the extracellular matrix in the mouse embryo.

Interestingly, several extracellular matrix associated genes and actin assembly regulators were found to be misregulated in *Hand1*-null embryoid bodies made from *Hand1* homozygous mutant ES cells, compared to wild type embryoid bodies (Smart et al., 2002). *Fibronectin* and *Tripartite motif protein 28* (*Trim28*) were among the list of genes downregulated greater than 2.5-fold in *Hand1*-null embryoid bodies (Smart et al., 2002).

Zfp568 and *Trim28*

ZFP568 belongs to the Kruppel-associated box (KRAB) zinc finger protein family, which is found only in tetrapod vertebrates. Mouse embryos mutant for *Zfp568* arrest at midgestation with yolk sac ruffling and defects in embryonic elongation along the anterior posterior axis (Garcia-Garcia et al., 2008). *Zfp568* is expressed ubiquitously from E7.5 to E8.5, and affects the morphogenesis of all major embryonic cell types (Garcia-Garcia et al., 2008). My work in this thesis describes severe extraembryonic defects in *Zfp568* mutants, which resemble defects in *Hand1* and *Yap1* mutants. In addition, my thesis describes a hypomorphic allele for *Trim28*, a binding partner for KRAB zinc finger proteins, which causes similar extraembryonic and embryonic defects.

B. KRAB zinc finger proteins and TRIM28

KRAB zinc finger transcription factors are conserved only in tetrapod vertebrates

KRAB zinc finger proteins are a large family of proteins found only in tetrapod vertebrate organisms (Urrutia, 2003). Proteins in this family contain a N-terminal KRAB domain and C-terminal C_2H_2 zinc finger domains. They have been proposed to act as transcriptional repressors by recruiting other corepressor proteins and targeting them to specific DNA sequences that are recognized by their zinc finger domains (Urrutia, 2003).

KRAB zinc finger proteins have been found in genomes of human, mouse, rat, chicken, and frog (Urrutia, 2003). In the human genome, 423 KRAB zinc finger protein-coding loci have been identified (Huntley et al., 2006). Of these, 103 are conserved in human, chimpanzee, dog and mouse, and at least 136 are thought to be primate specific (Huntley et al., 2006).

The KRAB domain consists of two subtypes, KRAB A and KRAB B. The KRAB A box binds to corepressor proteins and is essential for transcriptional repression. The KRAB B box is a domain that can enhance the repression of the KRAB A box, but not all KRAB zinc finger proteins contain this domain. In addition to a KRAB A box, some KRAB zinc finger proteins also contain an additional domain called the SCAN (SRE-ZBP, CTfin51, AW-1 and Number 18 cDNA) domain, which is found only in vertebrates, and allows for dimerization with other proteins containing SCAN-domains (Urrutia, 2003).

In most cases, the C_2H_2 zinc finger motif is encoded by a single exon (Urrutia, 2003). KRAB zinc finger proteins in the human genome contain an average of 12 zinc fingers per gene (Huntley et al., 2006). It has been proposed that each zinc finger interacts with 3 or 4 DNA bases, although it is possible that not all zinc fingers in a KRAB zinc finger protein may be used for binding to specific DNA sequences (Urrutia, 2003). Mouse ZFP568*,* the KRAB zinc finger protein described in this thesis, contains two KRAB A and B domains and 11 C_2H_2 zinc finger domains (Figure 1.5A, Garcia-Garcia et al., 2008). It is not known whether functional orthologs of mouse *Zfp568* exist in other organisms.

TRIM28 is a corepressor for KRAB zinc finger proteins

Tripartite motif protein 28 (TRIM28), also known as KRAB-associated protein 1 (KAP1), Transcription intermediary factor 1 β (TIF1β) or KRAB interacting protein 1 (KRIP-1), is proposed to be a universal corepressor protein that binds to all KRAB zinc finger proteins (Friedman et al., 1996). TRIM28 contains an N-terminal RBCC (RING finger, B box, coiled coil) domain that interacts with the KRAB domains of KRAB zinc finger proteins, and C-terminal plant homeodomain (PHD) finger and bromodomains that mediate transcriptional repression (Urrutia, 2003).

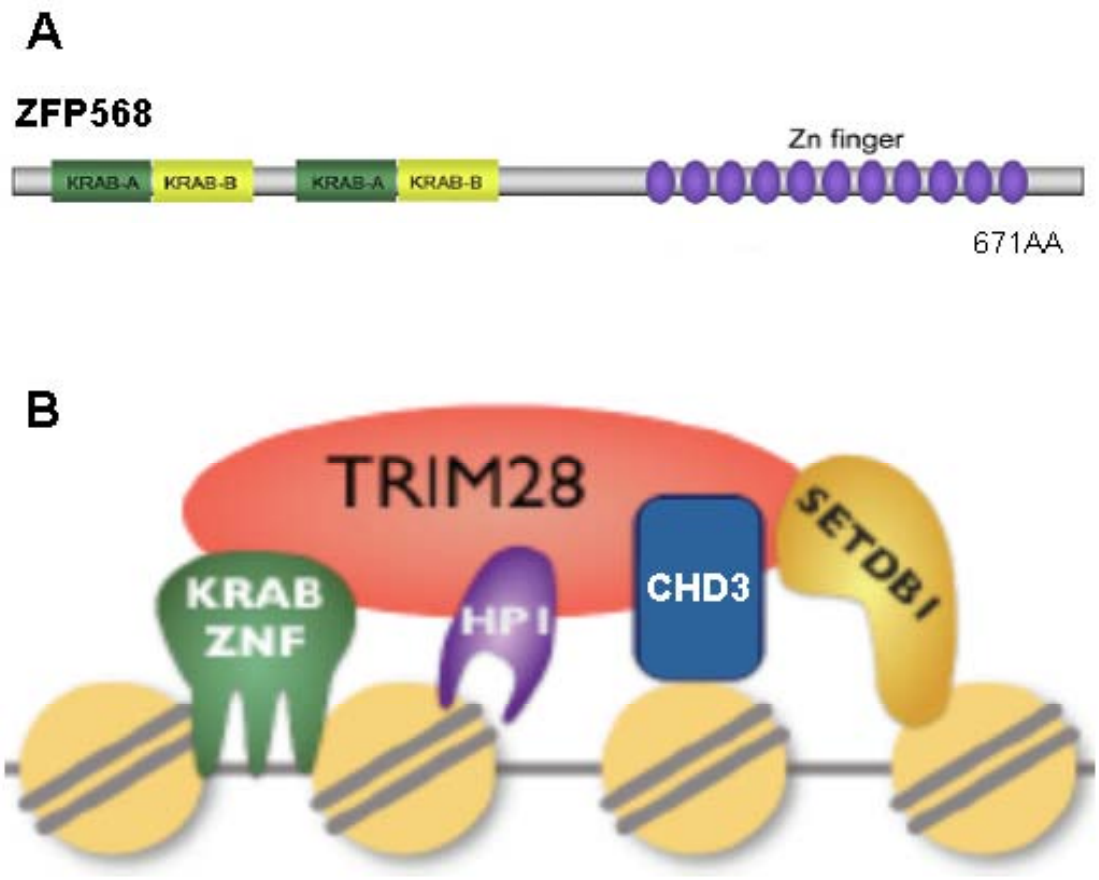

Figure 1.5. KRAB zinc finger protein ZFP568 and a proposed model for a TRIM28 mediated repression complex. (A) Diagram of KRAB zinc finger protein ZFP568 domains. ZFP568 contains two KRAB domains and 11 zinc fingers. Figure modified from Garcia-Garcia et al., 2008. **(B)** KRAB zinc finger proteins (KRAB ZNF) have been proposed to bind specific DNA sequences and recruit a transcriptional repression complex containing TRIM28, which binds to other proteins to modify chromatin structure.

The PHD and bromodomains of TRIM28 recruit the SETDB1 histone H3 lysine 9 methytransferase and CHD3, a protein in the nucleosome remodeling and histone deacetylation (NuRD) complex. The TRIM28 PHD domain also binds to the ubiquitin E2 transfer enzyme UBC9 and functions as an intramolecular SUMO E3 ligase, SUMOylating lysine residues in the TRIM28 bromodomain (Ivanov et al., 2007). SUMOylation of TRIM28 is important for its interaction with SETDB1 and CDH3, and mutation of all six SUMOylation sites in TRIM28 causes a loss of repression activity (Ivanov et al., 2007). The PHD and bromodomains in TRIM28 also function cooperatively with another domain, the heterochromatin protein 1 (HP1) binding domain, to recruit HP1 proteins which can bind to histone H3 lysine 9 and condense chromatin (Figure 1.5B, Nielsen et al., 1999; Ryan et al., 1999; Sripathy et al., 2006).

TRIM28 belongs to the TRIM (tripartite motif-containing) family of proteins, which are conserved across metazoans. Approximately 10 TRIM proteins are found in fly genomes, and approximately 20 TRIM proteins are found in worms. This protein family has expanded rapidly in vertebrates, with over 60 TRIM proteins identified in human and mouse genomes (Ozato et al., 2008). The TRIM proteins vary in their tissue specific expression patterns and subcellular localization, and function in a broad range of biological processes (Ozato et al., 2008).

The C-terminal PHD finger and bromodomain motifs found in TRIM28 are unique to the TIF1 family of TRIM proteins, and are found only in 2 other TRIM proteins (TRIM24 and TRIM33). The TIF1 family is conserved form flies to mammals, though in *Drosophila,* the *bonus* (*bon*) gene encodes the single homolog for the TIF1 family (Beckstead et al., 2001). Comparisons between Bon and mouse TRIM28 indicate an amino acid identity of approximately 30% and similarity of approximately 50% (Beckstead et al., 2001). Orthologs for all 3 family members

(TRIM24, TRIM28 and TRIM33) are found in humans, mice and chick, whereas in fish, orthologs for only TRIM33, and not TRIM24 or TRIM28 have been identified (Sardiello et al., 2008).

Levels of protein conservation are highest at the N and C terminal domains of the TIF1 family members (Hongzhuang Peng et al., 2002). However, TRIM24 and TRIM33 are more similar to each other than to TRIM28 (Hongzhuang Peng et al., 2002). TRIM24 and TRIM33 can hetero-dimerize with each other, though TRIM28 does not (Hongzhuang Peng et al., 2002). All three proteins have evolved specific functions, and only TRIM28 can interact with the KRAB domains of KRAB zinc finger proteins (Abrink et al., 2001). It is possible that TRIM28 evolved specifically to mediate functions of KRAB zinc finger proteins, as both TRIM28 and KRAB zinc finger proteins are found only in genomes of tetrapod vertebrates.

Mechanisms of KRAB zinc finger protein and TRIM28 function

KRAB zinc finger proteins have been proposed to target TRIM28 and chromatin modifying proteins to specific regions of the genome (Urrutia, 2003), however less is known about the DNA targets of specific KRAB zinc finger proteins. In a recent study, binding sites for ZNF263 (ZFP263 in mouse), a KRAB domain containing protein with 9 zinc finger domains, were identified using a genome-wide ChIP-seq approach (Frietze et al., 2009). ZNF263 was found to bind to over 5000 sites in K-562 human chronic myelogenous leukemia cells (Frietze et al., 2009). Of these sites, siRNA knockdown of ZNF263 resulted in an increase in expression of 61 genes and a decrease in expression of 37 genes, suggesting that ZNF263 may positively and negatively regulate transcription of specific genes (Frietze et al., 2009).

There is also evidence that the zinc finger regions of KRAB zinc finger proteins may mediate interactions with other proteins and not just DNA. ZFP128

(ZNF8 in human) is a KRAB zinc finger protein that interacts with SMAD1 through its zinc finger domains to represses TGF-β/BMP signaling (Jiao et al., 2002). Although a knockout for *Zfp128* has not been created, it is expressed ubiquitously in mouse embryos in a similar manner to *Smad1*, suggesting that ZFP128 may mediate BMP signaling during development.

The zinc finger region of KRAB zinc finger protein KRIM1B is highly expressed in the spleen and lymph nodes, and interacts with MYC protein, an oncogenic transcription factor, to decrease MYC activity (Hennemann et al., 2003). KRIM1B can also to bind to TRIM28, suggesting that the negative regulation of MYC may occur through a TRIM28 mediated mechanism (Hennemann et al., 2003).

APAK (ATM and p53-associated KRAB zinc finger protein) is a KRAB zinc finger protein containing an N terminal KRAB domain and 19 C_2H_2 zinc fingers. APAK can form a complex with P53, ATM, TRIM28 and histone deacetylase (HDAC1) to negatively regulate P53. Binding of APAK to P53 occurs through its zinc finger domain, whereas binding to ATM occurs through the KRAB domain of Apak (Tian et al., 2009). In addition to APAK, other KRAB zinc finger proteins may also be involved in the regulation of P53. ZNF8 (ZFP128 in mouse) and ZNF498 also bind to P53 and repress P53 activity, whereas ZNF182 and ZNF136 do not (Tian et al., 2009).

Functions of TRIM28 and KRAB zinc finger proteins in ES cells

TRIM28 is required for the maintenance of ES cell pluripotency, and is thought to control self-renewal in stem cells by binding to sites close to transcription start sites and regulating gene expression (Hu et al., 2009). Through biotin-mediated ChIP assays, over 3000 DNA binding sites for TRIM28 have been identified (Hu et al., 2009). Although a GCCGCGXX consensus binding motif was predicted (Hu et al.,

2009), specific KRAB zinc finger proteins for targeting TRIM28 to DNA for maintenance of ES cell pluripotency have not been identified.

Phosphorylation of TRIM28 at serine 824, a mark observed in ES cells and the inner cell mass regions of E3.5 blastocysts, but not in mouse embryonic fibroblasts (MEFs) or NIH3T3 cells, is necessary for the maintenance of pluripotency of ES cells (Seki et al., 2010). Phosphorylated TRIM28 forms a transcriptional activation complex with Oct3/4, and chromatin remodeling factors SMARCAD1, BRG1 and BAF155 which are part of a ES cell-specific chromatin remodeling complex called esBAF (Seki et al., 2010).

TRIM28 is also important for the silencing of retroviral elements in ES cells. TRIM28 directly associates with and silences IAP elements, a type of endogenous retrovirus (Rowe et al., 2010). TRIM28 has also been found to be required for the silencing of Moloney murine leukemia virus (M-MLV) (Wolf and Goff, 2007). Silencing of these elements in ES cells occurs through the recruitment of histone H3 lysine 9 trimethylation (H3K9me3) by the H3K9 methyltransferase SETDB1, and does not require DNA methyltranferases (Matsui et al., 2010). Furthermore, ZFP809 has been indentified as a KRAB zinc finger protein involved in the silencing of M-MLV retroviral DNA in mouse ES cells. ZFP809 can recognize an 18-base pair primer binding site of retroviral DNA and recruit TRIM28 (Wolf and Goff, 2009). These findings suggest that some KRAB zinc finger proteins may have evolved to restrict specific retroviruses using a TRIM28 mediated mechanism.

TRIM28 and KRAB zinc finger proteins in development

Interestingly, all but 39 of the KRAB zinc finger proteins found in humans are found in clusters containing other KRAB zinc finger proteins (Huntley et al., 2006). Despite this clustering, analysis of expression patterns of KRAB zinc finger proteins using

publicly available microarray data indicated that many KRAB zinc finger proteins have distinct patterns of expression, and that expression patterns of recent paralogs have diverged (Huntley et al., 2006). The distinct expression patterns suggest that KRAB zinc finger proteins have evolved diverse functions.

Targeted knockout mice (*Trim28*$^{-/-}$) with a truncated TRIM28 protein are embryonic lethal, arresting at approximately embryonic day 5.5 (Cammas et al., 2000). *Trim28*$^{-/-}$ embryos implant normally, but display defects in gastrulation and fail to express *Brachyury*, a marker of the primitive streak (Cammas et al., 2000). This finding suggests that there are likely to be KRAB zinc finger proteins that require TRIM28 function during early postimplantation development.

Aside from *Zfp568,* which will be the focus of my thesis, there is only one other KRAB zinc finger protein that has been identified to be important for embryonic development. *Zfp57* encodes a KRAB zinc finger protein, and is expressed in maturing oocytes and preimplantation embryos (Li et al., 2008). Homozygous knockout mice lacking zygotic *Zfp57* display partial lethality (Li et al., 2008). However, phenotypes of embryos lacking both maternal and zygotic *Zfp57* are more severe, with ~80% of mice dying prior to E16.5. Maternal ZFP57 is required in oocytes for the establishment of maternal methylation imprints at the *Snrpn* imprinted domain. In addition, zygotic ZFP57 has been shown to play a role in the maintenance of methylation at both *Dlk1-Dio3* and *Snrpn* imprinted domains. However, not all imprinted loci are affected in *Zfp57* mutants (Li et al., 2008).

The creation of a conditional allele for *Trim28* has expanded the understanding of TRIM28 functions in a few specific tissues. Removal of TRIM28 from spermatogonia and spermatocytes using an inducible testis specific Cre recombinase revealed a requirement for TRIM28 for maintaining spermatogenesis (Weber et al., 2002). Removal of TRIM28 from the adult forebrain of mice affects vulnerability of

the mice to stress, and results in the misregulation of a small number of genes in the hippocampus (Jakobsson et al., 2008). Decreased histone H3 K9 and increased histone 4 acetylation marks were confirmed at the promoters of two of the misregulated genes, and expression of at least 45 KRAB zinc finger proteins has been noted in the hippocampus (Jakobsson et al., 2008). These findings support a model where KRAB zinc finger proteins may target TRIM28 to specific genes for transcriptional repression.

TRIM28 and KRAB zinc finger proteins in disease

It has been proposed that KRAB zinc finger proteins may have evolved functions key to vertebrates such as the development of an elaborate immune system or the nervous system (Urrutia, 2003). Interestingly, three KRAB zinc finger proteins, ZNF41, ZNF81 and ZNF674, have been associated with X-linked mental retardation in humans (Emerson and Thomas, 2009). Mutations in another KRAB zinc finger protein, ZNF57 (ZFP57 in mouse) have been identified in seven human pedigrees associated with transient neonatal diabetes (Mackay et al., 2008). Similar to the findings in mice, human ZNF57 appears to have a global affect on imprinting, as hypomethylation of several imprinted loci were identified in individuals with mutations in *Znf57* (Mackay et al., 2008).

Evidence that TRIM28 may be associated with cancer metastasis has also emerged. In clinical samples, protein expression of TRIM28 was increased in about 40% of metastic carcinomas compared to invasive primary breast tumors, suggesting that TRIM28 may play a role in breast cancer metastasis (Ho et al., 2009). Upregulation of *Trim28* expression, found in 68% of tumor tissues from gastric cancers, is associated with a reduced 5 year overall survival rate (Yokoe et al., 2009). Given the increasing evidence that TRIM28 and KRAB zinc finger proteins may

affect human health, it is important to understand the functions of specific KRAB zinc finger proteins and the reasons for the rapid evolution of this family.

C. Organization of thesis

The goal of the research presented in this thesis is to understand the role of a specific KRAB zinc finger protein, ZFP568 and its partner, TRIM28, during embryonic development in the mouse. The results presented here suggest that KRAB zinc finger protein ZFP568 may have evolved specifically to control extraembryonic development in the mouse.

In Chapter 2, I present work on the characterization of extraembryonic defects in *Zfp568* mutant embryos, and results from analysis of chimeric embryos to study the tissue specific requirements for *Zfp568.* These results indicate that *Zfp568* is required in the extraembryonic mesoderm for proper morphogenesis of extraembryonic tissues in the mouse.

In Chapter 3, I present results from the analysis and characterization of a mutation that creates a hypomophic allele of *Trim28. Trim28*^{chatwo} mutants strongly resemble *Zfp568* embryos. I also describe results from analyses of tissue specific requirements for TRIM28, which suggest that ZFP568 is major mediator of TRIM28 functions in embryonic tissues.

In Chapter 4, I present a summary and discussion of how these studies expand our knowledge of the biological functions of KRAB zinc finger proteins and their binding partners during embryonic development, and propose ideas for future research.

Appendices A, B, C and D contain unpublished results that were not included in previous chapters as they are either preliminary or inconclusive. In Appendix A, I describe the analysis of mutants carrying a hypomorphic allele for *Zfp568*. In

Appendix B, I describe experiments I conducted to study the subcellular localization of ZFP568 and TRIM28. Appendix C contains information from microarray analyses conducted to identify genes misregulated in *Zfp568* and *Trim28*^{chatwo} mutants. Appendix D contains data from studies I have conducted to study epigenetic defects in *Trim28*^{chatwo} mutants.

REFERENCES

Abrink, M., Ortiz, J. A., Mark, C., Sanchez, C., Looman, C., Hellman, L., Chambon, P., and Losson, R. (2001). Conserved interaction between distinct Krüppel-associated box domains and the transcriptional intermediary factor 1 β. *Proceedings of the National Academy of Sciences of the United States of America*, **98**, 1422 -1426.

Alarcón, C., Zaromytidou, A., Xi, Q., Gao, S., Yu, J., Fujisawa, S., Barlas, A., Miller, A. N., Manova-Todorova, K., and Macias, M. J. (2009). Nuclear CDKs Drive Smad Transcriptional Activation and Turnover in BMP and TGF-β Pathways. *Cell*, **139**, 757-769.

Angelo, S., Lohr, J., Lee, K. H., Ticho, B. S., Breitbart, R. E., Hill, S., Yost, H. J., and Srivastava, D. (2000). Conservation of sequence and expression of Xenopus and zebrafish dHAND during cardiac, branchial arch and lateral mesoderm development. *Mechanisms of Development*, **95**, 231-237.

Argraves, W. S. and Drake, C. J. (2005). Genes critical to vasculogenesis as defined by systematic analysis of vascular defects in knockout mice. *The anatomical record Part A, Discoveries in molecular, cellular, and evolutionary biology*, **286**, 875–84.

Beckstead, R., Ortiz, J. A., Sanchez, C., Prokopenko, S. N., Chambon, P., Losson, R., and Bellen, H. J. (2001). Bonus, a Drosophila Homolog of TIF1 Proteins, Interacts with Nuclear Receptors and Can Inhibit βFTZ-F1-Dependent Transcription. *Molecular Cell*, **7**, 753-765.

Bianchi, D. W. et al. (1993). Origin of extraembryonic mesoderm in experimental animals: relevance to chorionic mosaicism in humans. *Am. J. Med. Genet*, **46**, 542-550.

Bohnsack, B. L., Lai, L., Dolle, P., and Hirschi, K. K. (2004). Signaling hierarchy downstream of retinoic acid that independently regulates vascular remodeling and endothelial cell proliferation. *Genes & development*, **18**, 1345-1358.

Cammas, F., Mark, M., Dollé, P., Dierich, A., Chambon, P., and Losson, R. (2000). Mice lacking the transcriptional corepressor TIF1beta are defective in early postimplantation development. *Development*, **127**, 2955-2963.

Chang, H., Huylebroeck, D., Verschueren, K., Guo, Q., Matzuk, M. M., and Zwijsen, A. (1999). Smad5 knockout mice die at mid-gestation due to multiple embryonic and extraembryonic defects. *Development*, **126**, 1631–42.

Coultas, L., Chawengsaksophak, K., and Rossant, J. (2005). Endothelial cells and

VEGF in vascular development. *Nature*, **438**, 937-945.

Drake, C. J. and Fleming, P. A. (2000). Vasculogenesis in the day 6.5 to 9.5 mouse embryo. *Blood*, **95**, 1671-1679.

Eakin, G. S. and Behringer, R. R. (2004). Diversity of germ layer and axis formation among mammals. *Seminars in Cell & Developmental Biology*, **15**, 619-629.

Emerson, R. and Thomas, J. (2009). Adaptive Evolution in Zinc Finger Transcription Factors. *PLoS Genetics*.

Ferkowicz, M. J. and Yoder, M. C. (2005). Blood island formation: longstanding observations and modern interpretations. *Exp Hematol*, **33**, 1041–7.

Firulli, A. B., McFadden, D. G., Lin, Q., Srivastava, D., and Olson, E. N. (1998). Heart and extra-embryonic mesodermal defects in mouse embryos lacking the bHLH transcription factor Hand1. *Nature genetics*, **18**, 266–70.

Firulli, A. B. (2003). A HANDful of questions: the molecular biology of the heart and neural crest derivatives (HAND)-subclass of basic helix-loop-helix transcription factors. *Gene*, **312**, 27–40.

Freyer, C. and Renfree, M. (2008). The mammalian yolk sac placenta. *J Exp Zool B Mol Dev Evol*.

Friedman, J. R., Fredericks, W. J., Jensen, D. E., Speicher, D. W., Huang, X. P., Neilson, E. G., and Rauscher, F. J. (1996). KAP-1, a novel corepressor for the highly conserved KRAB repression domain. *Genes & Development*, **10**, 2067–78.

Frietze, S., Lan, X., Jin, V. X., and Farnham, P. J. (2009). Genomic targets of the KRAB and scan domain-containing zinc finger protein 263 (ZNF263). *Journal of Biological Chemistry*, 1–22.

Garavito-Aguilar, Z. V., Riley, H. E., and Yelon, D. (2010). Hand2 ensures an appropriate environment for cardiac fusion by limiting Fibronectin function. *Development*, **137**, 3215 -3220.

Garcia-Garcia, M. J., Shibata, M., and Anderson, K. V. (2008). Chato, a KRAB zinc-finger protein, regulates convergent extension in the mouse embryo. *Development*, **135**, 3053–3062.

George, E. L., Georges-Labouesse, E. N., Patel-King, R. S., Rayburn, H., and Hynes, R. O. (1993). Defects in mesoderm, neural tube and vascular

development in mouse embryos lacking fibronectin. *Development (Cambridge, England)*, **119**, 1079-1091.

Gilbert, S. F. and Singer, S. R. (2010). Developmental Biology Sinauer Associates, Incorporated.

Goumans, M. J., Zwijsen, A., Rooijen, M. A. V., Huylebroeck, D., Roelen, B. A., and Mummery, C. L. (1999). Transforming growth factor-beta signalling in extraembryonic mesoderm is required for yolk sac vasculogenesis in mice. *Development*, **126**, 3473–83.

Hennemann, H., Vassen, L., Geisen, C., Eilers, M., and Möröy, T. (2003). Identification of a novel Krüppel-associated box domain protein, Krim-1, that interacts with c-Myc and inhibits its oncogenic activity. *J. Biol. Chem*, **278**, 28799-28811.

Ho, J., Kong, J., Choong, L., Loh, M., Toy, W., Chong, P., Wong, C., Wong, C., Shah, N., and Lim, Y. (2009). Novel Breast Cancer Metastasis-Associated Proteins. *Journal of Proteome Research*, **8**, 583-594.

Hu, D. and Cross, J. C. (2010). Development and function of trophoblast giant cells in the rodent placenta. *Int J Dev Biol*, **54**, 341–54.

Hu, G., Kim, J., Xu, Q., Leng, Y., Orkin, S. H., and Elledge, S. J. (2009). A genome-wide RNAi screen identifies a new transcriptional module required for self-renewal. *Genes & Development*, **23**, 837–48.

Huminiecki, L., Goldovsky, L., Freilich, S., Moustakas, A., Ouzounis, C., and Heldin, C. (2009). Emergence, development and diversification of the TGF-beta signalling pathway within the animal kingdom. *BMC Evolutionary Biology*, **9**, 28.

Huntley, S., Baggott, D. M., Hamilton, A. T., Tran-Gyamfi, M., Yang, S., Kim, J., Gordon, L., Branscomb, E., and Stubbs, L. (2006). A comprehensive catalog of human KRAB-associated zinc finger genes: insights into the evolutionary history of a large family of transcriptional repressors. *Genome Res*, **16**, 669–77.

Inman, K. E. and Downs, K. M. (2007). The murine allantois: emerging paradigms in development of the mammalian umbilical cord and its relation to the fetus. *genesis*, **45**, 237–58.

Ivanov, A. V., Peng, H., Yurchenko, V., Yap, K. L., Negorev, D. G., Schultz, D. C., Psulkowski, E., Fredericks, W. J., White, D. E., Maul, G. G., et al. (2007). PHD domain-mediated E3 ligase activity directs intramolecular

sumoylation of an adjacent bromodomain required for gene silencing. *Molecular cell*, **28**, 823-837.

Jakobsson, J., Cordero, M. I., Bisaz, R., Groner, A. C., Busskamp, V., Bensadoun, J., Cammas, F., Losson, R., Mansuy, I. M., Sandi, C., et al. (2008). KAP1-mediated epigenetic repression in the forebrain modulates behavioral vulnerability to stress. *Neuron*, **60**, 818–31.

Jiao, K., Zhou, Y., and Hogan, B. L. M. (2002). Identification of mZnf8, a mouse Krüppel-like transcriptional repressor, as a novel nuclear interaction partner of Smad1. *Mol Cell Biol*, **22**, 7633–44.

Knöfler, M., Meinhardt, G., Bauer, S., Loregger, T., Vasicek, R., Bloor, D. J., Kimber, S. J., and Husslein, P. (2002). Human Hand1 basic helix-loop-helix (bHLH) protein: extra-embryonic expression pattern, interaction partners and identification of its transcriptional repressor domains. *Biochem J*, **361**, 641-651.

Lawson, K. A., Dunn, N. R., Roelen, B. A., Zeinstra, L. M., Davis, A. M., Wright, C. V., Korving, J. P., and Hogan, B. L. (1999). Bmp4 is required for the generation of primordial germ cells in the mouse embryo. *Genes Dev*, **13**, 424-436.

Li, X., Ito, M., Zhou, F., Youngson, N., Zuo, X., Leder, P., and Ferguson-Smith, A. C. (2008). A maternal-zygotic effect gene, Zfp57, maintains both maternal and paternal imprints. *Developmental cell*, **15**, 547-557.

Mackay, D. J. G., Callaway, J. L. A., Marks, S. M., White, H. E., Acerini, C. L., Boonen, S. E., Dayanikli, P., Firth, H. V., Goodship, J. A., Haemers, A. P., et al. (2008). Hypomethylation of multiple imprinted loci in individuals with transient neonatal diabetes is associated with mutations in ZFP57. *Nat. Genet*, **40**, 949-951.

Matsui, T., Leung, D., Miyashita, H., Maksakova, I. A., Miyachi, H., Kimura, H., Tachibana, M., Lorincz, M. C., and Shinkai, Y. (2010). Proviral silencing in embryonic stem cells requires the histone methyltransferase ESET. *Nature*, **464**, 927-931.

Morikawa, Y. and Cserjesi, P. (2004). Extra-embryonic vasculature development is regulated by the transcription factor HAND1. *Development*, **131**, 2195–2204.

Morin-Kensicki, E. M., Boone, B. N., Howell, M., Stonebraker, J. R., Teed, J., Alb, J. G., Magnuson, T. R., O'Neal, W., and Milgram, S. L. (2006). Defects in yolk sac vasculogenesis, chorioallantoic fusion, and embryonic axis elongation in mice with targeted disruption of Yap65. *Mol Cell Biol*, **26**, 77–

87.

Nagy, A. (2003). Manipulating the mouse embryo : a laboratory manual Cold Spring Harbor Laboratory Press, Cold Spring Harbor, N.Y.

Nielsen, A. L., Ortiz, J. A., You, J., Oulad-Abdelghani, M., Khechumian, R., Gansmuller, A., Chambon, P., and Losson, R. (1999). Interaction with members of the heterochromatin protein 1 (HP1) family and histone deacetylation are differentially involved in transcriptional silencing by members of the TIF1 family. *EMBO J*, **18**, 6385-6395.

O'Farrell, P. H., Stumpff, J., and Tin Su, T. (2004). Embryonic Cleavage Cycles: How Is a Mouse Like a Fly? *Current Biology*, **14**, R35-R45.

Ozato, K., Shin, D., Chang, T., and Morse, H. C. (2008). TRIM family proteins and their emerging roles in innate immunity. *Nat Rev Immunol*, **8**, 849-860.

Peng, H., Feldman, I., and Rauscher III, F. J. (2002). Hetero-oligomerization Among the TIF Family of RBCC/TRIM Domain-containing Nuclear Cofactors: A Potential Mechanism for Regulating the Switch Between Coactivation and Corepression. *Journal of Molecular Biology*, **320**, 629-644.

Riley, P., Anson-Cartwright, L., and Cross, J. C. (1998). The Hand1 bHLH transcription factor is essential for placentation and cardiac morphogenesis. *Nature genetics*, **18**, 271–275.

Riley, P., Gertsenstein, M., Dawson, K., and Cross, J. (2000). Early Exclusion of Hand1-Deficient Cells from Distinct Regions of the Left Ventricular Myocardium in Chimeric Mouse Embryos. *Developmental Biology*, **227**, 156–168.

Ross, S. and Hill, C. S. (2008). How the Smads regulate transcription. *The International Journal of Biochemistry & Cell Biology*, **40**, 383-408.

Rossant, J. and Cross, J. C. (2001). Placental development: Lessons from mouse mutants. *Nat Rev Genet*, **2**, 538-548.

Rowe, H. M., Jakobsson, J., Mesnard, D., Rougemont, J., Reynard, S., Aktas, T., Maillard, P. V., Layard-Liesching, H., Verp, S., Marquis, J., et al. (2010). KAP1 controls endogenous retroviruses in embryonic stem cells. *Nature*, **463**, 237–240.

Ryan, R., Schultz, D., Ayyanathan, K., Singh, P., Friedman, J., Fredericks, W., and Rauscher, F. (1999). KAP-1 corepressor protein interacts and colocalizes with heterochromatic and euchromatic HP1 proteins. *Mol Cell Biol*.

Sardiello, M., Cairo, S., Fontanella, B., Ballabio, A., and Meroni, G. (2008). Genomic analysis of the TRIM family reveals two groups of genes with distinct evolutionary properties. *BMC Evolutionary Biology*, **8**, 225.

Sawada, A., Kiyonari, H., Ukita, K., Nishioka, N., Imuta, Y., and Sasaki, H. (2008). Redundant Roles of Tead1 and Tead2 in Notochord Development and the Regulation of Cell Proliferation and Survival. *Mol. Cell. Biol.*, **28**, 3177-3189.

Seki, Y., Kurisaki, A., Watanabe-Susaki, K., Nakajima, Y., Nakanishi, M., Arai, Y., Shiota, K., Sugino, H., and Asashima, M. (2010). TIF1β regulates the pluripotency of embryonic stem cells in a phosphorylation-dependent manner. *Proceedings of the National Academy of Sciences*, **107**, 10926-10931.

Smart, N., Hill, A. A., Cross, J. C., and Riley, P. R. (2002). A differential screen for putative targets of the bHLH transcription factor Hand1 in cardiac morphogenesis. *Mech Dev*, **119 Suppl 1**, S65–71.

Sripathy, S. P., Stevens, J., and Schultz, D. C. (2006). The KAP1 Corepressor Functions To Coordinate the Assembly of De Novo HP1-Demarcated Microenvironments of Heterochromatin Required for KRAB Zinc Finger Protein-Mediated Transcriptional Repression. *Mol Cell Biol*, **26**, 8623–8638.

Tallquist, M. and Soriano, P. (2000). Epiblast-restricted Cre expression in MORE mice: a tool to distinguish embryonic vs. extra-embryonic gene function. *Genesis*.

Tam, P. P. L. and Loebel, D. A. F. (2007). Gene function in mouse embryogenesis: get set for gastrulation. *Nat Rev Genet*, **8**, 368-381.

Tam, P. P. L. and Rossant, J. (2003). Mouse embryonic chimeras: tools for studying mammalian development. *Development*, **130**, 6155 -6163.

Tian, C., Xing, G., Xie, P., Lu, K., Nie, J., Wang, J., Li, L., Gao, M., Zhang, L., and He, F. (2009). KRAB-type zinc-finger protein Apak specifically regulates p53-dependent apoptosis. *Nat Cell Biol*, **11**, 580-591.

Tremblay, K. D., Dunn, N. R., and Robertson, E. J. (2001). Mouse embryos lacking Smad1 signals display defects in extra-embryonic tissues and germ cell formation. *Development*, **128**, 3609–21.

Urrutia, R. (2003). KRAB-containing zinc-finger repressor proteins. *Genome biology*, **4**, 231.

Watson, E. D. and Cross, J. C. (2005). Development of Structures and Transport Functions in the Mouse Placenta. *Physiology*, **20**, 180-193.

Weber, P., Cammas, F., Gerard, C., Metzger, D., Chambon, P., Losson, R., and Mark, M. (2002). Germ cell expression of the transcriptional co-repressor TIF1beta is required for the maintenance of spermatogenesis in the mouse. *Development*, **129**, 2329–37.

Winnier, G., Blessing, M., Labosky, P. A., and Hogan, B. L. (1995). Bone morphogenetic protein-4 is required for mesoderm formation and patterning in the mouse. *Genes & Development*, **9**, 2105–16.

Wolf, D. and Goff, S. P. (2009). Embryonic stem cells use ZFP809 to silence retroviral DNAs. *Nature*, **458**, 1201–1204.

Wolf, D. and Goff, S. P. (2007). TRIM28 mediates primer binding site-targeted silencing of murine leukemia virus in embryonic cells. *Cell*, **131**, 46–57.

Wu, M. Y. and Hill, C. S. (2009). Tgf-beta superfamily signaling in embryonic development and homeostasis. *Dev. Cell*, **16**, 329-343.

Yang, J. T., Rayburn, H., and Hynes, R. O. (1993). Embryonic mesodermal defects in alpha 5 integrin-deficient mice. *Development*, **119**, 1093-1105.

Yelon, D., Ticho, B., Halpern, M., Ruvinsky, I., Ho, R., Silver, L., and Stainier, D. (2000). The bHLH transcription factor hand2 plays parallel roles in zebrafish heart and pectoral fin development. *Development*, **127**, 2573 -2582.

Yin, C., Kikuchi, K., Hochgreb, T., Poss, K. D., and Stainier, D. Y. (2010). Hand2 Regulates Extracellular Matrix Remodeling Essential for Gut-Looping Morphogenesis in Zebrafish. *Developmental Cell*, **18**, 973-984.

Yokoe, T., Toiyama, Y., Okugawa, Y., Tanaka, K., Ohi, M., Inoue, Y., Mohri, Y., Miki, C., and Kusunoki, M. (2009). KAP1 Is Associated With Peritoneal Carcinomatosis in Gastric Cancer. *Ann Surg Oncol*, **17**, 821-828.

Zhao, B., Li, L., Lei, Q., and Guan, K. (2010). The Hippo–YAP pathway in organ size control and tumorigenesis: an updated version. *Genes & Development*, **24**, 862-874.

CHAPTER 2

THE MOUSE KRAB ZINC-FINGER PROTEIN CHATO IS REQUIRED IN EMBRYONIC-DERIVED TISSUES TO CONTROL YOLK SAC AND PLACENTA MORPHOGENESIS[1]

[1] This work has been published as **Shibata, M. and Garcia-Garcia, M. J.** (2010). The mouse KRAB Zinc-Finger protein CHATO is required in embryonic-derived tissues to control yolk sac and placenta morphogenesis. *Dev. Biol.* doi:10.1016/j.ydbio.2010.11.015. Minor modifications have been made.

ABSTRACT

Yolk sac and placenta are required to sustain embryonic development in mammals, yet our understanding of the genes and processes that control morphogenesis of these extraembryonic tissues is still limited. The *chato* mutation disrupts ZFP568, a Krüppel-Associated-Box (KRAB) domain Zinc finger protein, and causes a unique set of extraembryonic malformations, including ruffling of the yolk sac membrane, defective extraembryonic mesoderm morphogenesis and vasculogenesis, failure to close the ectoplacental cavity and incomplete placental development. Phenotypic analysis of *chato* embryos indicated that ZFP568 does not control proliferation or differentiation of extraembryonic lineages, but rather regulates the morphogenetic events that shape extraembryonic tissues. Analysis of chimeric embryos showed that *Zfp568* function is required in embryonic-derived lineages, including the extraembryonic mesoderm. Depleting *Zfp568* affects the ability of extraembryonic mesoderm cells to migrate. However, explanted *Zfp568* mutant cells could migrate properly when plated on appropriate extracellular matrix conditions. We show that expression of Fibronectin and Indian Hedgehog are reduced in *chato* mutant yolk sacs. This data suggests that ZFP568 controls the production of secreted factors required to promote morphogenesis of extraembryonic tissues. Our results support previously undescribed roles of the extraembryonic mesoderm in yolk sac morphogenesis and in the closure of the ectoplacental cavity and identify a novel role of ZFP568 in the development of extraembryonic tissues.

INTRODUCTION

Yolk sac and placenta are extraembryonic tissues that play critical roles in the early development of mammalian species. Although extraembryonic tissues do not contribute to the adult organism, they are critical to sustain embryonic life inside the

uterus by providing nourishment and secreting factors that maintain pregnancy (Watson and Cross, 2005). At early embryonic stages, the yolk sac forms a diffusion barrier that mediates the absorption of nutrients directly from the uterine compartment (Jollie, 1990; Rossant and Tam, 2002). Additionally, the yolk sac functions as the first hematopoietic organ, playing a critical role nourishing embryos once they depend on a circulatory system to deliver nutrients (Ferkowicz and Yoder, 2005; Fraser and Baron, 2009). Once embryonic blood circulation is established, the chorio-allantoic placenta (referred onwards as placenta) becomes essential for embryonic survival, as it mediates the exchange of gases, metabolites and waste products between the maternal and fetal circulatory systems. Placental cell types also secrete hormones that maintain pregnancy and impede immunological rejection of the fetus by the maternal immune system (Watson and Cross, 2005). The importance of extraembryonic tissues is underscored by the embryonic growth restriction and early lethality observed in mouse mutants that disrupt yolk sac and placental development (Argraves and Drake, 2005; Baron, 2003; Watson and Cross, 2005).

There are three critical stages in the morphogenesis of extraembryonic tissues: the early specification of trophectoderm (TE) and visceral endoderm (VE) as extraembryonic lineages separate from the embryonic inner cell mass; the contribution of extraembryonic mesoderm during gastrulation; and the subsequent differentiation and morphogenesis of these cell types to form the mature yolk sac and placenta (Rossant and Tam, 2009). Especially relevant is the emergence of the extraembryonic mesoderm, an embryonic-derived cell type that delaminates from the primitive streak and triggers a profound rearrangement in the other extraembryonic lineages (Inman and Downs, 2007). Starting at embryonic day (E) 6.5, mesoderm cells migrate into the extraembryonic region, displacing TE lineages proximally into the conceptus and originating the exocoelomic and ectoplacental cavities. As the extraembryonic

mesoderm thins out to line the exocoelom, it apposes the VE and forms the yolk sac. Additionally, the extraembryonic mesoderm contacts TE lineages and forms the chorion, an extraembryonic membrane essential for placental formation (Rossant and Cross, 2001; Watson and Cross, 2005). Completion of placental morphogenesis also requires the contribution of the allantois, another mesoderm-derived structure that extends and fuses with the chorion, becoming the umbilical cord (Inman and Downs, 2007). Simultaneously, the chorion rises and the ectoplacental cavity collapses, causing the apposition of the chorion with the ectoplacental cone, a pre-requisite for the formation of the labyrinth, the vascularized portion of the placenta where maternal and fetal circulation contact (Inman and Downs, 2007; Watson and Cross, 2005).

The study of mouse mutants has greatly contributed to our understanding of the genes and processes that underlie yolk sac and placenta morphogenesis. More than 90 genes have been described to affect the development of these extraembryonic tissues (for a comprehensive review of mouse mutants with placental phenotypes see Inman and Downs, 2007; Watson and Cross, 2005). Some mutations affect differentiation of extraembryonic cell types: for instance, transcription factors Achaete-Scute complex homolog-2 (ASCL2) and Heart and neural crest derivatives expressed transcript-1 *(*HAND1) regulate the differentiation of trophoblast giant cells from TE stem cell precursors (El-Hashash et al., 2010; Hu and Cross, 2010). Other mutants affect extraembryonic mesoderm cells or their derivatives, as in the case of mutations in *Brachyury* (*T*) and *Bone morphogenetic protein (Bmp)* signaling, which affect extraembryonic mesoderm morphogenesis and the formation of the allantois (Downs et al., 2004; Inman and Downs, 2006; Rashbass et al., 1991; Tremblay et al., 2001; Winnier et al., 1995). Mouse studies have also highlighted the mutual dependence of TE, VE and extraembryonic mesoderm for morphogenesis of extraembryonic tissues, and have identified signaling molecules that mediate these

interactions, including Vascular endothelial growth factor (VEGF), Indian Hedgehog (IHH), Fibroblast growth factor (bFGF), Fibronectin (FN) and Transforming growth factor β (TGFβ) (Bohnsack et al., 2004; Byrd et al., 2002; Damert et al., 2002; Flamme and Risau, 1992; Goumans et al., 1999). Also, TE derived lineages secrete polypeptide hormones that impact proliferation and differentiation of the placenta (Rossant and Cross, 2001; Watson and Cross, 2005). Studies on mouse mutants have also identified many other genes that control placental morphogenetic processes such as chorioallantoic attachment, labyrinth branching morphogenesis and labyrinth vascularization (reviewed in Inman and Downs, 2007; Watson and Cross, 2005). These include growth factors, adhesion proteins, transmembrane receptors, protein kinases, transcription factors and epigenetic regulators (Bartholin et al., 2008; Inman and Downs, 2007; Papadaki et al., 2007; Rossant and Cross, 2001; Tian et al., 2009; Watson and Cross, 2005).

KRAB Zinc finger proteins represent one of the largest families of transcriptional regulators in mammals, with more than 300 genes (Urrutia, 2003). However, the biological processes controlled by these proteins have been elusive, mostly due to the lack of mouse mutants in individual KRAB-domain proteins. Here we report the characterization of the extraembryonic defects of *chato* mouse mutants. *chato* disrupts ZFP568, a KRAB Zinc finger protein previously described to disrupt mammalian convergent extension (Garcia-Garcia et al., 2008). *chato* mutants display strong extraembryonic defects, including a ruffling of the yolk sac, defective vasculogenesis and incomplete placental morphogenesis. Analysis with markers of different extraembryonic cell types showed proper specification of extraembryonic lineages in *chato* embryos, but morphogenetic cellular and tissue rearrangements were disrupted. *Zfp568* is expressed ubiquitously throughout mid-gestation, but at high levels in TE-derived tissues, including the ectoplacental cone and the extraembryonic

ectoderm (Garcia-Garcia et al., 2008). Analysis of chimeric *Zfp568* embryos obtained through tetraploid complementation and through the use of a Cre-responsive *Zfp568* reversible allele indicated that *Zfp568* is required in embryonic-derived tissues for the morphogenesis of both yolk sac and placenta. *chato* mutant yolk sacs contained clumped extraembryonic mesoderm cells, indicating that yolk sac and trophoblast defects in *chato* mutants could be caused by an inability of extraembryonic mesoderm to migrate. We show that *chato* yolk sac explants migrate and behave similar to wild type when plated in appropriate tissue culture conditions, but their migratory ability is diminished in the absence of Fibronectin. Expression of *Fn1* and other factors involved in morphogenesis of extraembryonic tissues is decreased in *chato* mutant embryos. Taken together, these results indicate that *Zfp568* is required in embryonic-derived tissues to provide an environment that supports proper morphogenesis of extraembryonic tissues. Our data attests to the important role of the extraembryonic mesoderm in the morphogenesis of the yolk sac and placenta and defines a requirement of ZFP568 for proper development of these tissues.

MATERIALS AND METHODS

Mouse strains

Extraembryonic phenotypes of $Zfp568^{chato}$ and $Zfp568^{null}$ alleles (Garcia-Garcia et al., 2008) were characterized on C3H/FeJ, CAST/Ei and 129Sv/ImJ. *Meox2Cre* (Tallquist and Soriano, 2000), *Sox2Cre* (Hayashi et al., 2002) and *ROSA 26* (Friedrich and Soriano, 1991) mice were obtained from Jackson Laboratory. myr-VENUS mice were obtained from Dr. Kat Hadjantonakis (Rhee et al., 2006). The $Zfp568^{rGT\text{-}mutant}$ reversible allele was generated from the German Gene Trap Consortium (GGTC) clone P103E09 (Schnutgen *et al*., 2005). Complete disruption of *Zfp568* splicing in

Zfp568$^{rGT\text{-}mutant}$ was confirmed by RT-PCR using primers in *Zfp568* first and second coding exons. For creation of chimeras, *Meox2Cre*$^{+/-}$; *Zfp568*$^{+/null}$ or *Sox2Cre*$^{+/-}$; *Zfp568*$^{+/null}$ males were crossed to *Zfp568*$^{rGT\text{-}mutant/+}$ females.

Embryo analysis

Embryos were dissected in 0.4% BSA PBS. Scanning electron microscopy samples were prepared as described (Garcia-Garcia et al., 2008) and imaged with a Hitachi 4500 microscope. *In situ* hybridizations using DIG-labeled RNA probes were conducted as previously described (Garcia-Garcia and Anderson, 2003; Welsh and O'Brien, 2000). Embryos were imaged in methanol, then processed for 16 μm cryosections. Immunohistochemistry was performed as described (Nagy, 2003) on 8 μm cryosections or whole embryos. Antibodies were anti-phospho-histone H3 (1:200; Upstate); anti-VCAM1 (1:250; BD Biosciences), anti-α4 integrin (1:250; Millipore), anti-Laminin (1:50; Sigma-Aldrich), anti-Fibronectin (1:1000 Sigma-Aldrich), anti-E-Cadherin (1:500 Sigma-Aldrich) and anti-rabbit/anti-rat Alexa Fluor 488 (1:200; Molecular Probes). Alexa Fluor 488 Phalloidin (1:20; Molecular Probes) was used for counterstaining. TUNEL was conducted using the ApopTag Kit (Chemicon) as previously described (Garcia-Garcia *et al.,* 2008). Western blot analysis was performed on yolk sacs from E8.5 embryos using standard protocols and anti-Laminin (1:1000; Sigma-Aldrich), anti-Fibronectin (1:1000; Sigma-Aldrich), anti-GAPDH HRP (1:8000; Abcam) and anti-rabbit HRP (1:10000; Jackson ImmunoResearch) antibodies. Intensity of Western blot bands was quantified with ImageJ. Images of mutant embryos and their respective wild type controls are shown at the same magnification. Expression of molecular markers in *chato* mutants of different categories was assayed, but has not been reported unless a modification in the expression pattern was detected. Similarly, analysis of proliferation and apoptosis

includes results from *chato* embryos of different classes unless stated. Statistical analysis used two-tailed *t*-tests and the Prism software (GraphPad).

Tetraploid complementation assays

Generation of *Rosa26 lacZ*$^{+}$ *Zfp568*^{chato} and *Zfp568*$^{chato/+}$ ES cell lines, tetraploid complementation experiments and staining for β -galactosidase activity were conducted as described (Nagy, 2003). Similar results were obtained using either of two *Zfp568*^{chato} ES cell lines.

Cell migration assays

Yolk sacs from GFP+ (myr-VENUS; Rhee et al., 2006) wild type embryos and from *chato* mutants were dissected at E8.5 and treated with 0.*25*% trypsin. Trypsinized cells were mixed, then plated onto 5μg/cm^2 Fibronectin-coated chambers. 24 hours after plating, confluent cells were scratched and cultured in media containing 5% FBS. Cell migration was assessed after 16 hours. Individually grown yolk sac explants were performed as described (Nagy, 2003) using Lab-Tek II Chamber Slides (Nunc) coated with 5μg/cm^2 Fibronectin, 5μg/cm^2 Laminin, 0.1% gelatin or without coating. Quantification of migration areas was done at 16 hours using ImageJ. Explants lacking migrating cells at 16 hours (30-60%) were not used to quantify the migratory ability of explants. Differences in explant attachment efficiency between wild type and *chato* mutant embryos, or between different substrate conditions, were not significant.

qRT-PCR

For quantitative reverse transcription PCR analysis of yolk sac samples, RNA was purified from two independent pools of E8.5 wild type and mutant yolk sacs (RNA STAT-60, Tel-Test). SYBR Green real-time PCR was conducted under standard conditions with cDNA prepared using Superscript III First-Strand Synthesis System

(Invitrogen). Calculations were conducted using the $2^{-\Delta\Delta CT}$ method (Livak and Schmittgen, 2001) with *Gapdh* as standard. For primer sequences, see Table 2.1.

RESULTS

ZFP568 is required for yolk sac morphogenesis

chato is a recessive chemically-induced null mutation in the KRAB domain Zinc Finger protein ZFP568 that disrupts embryo elongation and causes lethality at E9 (Garcia-Garcia et al., 2008). In addition to previously characterized embryonic defects, *chato* mutants display malformations in extraembryonic tissues. In most *chato* embryos (96% n=73), the yolk sac is noticeably ruffled by E8.5 (Figure 2.1A-B; Garcia-Garcia et al., 2008). These yolk sac bubble-like protrusions were observed in embryos as early as E7.5, although at this stage the yolk sac ruffles were not as large and profuse (Figure 2.1C-D; Garcia-Garcia et al., 2008). We investigated whether *chato* yolk sac defects originate from abnormalities in the VE or extraembryonic mesoderm, the two cell types that constitute the yolk sac. Analysis of VE markers showed that expression of *α-fetoprotein (Afp)* (Dziadek and Andrews, 1983), *Transthyretin* (*Ttr*) (Barron et al., 1998) and *HNF1 Homeobox B* (*HNF1b*) (Coffinier et al., 1999) was unaffected in *chato* mutants (Figure 2.1E-H, Figure 2.2A-D). Likewise, molecular markers of the extraembryonic mesoderm, including *Hand1* (Firulli et al., 1998) and the *Forkhead box F1a* gene (*Foxf1*) (Mahlapuu et al., 2001), were correctly expressed (Figure 1I-L and not shown). We evaluated whether an overgrowth of the VE layer may underlie the yolk sac ruffling in *chato* mutants. To this end, we quantified the number of mitotic cells in sagittal sections using phospho-histone H3 antibodies. The average number of VE mitotic cells in *chato* mutants at

Table 2.1. Sequences of primer pairs used for genotyping and qRT-PCR experiments.

Genotyping Primers

chato (129 background, D7SKI10)	GGCTGTCTGAGGAGGACAAA TCCATCTTTCCCACTTCTCC
chato (129 background, D7SKI26)	TGGTAAAGCCCTGGACATCT CCTCTTCCTTCCAAGTGCAT
Zfp568^{null}	CGTTGAGTTCTCGGCATACA GGCTACCGGCTAAAACTTGA
Zfp568$^{rGT\text{-}mutant}$	CAAGGCGATTAAGTTGGGTAACG ATCGATTCAAGCCACTATGC
Zfp568$^{rGT\text{-}restored}$	CGTTGGCTACCCGTGATATT ATCGATTCAAGCCACTATGC

qRT-PCR Primers

Vegfa (PrimerBank ID 6678563a2)	CTTGTTCAGAGCGGAGAAAGC ACATCTGCAAGTACGTTCGTT
Kdr	TCCAGAATCCTCTTCCATGC CCAGAGACCCTCGTTTTCAG
Tgfb1 (PrimerBank ID 6755775a3)	CCGCAACAACGCCATCTATG CTCTGCACGGGACAGCAAT
Ihh	TGACAGAGATGGCCAGTGAG CAATCCCGACATCATCTTCA
Fn1 (PrimerBank ID 1181242a1)	ATGTGGACCCCTCCTGATAGT GCCCAGTGATTTCAGCAAAGG
Gapdh	ACTGCCACCCAGAAGACTGT GATGCAGGGATGATGTTCTG
Zfp568	TGACCCAGCCTTGAAATACC AGGCCTGGTCCTGTCTTCTT

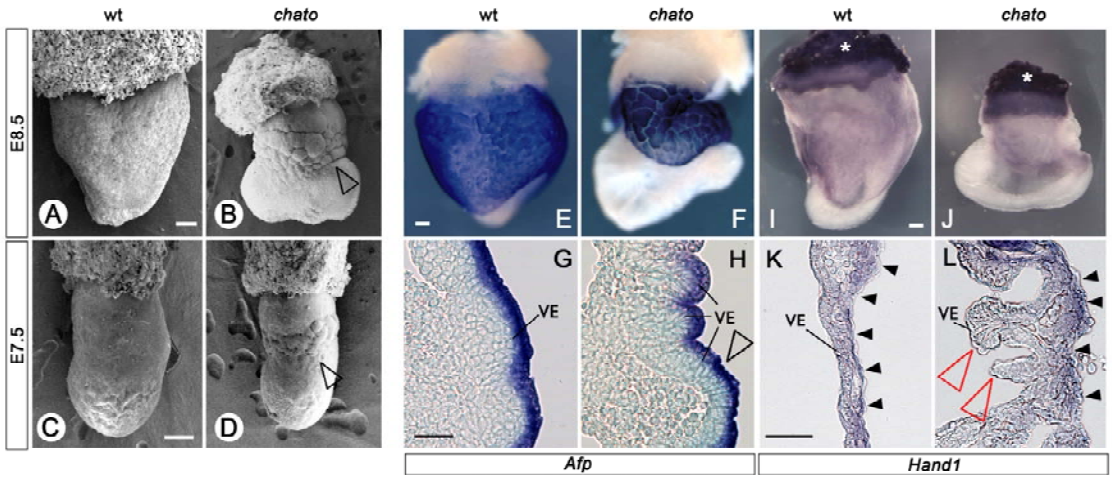

Figure 2.1. Yolk sac defects in *chato* embryos. (A-D) Scanning electron micrographs of E8.5 (A,B) and E7.5 embryos (C,D). **(E-L)** *In situ* hybridizations in whole mount embryos (E,F, I,J) and yolk sac sections (G,H, K, L) with *Afp* (E-H) and *Hand1* (I-L) probes in E8.5 wild type (E,G, I, K) and *chato* (F, H, J, L) embryos. The *chato* embryos shown in F, H, J and L correspond to the class II category as specified in Figure 3. In this and other figures, the expression of markers in their respective cell types did not change between embryos of different categories unless otherwise noted. Arrowheads in B and D indicate yolk sac ruffles. Arrowhead in H marks compression of VE cells. Red arrowheads in L highlight detachment of VE from extraembryonic mesoderm. Black arrowheads in K, L point to extraembryonic mesoderm cells. Asterisks (I,J) indicate placental expression of *Hand1*. VE, visceral endoderm. Scale bars represent 100µm in A, B, C, D, E and I; and 50µm in G and K. In this and following figures, pictures of wild type and mutant embryos are taken at the same magnification.

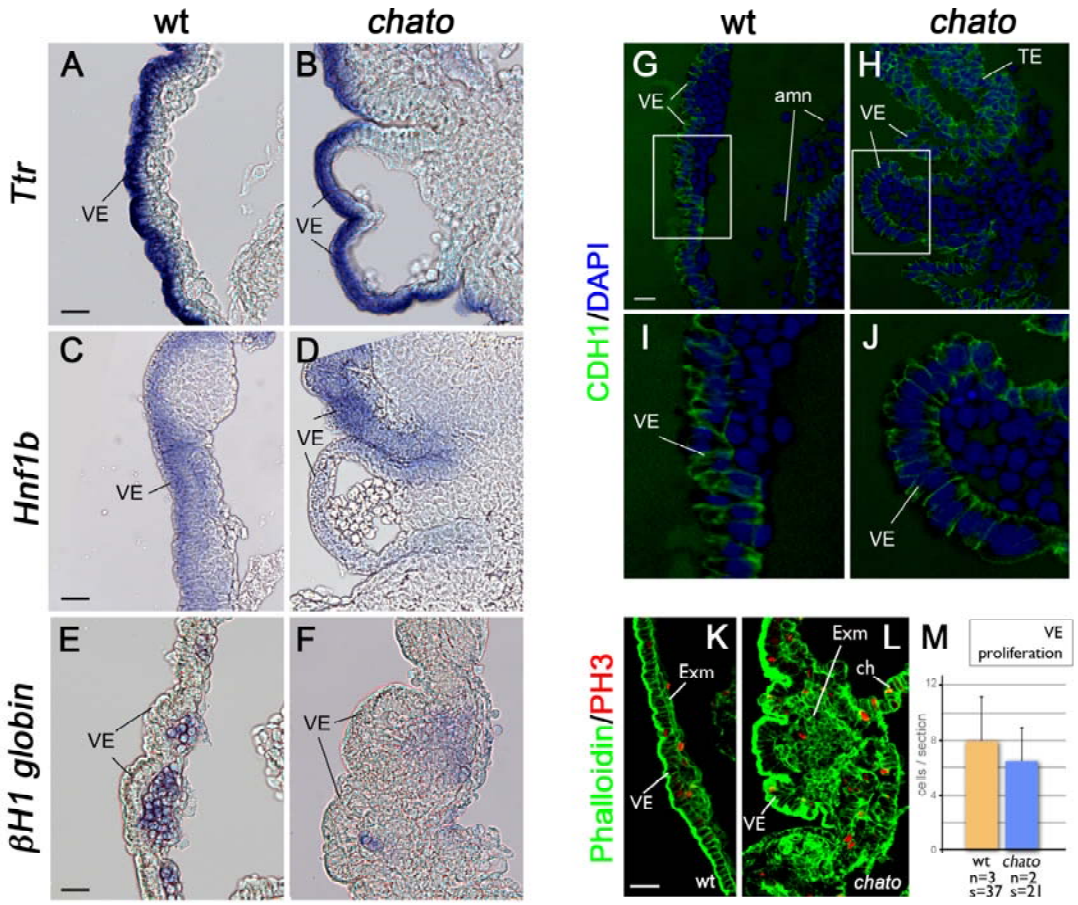

Figure 2.2. Analysis of yolk sac defects in *chato* embryos. (A-F) *In situ* hybridizations in E8.5 wild type (A, C, E) and *chato* mutants (B, D, F) with *Ttr* (A,B) *Hnf1b* (C,D) and β*H1 globin* (E,F) probes. High magnifications of sagittal sections through the yolk sac region are shown. (B) class III and (D, F) class II *chato* mutants **(G-J)** Wild type (G) and *chato* mutant sagittal sections were stained with anti-CDH1 antibody (green) and counterstained with DAPI (blue). (I,J) higher magnifications of boxed areas in G, H respectively. (H, J) show a class II *chato* mutant. **(K-L)** Immunohistochemistry with anti-phospho-histone H3 antibodies (PH3, red) counterstained with Phalloidin (green) as shown on a class III *chato* mutant **(M)** Quantification of the number of PH3 positive cells per section in the VE of wild type (orange; 7.97±3.18) and *chato* (blue; 6.48±2.38) embryos (p=0.0655). Error bars indicate s.d.; n=embryos and s=sections quantified. VE, visceral endoderm; amn, amnion; TE, trophectoderm; Exm, extraembryonic mesoderm; ch, chorion. Scale bars represent 25μm.

E8.5 (6.48±2.38; Figure 2.2L-M, blue) was slightly smaller than in wild type littermates (7.97±3.18; Figure 2.2K & 2.2M, orange), although the difference was not statistically significant (p=0.0655). To evaluate whether the ruffled yolk sac could originate from an excess of VE cells due to increased cell survival, we quantified apoptosis using TUNEL. Consistent with previous reports, we found that wild type yolk sac (Goh et al., 1997) and extraembryonic tissues (Gladdy et al., 2006) have very low levels of apoptosis, and that these levels were similarly low in *chato* mutants (Figure 2.3). Therefore, our data does not support overproliferation or increased cell survival of the VE as the causes of yolk sac ruffling.

Analysis of *chato* embryo sections revealed abnormalities in the organization of both VE and extraembryonic mesoderm. In *chato* embryos, VE cells were compressed at some areas (Figure 2.1H, black arrowhead) and detached from the underlying extraembryonic mesoderm at other locations (Figure 1L, red arrowheads; Figure 2.2B, 2.2D). These defects were not accompanied by abnormal VE epithelial integrity or polarity, as assessed by analysis of Cadherin 1 (CDH1) and actin localization in *chato* mutants (Figure 2.2G-J and 2.2K-L). Integrity and composition of extraembryonic basement membranes were not noticeably changed in *chato* embryos, as judged from immunohistochemistry analysis of Fibronectin and Laminin (Figure 2.4). Also, expression of receptors for these extracellular components such as α4-Integrin and β1 -Integrin was not affected in *chato* mutants (Figure 2.5 and not shown). Similar to wild type embryos, *chato* mutants contained mesoderm cells lining interiorly the exocoelomic cavity (Figure 2.1K-L, small arrowheads). However, in *chato* mutants extraembryonic mesoderm cells clumped at the embryonic-extraembryonic junction (Figure 2.1H, 2.2, 2.6D, 2.6F). Analysis of *Tbx4*, a marker of allantoic mesoderm (Chapman et al., 1996), revealed that posteriorly accumulated cells in *chato* embryos correspond to the allantois, which failed to extend as compared

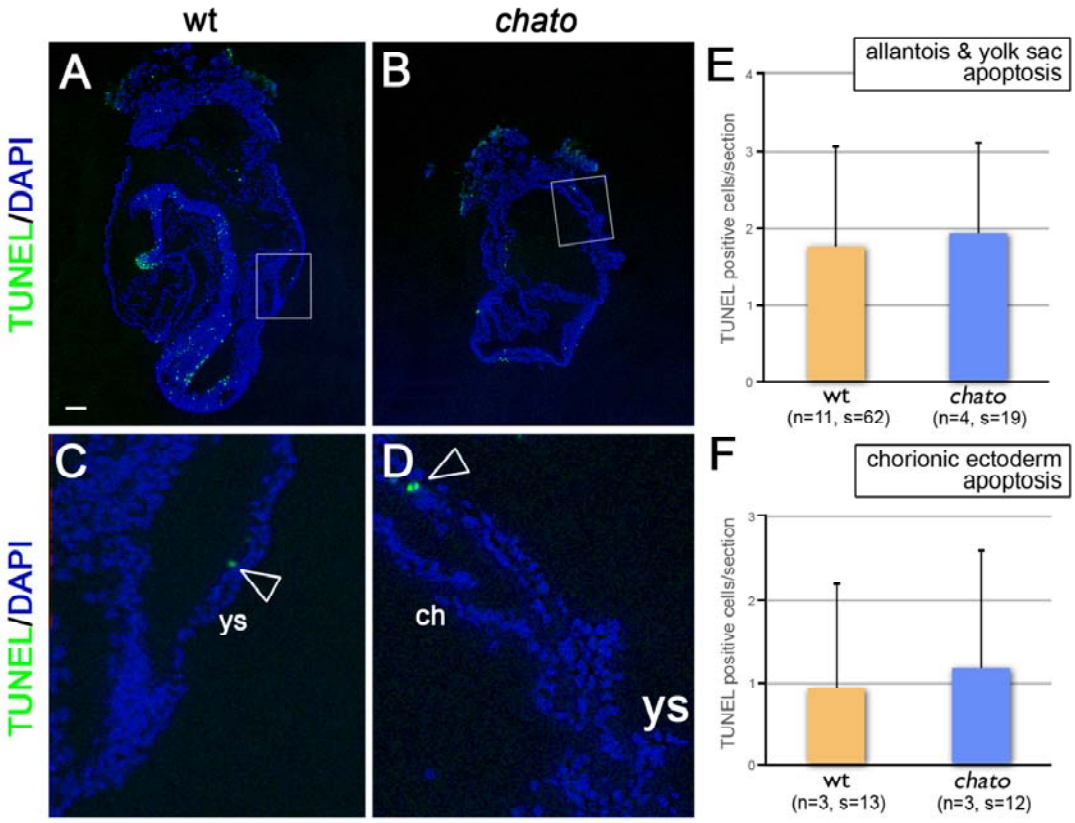

Figure 2.3. Apoptosis in *chato* mutants. **(A-D)** TUNEL (green) and DAPI (blue) staining on sagittal sections of wild type (A) and a class II *chato* (B) embryo. **(C,D)** Higher magnifications of boxed regions in A, B. Arrowheads point to TUNEL positive nuclei. **(E,F)** Quantification of total TUNEL positive cells per section in allantois and yolk sac (E) and chorionic ectoderm (F). Error bars indicate s.d.; n=embryos and s=sections quantified. ys=yolk sac, ch=chorion. Scale bar represents 100µm.

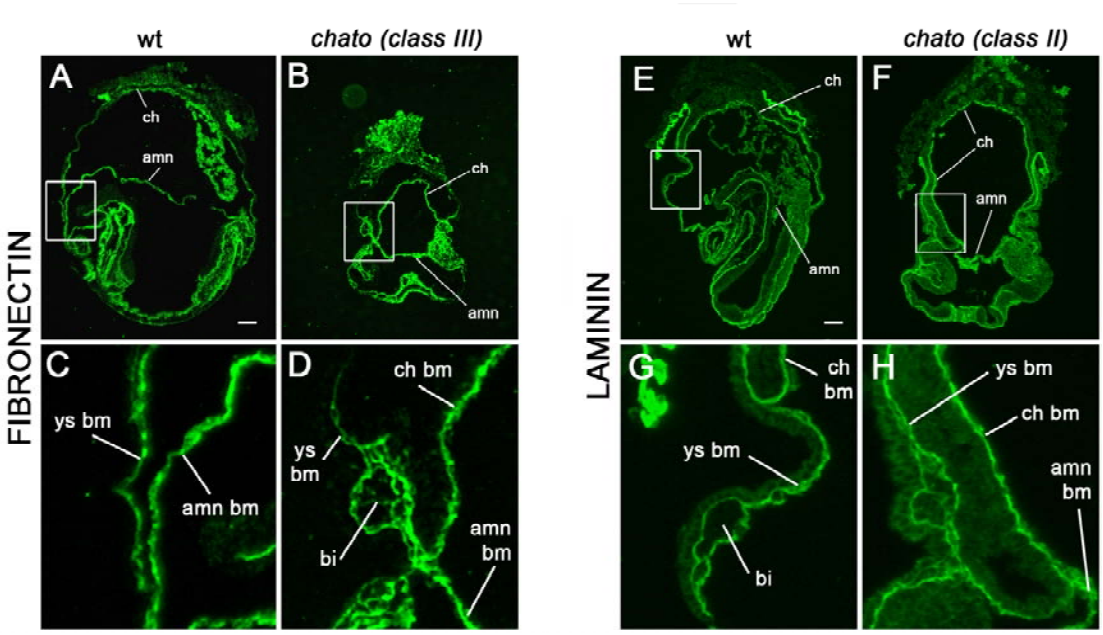

Figure 2.4. Localization of extracellular matrix components in *chato* extraembryonic tissues. Immunohistochemistry of sagittal sections from E8.5 wild type **(A, E)** and *chato* mutant **(B, F)** embryos with anti-Fibronectin (green, A-D) and anti-Laminin (green, E-H) antibodies. C-D and G-H are high magnifications of boxed areas in A-B and E-F, respectively. Both wild type and *chato* mutants contained Fibronectin and Laminin in the basement membranes of the yolk sac (ys bm), the chorion (ch bm) and the amnion (amn bm), as well as in the area surrounding blood islands (bi). Scale bars in A and E represent 100μm.

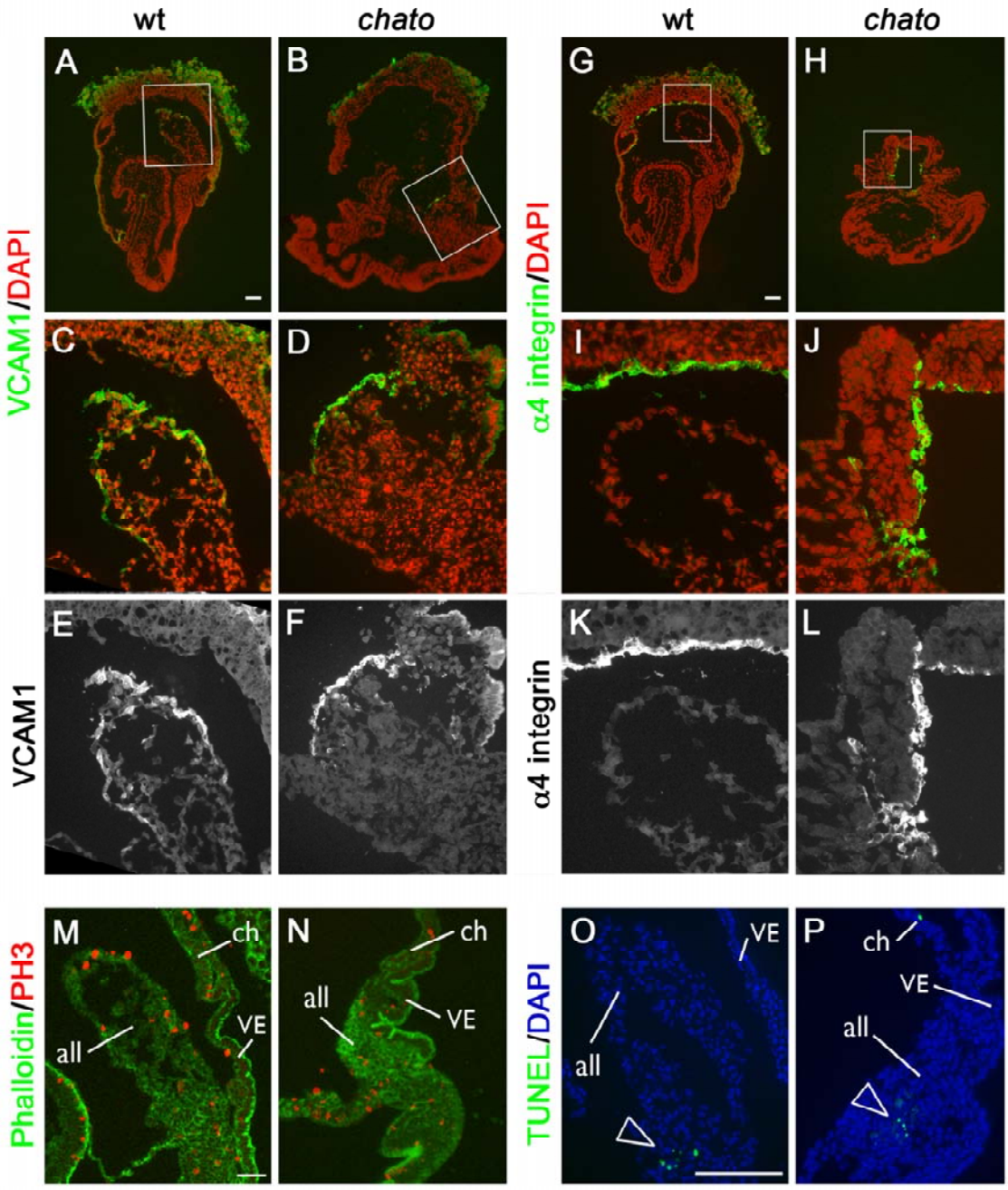

Figure 2.5. VCAM1 and α4 integrin expression in *chato* embryos. Sagittal sections of E8.5 wild type (A,G) and class II *chato* (B,H) embryos labeled with anti-VCAM (A,B; green) or anti-α4 integrin (G,H; green) antibodies and DAPI (red) counterstaining. C-F,I-L, are magnifications of boxed regions in A,B,G,H, respectively (E-F,K-L; green channel only). **(M-P)** Sagittal sections of wild type (M, O) and class II *chato* mutant embryos (N, P) stained with anti-phospho-histone H3 antibodies (PH3, red) and Phalloidin (green) (M-N) or with TUNEL (green) and DAPI (blue) (O-P). all, allantois; ch, chorion; VE, visceral endoderm. Arrowheads in O,P point to TUNEL positive nuclei in allantois. Scale bars in A,G,M,O represent 100μm.

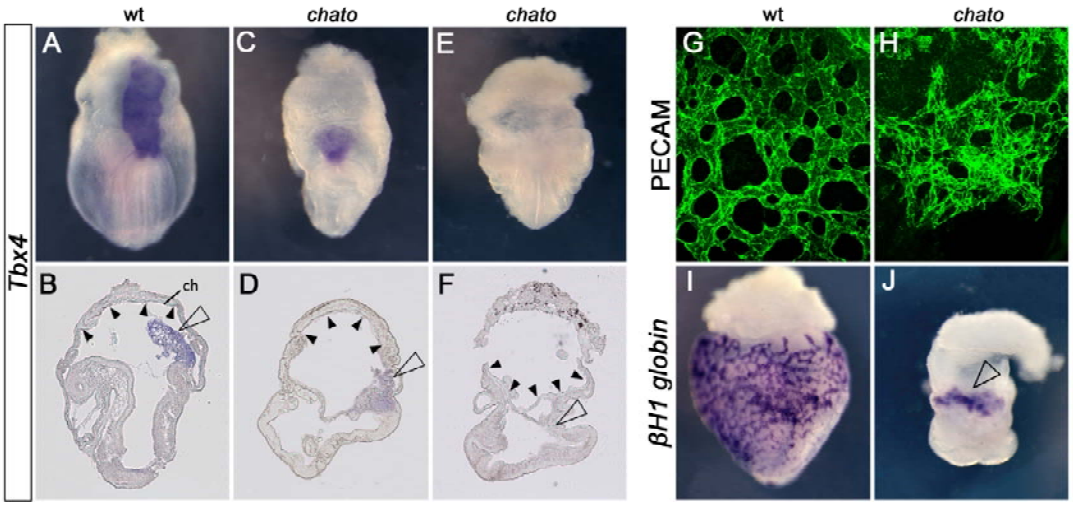

Figure 2.6. Abnormal extraembryonic mesoderm morphogenesis in *chato* mutants. (A-F) Whole mount *in situ* hybridizations of E8.5 wild type (A,B) and *chato* (C-F) embryos using *Tbx4* probe. (A,C,E) posterior views. (B,D,F) sagittal sections of the corresponding embryos. According to the categories specified in Figure 3, panels D and F are a class I and a class III *chato* mutant, respectively. **(G,H)** Immunohistochemistry with anti-PECAM antibodies in E8.5 wild type (G) and *chato* (H) embryos. Endothelial cells in *chato* mutants are small and formed a collapsed vascular plexus. **(I,J)** *βH1-globin* whole mount *in situ* hybridizations in E8.5 wild type (I) and *chato* (J) embryos. Open arrowheads in B, D, F point to allantoic mesoderm. Arrowhead in J indicates accumulation of blood cells at blood islands. Small arrowheads in B, D and F mark the chorion (ch). Images in G and H were acquired with confocal microscopy using a 40x objective.

to wild type littermates (Figure 2.6A-F). In the most severe *chato* embryos, *Tbx4* failed to be expressed (Figure 2.6E-F). Analysis of markers of vascular and hematopoietic precursors revealed abnormalities in these extraembryonic mesoderm lineages. Immunohistochemistry using Platelet/endothelial cell adhesion molecule-1 (PECAM1) antibodies (Baldwin et al., 1994) showed that in *chato* mutants the vascular endothelial cells are specified, but the extraembryonic vascular plexus failed to extend throughout the yolk sac and remained restricted to the blood island region (Figure 2.6G-H). Hematopoietic cells were also specified in *chato* mutants (Figure 2.6I-J, Figure 2.2E-F) as highlighted by expression of the hematopoietic marker *βH1globin* (McGrath et al., 2003). However, consistent with the failure of the primitive plexus vasculature to extend in *chato* embryos, they remained confined to the blood island region in *chato* mutants (Figure 2.6I-J, arrowhead). Altogether, these results indicate that the yolk sac ruffling in *chato* embryos could originate from a loss of adhesiveness between VE and extraembryonic mesoderm, and/or by defective extraembryonic mesoderm morphogenesis.

chato disrupts placental morphogenesis

Morphogenesis of the labyrinth layer of the placenta requires that the allantois grows and makes contact with the chorion (Inman and Downs, 2007; Watson and Cross, 2005). Consistent with the inability of the allantois to extend in *chato* mutants (Figure 2.6A-F), we found that chorioallantoic attachment was disrupted in all *chato* embryos (n>76), preventing labyrinth formation (Figures 2.7A-D, 2.5 and 2.8). In *chato* mutants containing allantoic buds, adhesion molecules required for chorioallantoic attachment, including Vascular cell adhesion molecule-1 (VCAM1) and its ligand α4-integrin (Gurtner et al., 1995; Kwee et al., 1995; Yang et al., 1995), were localized in

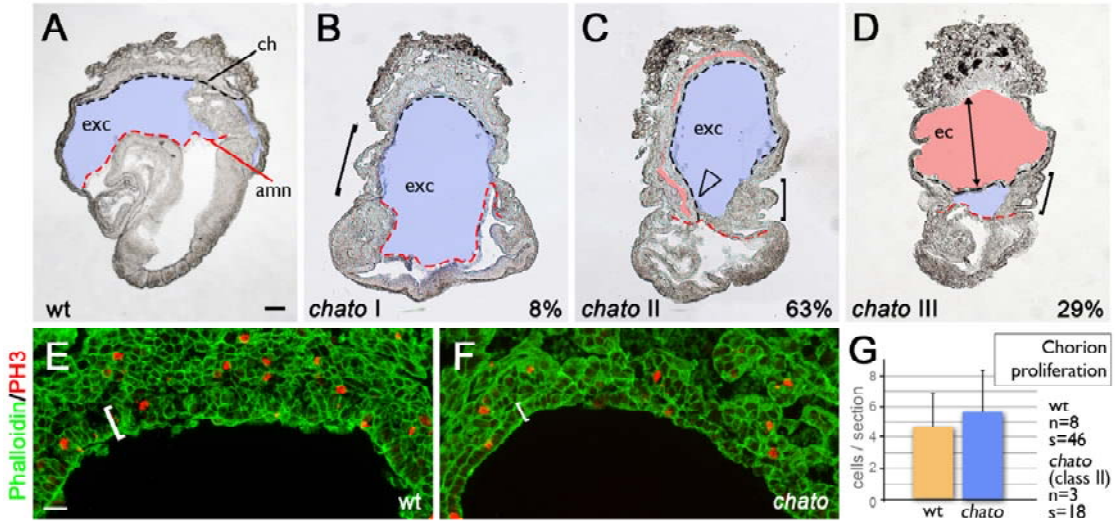

Figure 2.7. *chato* mutants display chorionic defects. (A-D) Sagittal sections of E8.5 wild type (A) and *chato* (B-D) embryos. Mutants were categorized into class I, II and III based on the severity of chorionic ectoderm expansion. Original pictures of these embryos without labeling signs are shown in Figure S4. **(E-F)** Immunohistochemistry with anti-phospho-histone H3 antibodies (PH3, red) in E8.5 sagittal sections of the chorion in wild type (E) and *chato* (F) embryos counterstained with Phalloidin (green). **(G)** Quantification of the number of PH3 positive cells per section in the chorionic ectoderm of wild type (orange; 4.61±0.33) and *chato* class II (blue; 5.67±0/64) embryos (p=0.1178). Broken black lines mark the chorion (ch). Broken red lines mark the amnion (amn). Exocoelomic cavity (exc) is colored in blue, ectoplacental cavity (ec) is colored in red. Arrowhead in C highlights the expansion of the chorion. Arrow in D points to the enlarged ectoplacental cavity. Bracket in B indicate the relatively smooth yolk sac of class I *chato* mutants. Brackets in C and D indicate yolk sac bubbles concentrated at the embryonic-extraembryonic boundary. Brackets in E and F mark the developing labyrinth in a wild type embryo and the flat chorion of a *chato* mutant, respectively. Error bars indicate s.d.; n=embryos and s=sections quantified. Scale bars represent 100µm in A and 25µm in E.

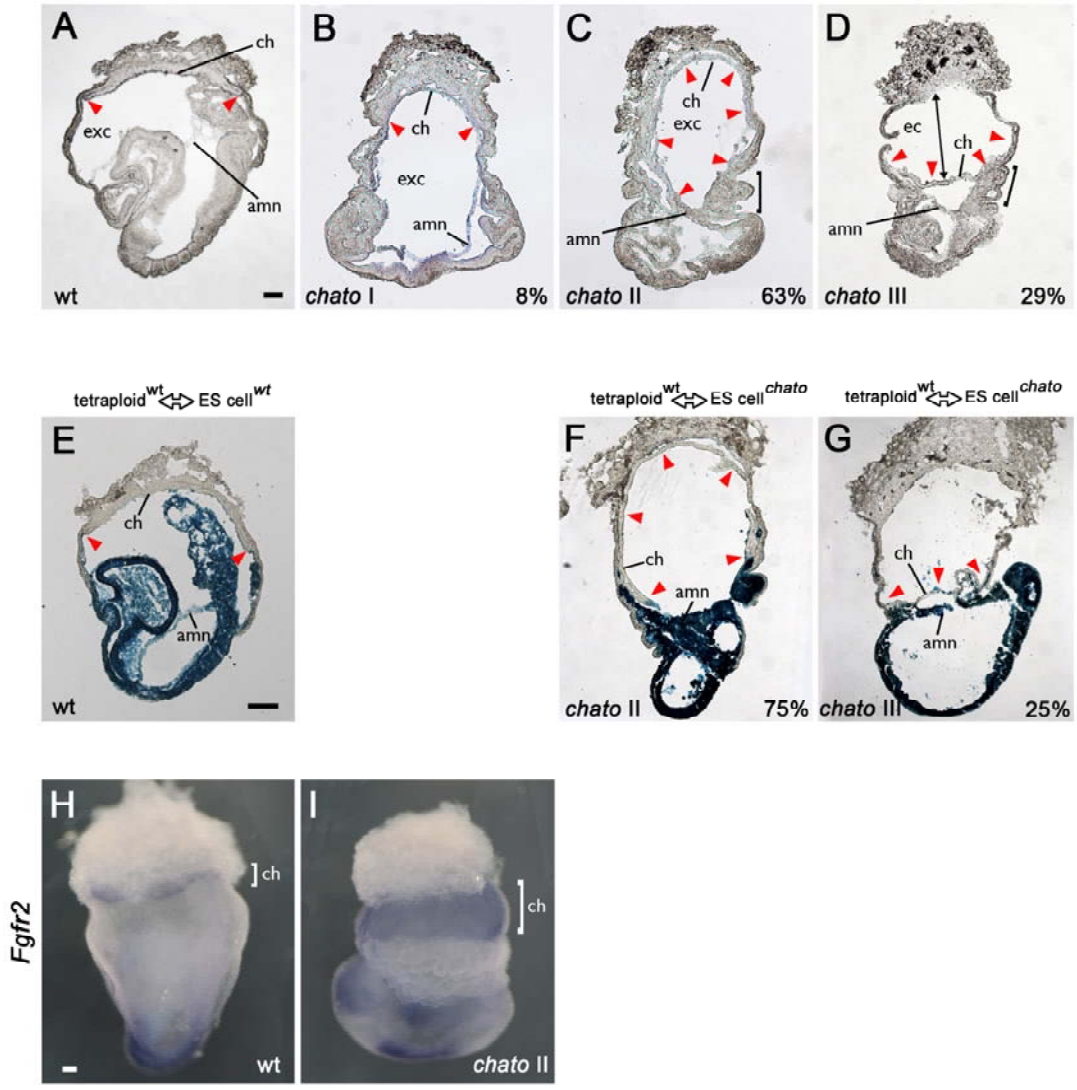

Figure 2.8. Trophoblast defects in *chato* mutants and *chato* tetraploid chimeras. **(A-D)** Raw images of the sagittal sections of E8.5 wild type (A) and *chato* (B-D) embryos shown in Figure 3. **(E-G)** Sagittal sections of X-gal stained tetraploid chimeras obtained from aggregation of wild type ES cells (control tetraploid^{wt} ↔ ES cell^{wt} chimera) (E) and *chato* mutant ES cells (tetraploid^{wt} ↔ ES cell^{chato} chimeras) (F,G). We found that *chato* tetraploid chimeras (n=8) reproduced the characteristic defects of class II (F, 75%) and class III *chato* mutants (G, 25%). The Rosa26 allele in the ES cell lines used to generate these chimeras served as a lineage marker to differentiate embryonic-derived cells (embryo and extraembryonic mesoderm, Xgal positive) from VE and trophoblast tissues (Xgal negative). **(H, I)** Whole mount *in situ* hybridizations with a *Fgfr2* probe in wild type (H) and *chato* embryos (I). amn, amnion; ch, chorion; exc, exocoelomic cavity; ec, ectoplacental cavity. Red arrowheads point to chorion. Double-arrowed line in D points to the enlarged ectoplacental cavity. Brackets in C and D indicate yolk sac bubbles concentrated at the embryonic-extraembryonic boundary. Scale bars in A,E,H represent 100µm.

allantois and chorionic mesoderm at levels similar to those of wild type littermates (Figure 2.5). Also, allantoic cell proliferation and cell death were not significantly altered in *chato* mutants (Figure 2.5M-P). Altogether, these results indicate that *chato* impedes chorioallantoic attachment by disrupting either sustained growth of the allantois or the ability of allantoic cells to migrate.

Analysis of embryonic sections revealed additional malformations in developing placental tissues in *chato* mutants. The majority of *chato* embryos contained an enlarged chorion (92% n=73 Figure 2.7C-D, Figure 2.8). Depending on the expansion and arrangement of the chorion we established three *chato* phenotypic groups: In class II *chato* embryos (63%) the chorion expanded laterally in direct contact with the VE (Figure 2.7C, Figure 2.8C, 2.8F), in some cases reaching the embryonic-extraembryonic boundary (Figure 2.7C, arrowhead). In class III *chato* mutants (29%), the chorion failed to rise and the enlarged chorionic ectoderm formed an expanded ectoplacental cavity (Figure 2.7D, Figure 2.8D, 2.8G). Only 8% of *chato* mutants (class I) contained a normally sized chorion and an ectoplacental cavity that collapsed similar to wild type littermates (Figure 2.7B).

Expansion of the chorion and failure of the ectoplacental cavity to collapse have not been associated with defects in allantoic growth, as supported by the lack of these defects in mouse mutants that disrupt allantoic extension such as *Smad1* (Lechleider et al., 2001) and *Cdx2* (Chawengsaksophak et al., 2004). To further investigate the role of *Zfp568* in proper morphogenesis of the chorion, we explored whether the expanded chorion in class II and class III *chato* mutants could originate from overproliferation. We assessed the number of phospho-histone H3 positive cells in sagittal section of the chorionic ectoderm at E8.5, when chorioallantoic attachment had just occurred in wild type embryos (Rossant and Cross, 2001) and the chorionic

ectoderm cells could still be morphologically discerned from other placental cell types (bracket in Figure 2.7E). At this stage, we did not observe an overall dramatic difference in the number of phospho-histone H3 positive cells in the chorion of *chato* mutants as compared with wild type littermates (Figure 2.7E-F). To quantify possible differences, we counted the number of phospho-histone H3 positive cells in the flat chorionic ectoderm of class II *chato* mutants and compared it with the number of TE phospho-histone H3 positive cells closer to the exocoelomic cavity of wild type littermates. Using this method, we found that the chorionic plate of class II *chato* embryos contained only an average of 1.06 more phospho-histone H3 positive cells than those in wild type littermates (wt=4.61 *chato*=5.67; Figure 2.7G). The fact that this difference is not statistically significant, together with the consideration that our quantification method might slightly underestimate the number of proliferating chorionic ectoderm cells in wild type embryos, suggests that chorion proliferation is not substantially increased in *chato* mutants. As previously indicated, TUNEL analysis in extraembryonic tissues did not reveal different rates of cell apoptosis between wild type and *chato* littermates (Figure 2.3), indicating that differences in cell survival do not account for the excess of chorionic ectoderm cells in *chato* embryos.

We next explored whether the expanded chorionic ectoderm in class II and III *chato* mutants could originate from an imbalance amongst different TE lineages. The chorion contains trophoblast stem cells that perdure until the last stages of placental morphogenesis and differentiate to produce ectoplacental cone and trophoblast giant cells (Cross, 2000; Hu and Cross, 2010). Conditions that disrupt the differentiation of trophoblast stem cells lead to an expansion of certain cell types at the expense of others (Guillemot et al., 1994; Luo et al., 1997; Riley et al., 1998). However, analysis of molecular markers characteristic of different placental populations by *in situ* hybridization in whole mount embryos and in sections showed that expression of

markers of different placental cell types in *chato* embryos, regardless of their phenotypic class, was similar to that of wild type littermates (Figure 2.9). The trophoblast giant cell marker *Placental lactogen 1* (*Pl1*); (Linzer and Fisher, 1999) was correctly expressed in *chato* mutants (Figure 2.9A-D, 2.9O-P). Likewise, markers expressed in the ectoplacental cone and in precursors of the spongiotrophoblast and labyrinth, including *Ascl2* (Guillemot et al., 1994) and *Trophoblast specific protein alpha* (*Tpbpa*) (Lescisin et al., 1988), were expressed in *chato* embryos in the appropriate location and in a similar number of cells as in wild type littermates (Figure 2.9E-L). Also, *Glial cells missing homolog 1* (*Gcm1*), a transcription factor expressed in clusters of chorion cells that mark the sites of future labyrinth branching (Basyuk et al., 1999) was expressed in clusters of cells in the chorion of *chato* embryos (Figure 2.9M-N). These results indicate that *chato* does not influence the differentiation of trophoblast cell types.

Altogether, results from these experiments indicate that ZFP568 does not regulate cell proliferation, cell survival or differentiation of trophoblast lineages. Hypotheses about how the expansion of the chorion might originate in *chato* mutants are provided in the Discussion section.

The severity of trophoblast defects in *chato* embryos correlates with that of yolk sac ruffling and extraembryonic mesoderm defects

We observed that the severity of defects in *chato* trophoblast tissues correlated with that of the yolk sac ruffling and malformations in extraembryonic mesoderm derivatives. In particular, the amount and location of yolk sac ruffles correlated with the extent of chorion expansion. Thus, in *chato* mutants where the chorion expanded to the embryonic-extraembryonic boundary (class II and III), yolk sac protrusions

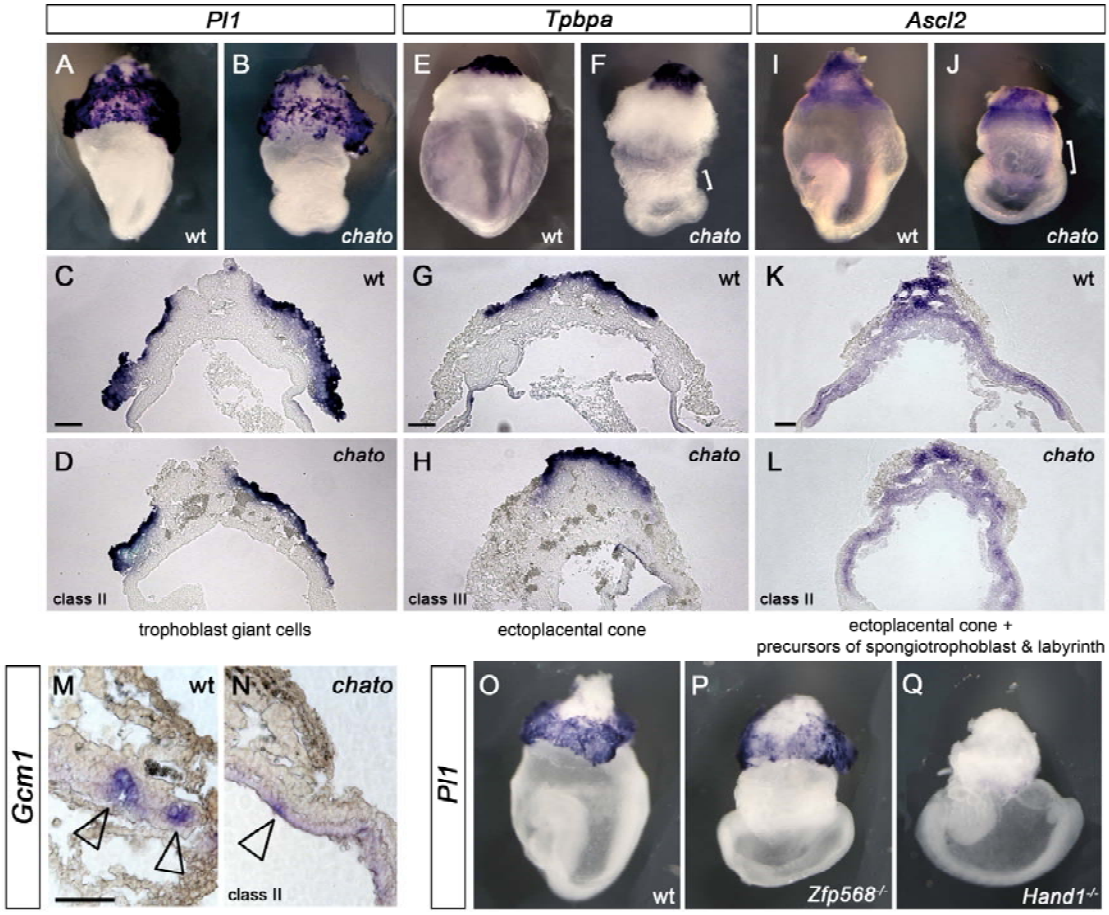

Figure 2.9. Specification of trophoblast cell types in *chato* mutants. Whole mount *in situ* hybridizations of E8.5 wild type (A,E,I, M) and *chato* mutant (B, F, J, N, P) embryos with *Pl1* (A-B, O-Q), *Tpbpa* (E-F), and *Ascl2 (*I-J) probes. **(C-D, G-H, K-L)** Sagittal sections of the trophoblast region of embryos in A-B, E-F, I-J, respectively. The trophoblast populations marked by these probes are indicated in the bottom margin. **(M-N)** High magnifications of E8.5 wild type (I) and *chato* mutant (J) sagittal sections showing *Gcm1* expression in clusters of chorionic cells (arrowheads). In *chato* embryos, *Gcm1* clusters are smaller. **(O-Q)** Whole mount *in situ* hybridizations of E8.5 wild type (O), *chato* (P) and *Hand1* mutant (Q) embryos with a *Pl1* probe. *Hand1* mutants have a severe reduction in the number of *Pl1*-expressing trophoblast giant cells (Riley et al., 1998). In contrast, the number of *Pl1*-expressing trophoblast giant cells in $Zfp568^{null}$ embryos is similar to that of wild type littermates. Brackets in F and J mark yolk sac ruffles. Scale bars represent 100μm.

were substantial and concentrated to a small band at this junction (brackets in Figure 2.7C-D, Figure 2.9F), while in embryos with a small chorion expansion (some class II) or no chorion expansion (class I), the yolk sac was smoother and the ruffles were distributed throughout a wider band (brackets in Figure 2.7B, Figure 2.9J).

Extraembryonic mesoderm defects in *chato* embryos also correlated with the yolk sac and chorion phenotypes. In class I *chato* mutants, clumps of extraembryonic mesoderm were not observed and, even though the vascular plexus was defective, an underdeveloped allantois was present (Figure 2.6D). However, class II and III *chato* mutants had more severe extraembryonic mesoderm defects such as presence of clumps of extraembryonic mesoderm (Figure 2.7C) and complete lack of an extended allantoic bud (Figure 2.6F, Figure 2.7D).

In contrast to the correlations between the severity of extraembryonic defects in *chato* mutants, we found that neither yolk sac ruffling, chorion expansion, nor extraembryonic mesoderm malformations matched up with the severity of *chato* embryonic phenotypes (not shown; Garcia-Garcia et al., 2008). Taken together, these observations suggest that defects in yolk sac and trophoblast tissues in *chato* mutants have a common developmental origin, while embryonic malformations likely originate from an independent requirement of ZFP568 in embryonic tissues. Analysis of *Zfp568* expression pattern did not resolve what tissues primarily require ZFP568 function, since *Zfp568* is expressed in all embryonic and extraembryonic tissues at early developmental stages, albeit with higher expression levels in TE cells (Garcia-Garcia et al., 2008; Figure 2.10).

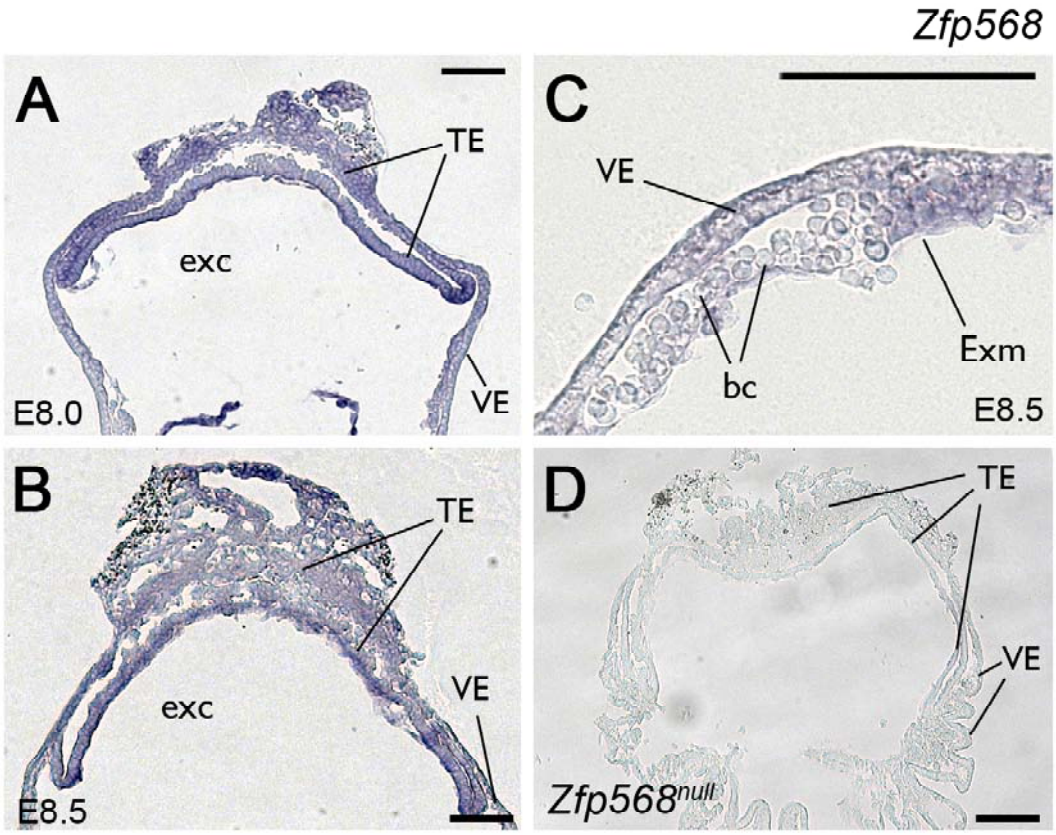

Figure 2.10. *Zfp568* expression in extraembryonic cells. Sections of whole mount *in situ* hybridizations of wild type (A-C) and *Zfp568*^{null} (D) embryos at E8.0 (A) and E8.5 (B,C,D) with a *Zfp568* probe. *Zfp568* expression was not detected in control *Zfp568*^{null} embryos (D). bc, blood cells; exc, exocoelomic cavity; TE, trophectoderm; VE, visceral endoderm; Exm, extraembryonic mesoderm. Scale bars represents 100μm.

ZFP568 is required in embryonic-derived tissues to control morphogenesis of embryonic and extraembryonic tissues

To investigate ZFP568 requirements in embryonic and extraembryonic lineages, we analyzed the phenotype of chimeric embryos obtained through tetraploid complementation assays. By aggregating wild type tetraploid embryos with *chato* mutant ES cells, we obtained tetraploid^{wt} ↔ ES cell^{chato} chimeras containing wild type VE and TE (Figure 2.11A, orange) and *chato* mutant embryonic-derived tissues, including the extraembryonic mesoderm (Figure 2.11A, blue). We found that tetraploid^{wt} ↔ ES cell^{chato} chimeric embryos (n=12) recapitulated all extraembryonic malformations observed in class II and III *chato* mutant embryos, including yolk sac ruffling (Figure 2.11B-C, arrowheads; Figure 2.8F-G), defective extraembryonic and allantoic mesoderm morphogenesis (Figure 2.11C, Figure 2.8F-G), expansion of the chorionic ectoderm (Figure 2.11C, Figure 2.8F-G) and failure of the chorion to rise and form the placenta (Figure 2.11C, arrow, Figure 2.8G). Additionally, tetraploid^{wt} ↔ ES cell^{chato} chimeric embryos displayed embryonic defects similar to *chato* mutants (Garcia-Garcia et al., 2008), including failure to undergo axial rotation and convergent extension defects in lateral plate mesoderm and definitive endoderm (Figure 2.11D-E). In comparison, control experiments using wild type tetraploid embryos and wild type ES cells, produced embryos without developmental defects (n=13, Figure 2.11F-I, Figure 2.11E). Therefore, these experiments demonstrate that wild type ZFP568 function in VE and TE tissues is not sufficient to rescue extraembryonic and embryonic malformations in *chato* mutants and that ZFP568 is required in embryonic-derived tissues to promote both extraembryonic and embryonic morphogenesis.

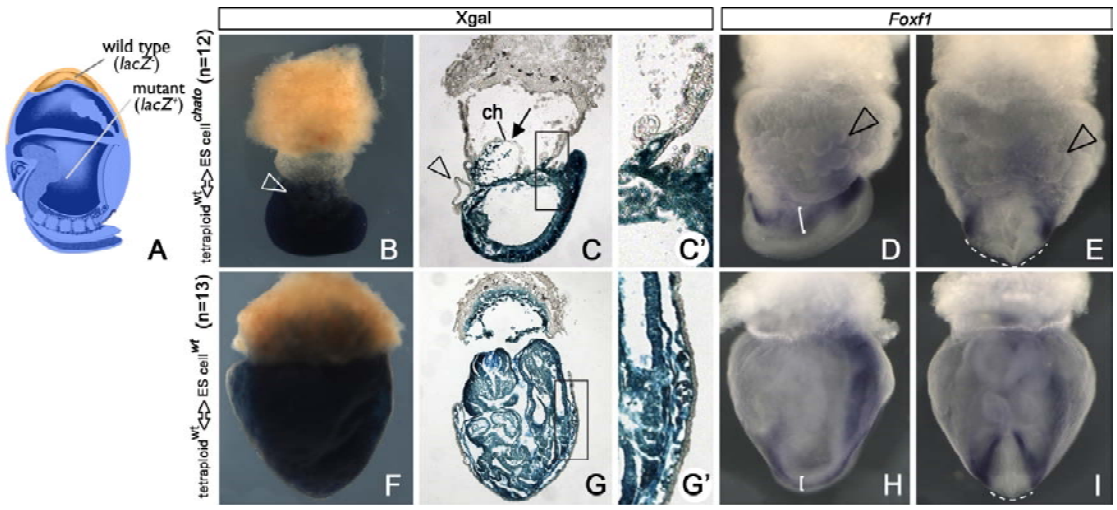

Figure 2.11. Tetraploid complementation assays. (A) Schematic representation of wild type (orange) and *chato* mutant (blue) cell types in tetraploid^{wt} ↔ ES cell^{chato} chimeric embryos shown in B-E. Tetraploid^{wt} ↔ ES cell^{chato} **(B-E)** and control tetraploid^{wt} ↔ ES cell^{wt} **(F-I)** chimeric embryos were processed for Xgal staining (B-C, F-G) or *Foxf1 in situ* hybridization (D-E, H-I). B, F, D, H; lateral views. E, I; anterior views. C, G; sagittal sections. C', G'; higher magnifications of boxed areas in C, G. Arrowheads indicate yolk sac ruffles. Arrow in C points to chorion (ch). Brackets in D, H highlight the lateral plate mesoderm. Discontinuous lines in E, I mark the width of the definitive endoderm.

Restoring *Zfp568* function in embryonic-derived tissues rescues embryonic and extraembryonic defects of *chato* mutants

To further confirm ZFP568 requirement in embryonic-derived tissues, we analyzed the phenotype of chimeric embryos reciprocal to those obtained through tetraploid complementation and thus containing *Zfp568* mutant VE and TE and wild type embryonic-derived tissues (VE+TE^{mutant} ↔ Em+Exm^{wt} chimeras, Figure 2.12C). To obtain these embryos, we used a *Zfp568* reversible allele in combination with the embryonic-specific Cre lines *Meox2Cre* (Tallquist and Soriano, 2000) and *Sox2Cre* (Hayashi et al., 2002). The *Zfp568* reversible allele (*Zfp568*$^{rGT\text{-}mutant}$) contains a genetrap insertion that completely disrupts the activity of *Zfp568* (Figure 2.12B), but, upon Cre recombinase expression, the orientation of the genetrap cassette can be inverted, restoring partial function to the *Zfp568* locus (*Zfp568*$^{rGT\text{-}restored}$ allele; Figure 2.13).

To resolve whether restoring *Zfp568* expression in embryonic-derived tissues is sufficient to rescue the extraembryonic and embryonic defects of *chato* mutants, we analyzed the phenotypes of *Meox2Cre; Zfp568*$^{rGT\text{-}mutant/null}$ and *Sox2Cre; Zfp568*$^{rGT\text{-}mutant/null}$ embryos. Both allelic combinations generate VE+TE$^{Zfp568\text{-}mutant}$ ↔ Em+Exm$^{Zfp568\text{-partially rescued}}$ chimeras (Figure 2.12C). The phenotypes of *Meox2Cre; Zfp568*$^{rGT\text{-}mutant/null}$ and *Sox2Cre; Zfp568*$^{rGT\text{-}mutant/null}$ chimeric embryos fell into one of the three following categories: some embryos showed all the phenotypic hallmarks of *chato* mutants (Figure 2.12F); in other embryos, yolk sac and chorion defects were rescued, but embryos still had *chato*-like defects in embryonic tissues (Figure 2.12E); finally, some chimeric embryos had a wild-type appearance in both embryonic and extraembryonic tissues (Figure 2.12D). The lack of rescue in some chimeric embryos (Figure 2.12E-F) could be due either to incomplete efficiency of the Cre recombinase

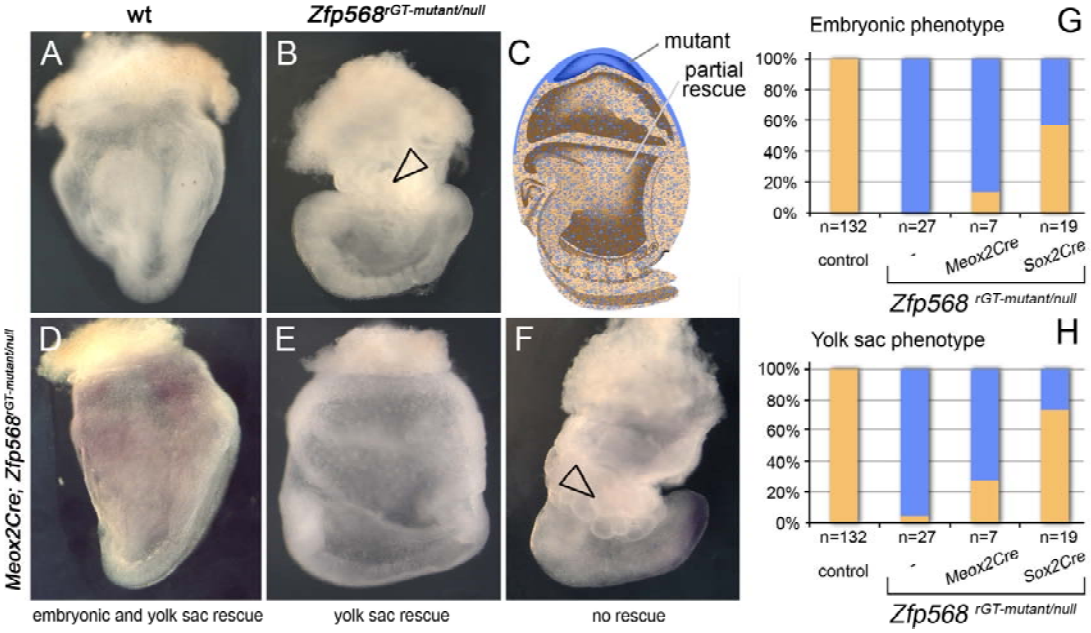

Figure 2.12. Analysis of chimeras with restored *Zfp568* expression in embryonic-derived tissues. Photographs of E8.5 wild type (A) and *Zfp568*$^{rGT\text{-}mutant/null}$ (B) embryos. **(C)** Schematic representation of the distribution of *Zfp568* mutant cells (blue) and cells with restored *Zfp568* function (orange) in *Meox2Cre; Zfp568* $^{rGT\text{-}mutant/null}$ and *Sox2Cre; Zfp568* $^{rGT\text{-}mutant/null}$ chimeric embryos. **(D-F)** Photographs of *Meox2Cre; Zfp568* $^{rGT\text{-}mutant/null}$ embryos. Blue staining in D and F corresponds to *Zfp568* and *T* expression, respectively. Other embryos were not assayed for expression of these markers. **(G,H)** Quantification of embryos with rescued embryonic (G) and yolk sac phenotypes (H) in *Meox2Cre; Zfp568* $^{rGT\text{-}mutant/null}$ and *Sox2Cre; Zfp568* $^{rGT\text{-}mutant/null}$ chimeras. Trophoblast defects could not be assessed in all chimeras, but severe chorionic defects such as those observed in class II and III *chato* mutants were detected in only 17% (2/12) *Sox2Cre; Zfp568* $^{rGT\text{-}mutant/null}$ embryos, suggesting that trophoblast defects were restored in some chimeras. Orange bars indicate the % embryos in which phenotypes were rescued. Blue bars represent % embryos with *chato*-like phenotypes. Note that yolk sacs were smooth in a small percentage of *Zfp568*$^{rGT\text{-}mutant/null}$ embryos without *Cre* (panel H; orange area in second column from the left; these embryos had a phenotype similar to those shown in panel E). Control embryos include *Sox2Cre/+* and *Meox2Cre/+* embryos. n = embryos quantified. Arrowheads highlight yolk sac ruffles.

in all embryonic cells, or to incomplete rescue of ZFP568 function due to the hypomorphic condition of the *Zfp568*$^{rGT\text{-}restored}$ allele (Figure 2.13). Quantification of embryos showing rescue of yolk sac and embryonic phenotypes showed that a larger percentage of embryos were rescued in experiments using *Sox2Cre* (Figure 2.12G-H). This result is consistent with the previously reported higher efficiency of *Sox2Cre vs. Meox2Cre* (Hayashi et al., 2002) and confirms that the extent of phenotypic rescue in the chimeras depends, at least partially, on the number of embryonic-derived cells in which ZFP568 function was restored. Regardless of the incomplete Cre efficiency and incomplete restoration of ZFP568 function, the fact that some VE+TE$^{Zfp568\text{-}mutant}$ ↔ Em+Exm$^{Zfp568\text{-partially rescued}}$ chimeras were completely wild type in appearance (Figure 2.12D, G, H) indicates that relatively small levels of *Zfp568* expression in embryonic-derived tissues can rescue both embryonic and extraembryonic defects. Additionally, the presence of embryonic defects in some VE+TE$^{Zfp568\text{-}mutant}$ ↔ Em+Exm$^{Zfp568\text{-partially rescued}}$ chimeras with rescued yolk sac and placental malformations (Figure 2.12E) indicates that embryonic defects are not a secondary consequence of the yolk sac and placental malformations in *chato* mutants.

Together with results from the analysis of tetraploid chimeras, these experiments demonstrate that *Zfp568* is not required in the VE or TE for early morphogenesis of the yolk sac, placenta and embryonic tissues. Furthermore, the rescue of extraembryonic, but not embryonic malformations in some VE+TE$^{Zfp568\text{-}mutant}$ ↔ Em+Exm$^{Zfp568\text{-partially rescued}}$ chimeras (Figure 2.12E) suggests that the requirements for *Zfp568* in extraembryonic mesoderm might be lower, and separate from the requirements of *Zfp568* in embryonic tissues.

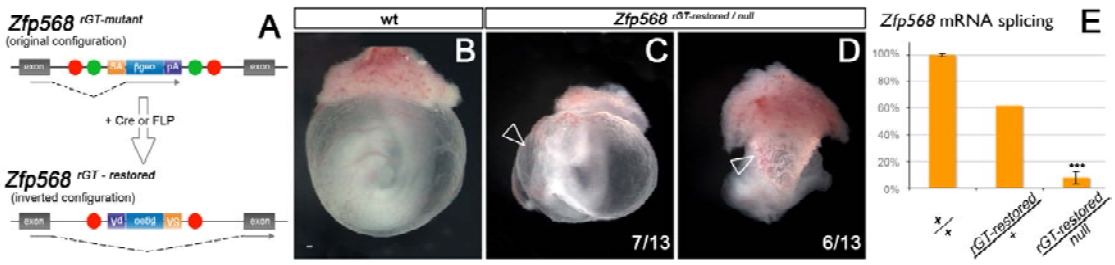

Figure 2.13. Characterization of the *Zfp568* reversible allele. (A) The *Zfp568* reversible allele (*Zfp568*$^{rGT\text{-}mutant}$) was generated from a German Gene Trap Consortium ES cell clone containing a FlipROSAbgeo genetrap vector inserted into the third intron of the *Zfp568* locus. The genetrap cassette in *Zfp568*$^{rGT\text{-}mutant}$ disrupted the *Zfp568* transcript and generated a truncated ZFP568 protein fused to βgeo (http://tikus.gsf.de/ggtc/). This truncated protein, which originated from splicing between the second exon of *Zfp568* and the splicing acceptor site in the genetrap cassette, contained only 11 N-terminal amino acids of ZFP568 and lacked all ZFP568 functional domains (KRAB domains and Zinc finger motifs). Complementation tests between *Zfp568*$^{rGT\text{-}mutant}$, *Zfp568*^{chato} and *Zfp568*^{null}, as well as RT-PCR experiments, all confirmed that *Zfp568*$^{rGT\text{-}mutant}$ genetrap insertion generates a null allele for *Zfp568*. The reversible capabilities of *Zfp568*$^{rGT\text{-}mutant}$ reside in the loxP and FRT recombination sites (red and green circles) flanking the FlipROSAßgeo genetrap cassette. These sites mediate the inversion of the genetrap cassette when Cre or FLP recombinases are present and release the effect of the genetrap cassette on *Zfp568*, therefore restoring wild type function to the *Zfp568* locus. **(B-D)** Complementation tests between *Zfp568rGT-restored* and *Zfp568null* alleles revealed that 7 out of 13 *Zfp568rGT-restored/null* embryos had a smooth yolk sac and wild type embryo morphology at E9.5 (C), whereas 6/13 embryos (D) had all the characteristic defects of *chato* mutants, including yolk sac ruffling. All other littermates were wild type in appearance (B). These results suggested that the inversion of the cassette did not fully restore wild type ZFP568 function and that *Zfp568rGT-restored* was likely a hypomorphic allele of *Zfp568*. Because the targeted insertion of vectors in intronic sequences has been previously reported to affect gene transcription (Meyers et al., 1998), we hypothesized that the presence of the genetrap allele in *Zfp568rGT-restored*, even in the wild type configuration, interferes with the normal splicing of the *Zfp568* transcript. **(E)** Quantification of the levels of splicing through the two exons flanking the genetrap insertion site using qRT-PCR on E9.5 embryonic tissues showed that *Zfp568rGT-restored/+* embryos have a 40% reduction in the levels of full length *Zfp568* transcript. *Zfp568rGT-restored/null* embryos only express 10% the level of full length transcript compared to wild type embryos. These results confirmed *Zfp568rGT-restored* is a hypomorphic allele of *Zfp568*. ***p=0.0007 compared to wt. Error bars represent s.d. SA, splice acceptor; pA, polyadenylation signal.

chato mutant cells migrate properly in explant assays

Since analysis of chimeric embryos showed that *Zfp568* is required in embryonic-derived tissues (including extraembryonic mesoderm), we sought to test whether extraembryonic defects in *chato* embryos are due to an inability of extraembryonic mesoderm cells to migrate properly. To this end, we compared the migratory ability of wild type and *chato* mutant cells side-by-side in yolk sac explant assays. Yolk sac tissues from GFP-labelled wild type embryos and *chato* mutants were individually trypsinized, then mixed. The resultant cell mixture was then plated onto Fibronectin-coated plates and the migratory behavior of wild type and *chato* mutant cells was evaluated through their ability to populate a scratch as previously described (materials and methods; Figure 2.14A). If the migratory ability of *chato* mutant cells were hindered, we anticipated that the wound would be preferentially populated by wild type (GFP+) cells. In our experiments, we observed that, at 16 hours after wounding, the scratch had completely healed and contained a similar number of wild type (GFP+) and *chato* mutant (GFP-) cells with mesenchymal morphology that were distributed evenly throughout the wounded area (Figure 2.14B-C, n=7 assays). We did not detect any abnormality in the morphology of *chato* mutant cells in our tests.

The lack of migratory defects in *chato* mutant explants contrasts with the extraembryonic and embryonic phenotypes we observed in *chato* mutants. As described previously, *chato* embryos contained clumps of extraembryonic mesoderm accumulated in the embryonic-extraembryonic boundary (Figure 2.6C-F) and extraembryonic mesoderm derivatives fail to properly rearrange to form the vascular plexus (Figure 2.6G-H). Additionally, *chato* mutants fail to undergo convergent extension (Garcia-Garcia et al., 2008). Since these phenotypes indicate that *chato*

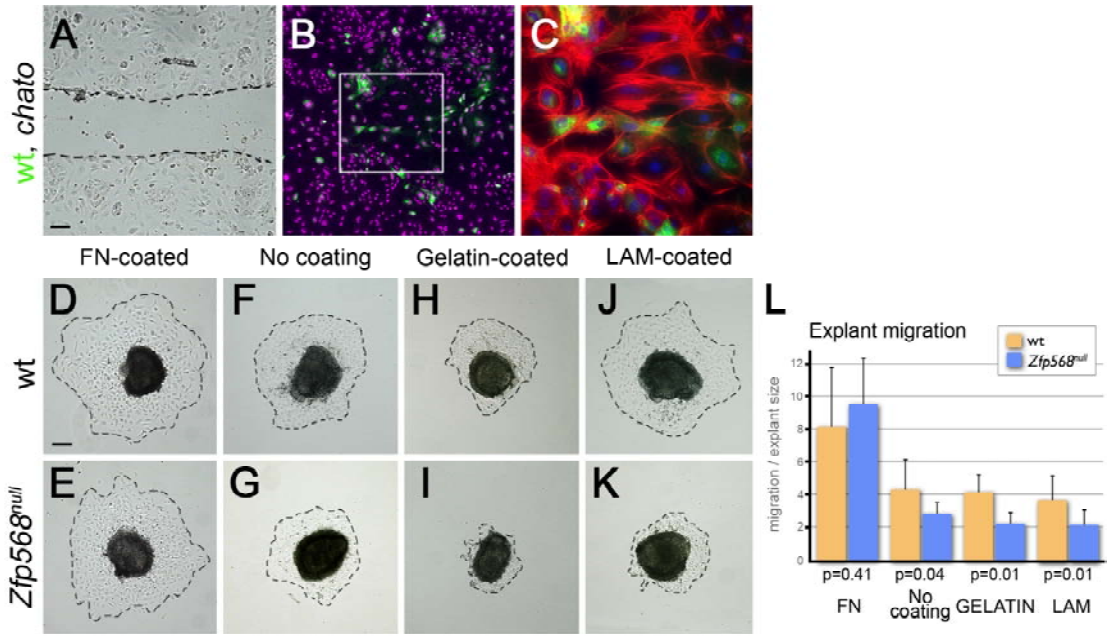

Figure 2.14. Yolk sac cell migration assays. (A) Bright field image of a scratch made 24 hours after plating a mix of GFP-positive wild type (green in B and C) and *chato* mutant cells from yolk sac explants onto Fibronectin-coated slides. **(B-C)** Phalloidin (red) and DAPI (purple/blue) staining on the same field of cells 16 hours later. C corresponds to the boxed region in B. **(D-K)** Yolk sacs from E7.5 wild type **(D, F, H, J)** and *Zfp568* mutant **(E, G, I, K)** embryos were cut into 2-4 fragments, plated (extraembryonic mesoderm face down) onto chambers coated with Fibronectin (D,E) not coated (F,G), coated with Gelatin (H,I) or Laminin (J,K) and imaged 16 hours afterwards. Images shown are representative examples of each category. For plots of all explants analyzed see Figure S8. **(L)** Quantification of explant migration shown as the area populated by migrating cells from the explant (traced by broken lines in D-K) relative to the size of the explant (dark area in D-K). Broken lines in A indicate edges of scratch. Broken lines in D-K indicate outer edge of migrating cells. Error bars in L represent s.d. between explants. Scale bars represent 100μm in A, D. Orange bars represent wt embryos, blue bars represent *Zfp568*^{null} embryos.

regulates cellular rearrangements, we reasoned that *Zfp568* might be required to influence the behavior and/or migration of mesenchymal cells in the context of the embryo. Cell migration depends on cues laid down in the extracellular environment, such as growth factors, adhesion molecules and chemotactic cues (Ridley et al., 2003). Hence, it is possible that in our explant assays, *chato* mutant cells migrated normally because these cues were provided by either the simultaneous presence of wild type cells or the cell culture conditions. To address this possibility, we tested the migratory ability of wild type and *chato* mutant yolk sac explants when grown separately and under different growth conditions.

We found that different cell culture substrates supported migration from wild type yolk sac explants, although migration was favored when slides were coated with FN (Figure 2.14D, F, H, J; orange bars in Figure 2.14L). Previous reports have described similar effects of different extracellular matrix components on cell culture behavior, with particular cell types showing distinct responses for a given protein substrate (Burdsal et al., 1993; Hashimoto et al., 1987; Tzu and Marinkovich, 2008). When plated on FN-coated slides, *chato* yolk sac explants migrated similar to wild type controls ($p=0.41$; Figure 2.14D-E, 2.14L, Figure 2.15). However, migration from *chato* yolk sacs was significantly reduced when plated on non-coated slides or onto slides coated with inactivated Collagen (gelatin) or Laminin (LAM) (Figure 2.14F-L, Figure 2.15). These results indicate that in the absence of FN, *chato* cells do not have the conditions appropriate for cell migration. These results support our previous observation that lack of ZFP568 does not impede cells from migrating in an appropriate environment and suggest that ZFP568 controls the production of specific secreted factors required for cell migration in the context of the embryo.

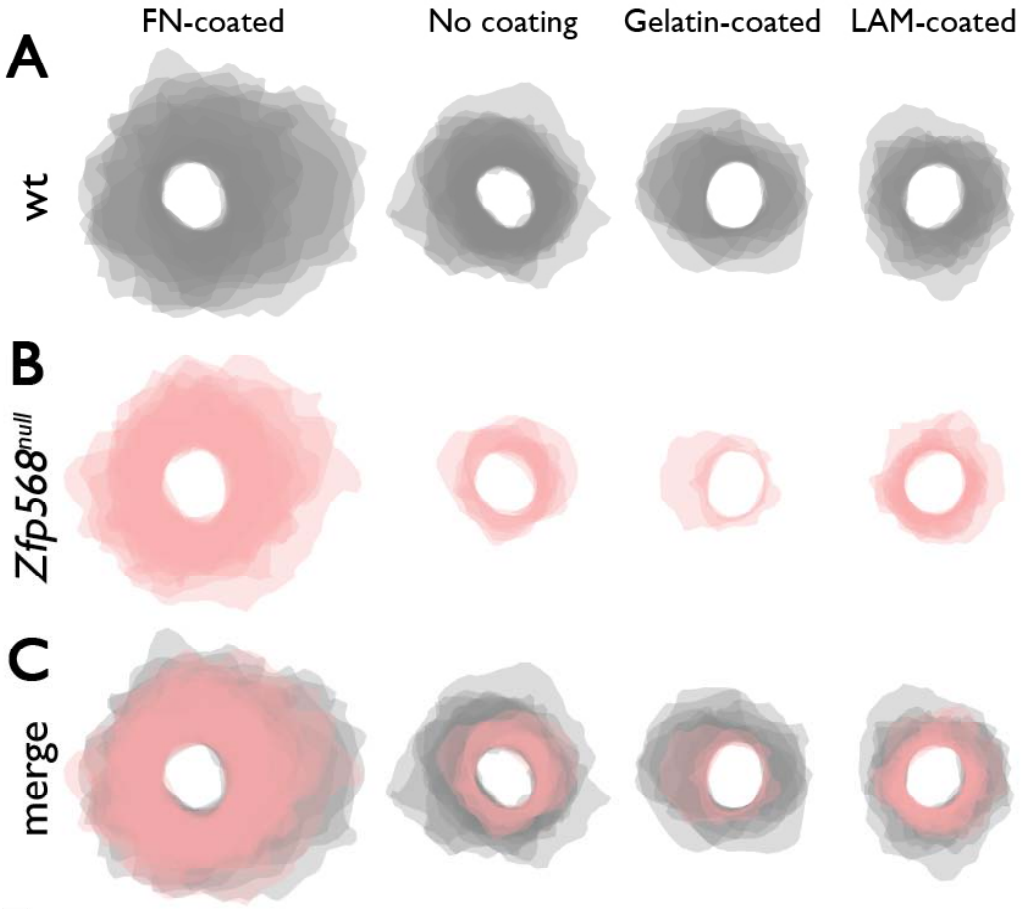

D

	FN			non-coating			gelatin			LAM		
	n	explant area (μm²)	migration area (μm²)	n	explant area (μm²)	migration area (μm²)	n	explant area (μm²)	migration area (μm²)	n	explant area (μm²)	migration area (μm²)
wt	12	69,904 ± 22,068	555,008 ± 270,337	18	117,902 ± 54,948	459,294 ± 165,572	9	73,830 ± 20,674	292,093 ± 73,879	10	87,737 ± 18,897	323,646 ± 135,824
chato	7	65,782 ± 24,335	611,228 ± 232,859	6	87,526 ± 40,059	246,294 ± 131,625	3	75,079 ± 11,407	158,972 ± 28,950	10	101,379 ± 30,818	234,617 ± 165,888

Figure 2.15. Migration assay using yolk sac explants. (A-C) Graphic representation of results from yolk sac explant assays plated onto Lab-Tek™ II (Nunc) slides coated with Fibronectin (FN), no coating, Gelatin, or Laminin (LAM). The regions containing migrating cells for each wt (A, grey) and *Zfp568* mutant (B, pink) explant were represented as shaded areas on different layers at 30% transparency, then scaled so that the size of the initial explant size (central white area) was constant across all explants. Darker areas represent regions most frequently populated by migrating cells. Overlays of wt and *Zfp568* mutant explants (C) highlight the reduced migration from mutant explants in the absence of Fibronectin-coating. **(D)** Table of average values ± standard deviation obtained in yolk sac explant assays. n = number of explants with migrating cells that were quantified. Explant area = area occupied by explant in μm^2. (B) Migration area = area occupied by cells migrating from the explant measured 16 hours after plating in μm^2.

chato disrupts signaling between VE and extraembryonic mesoderm

Within extraembryonic tissues, a number of molecules secreted to the extracellular environment are required for proper yolk sac morphogenesis. Amongst these, FN1 is known to be produced by extraembryonic mesoderm cells and promote both extraembryonic mesoderm development and VE survival and homeostasis (Bohnsack et al., 2004; Dickson et al., 1995; Goumans et al., 1999; Morikawa and Cserjesi, 2004). Since our explant assays indicated that FN-coating could restore migration from *chato* mutant explants (Figure 2.14L-M), we investigated whether FN1 was correctly expressed in *chato* embryos. We found that, in *chato* mutants, both FN1 and Laminin A1 (LAMA1) were localized at the basement membranes of extraembryonic and embryonic tissues similar to wild type littermates (Figure 2.4). However, the levels of FN1 in *chato* yolk sac extracts were 32.2% those of wild type controls as assayed by Western blotting (Figure 2.16A). Interestingly, the levels of LAMA1 were similar between *chato* and wild type samples (Figure 2.16B), indicating that *chato* specifically disrupts the production of some, but not all basement membrane components.

In addition to FN1, other secreted factors have been identified to play roles in yolk sac development. VEGF and IHH, are secreted by the VE and promote differentiation and morphogenesis of the vascular system in the adjacent extraembryonic mesoderm layer, where they are bound by receptors exclusively expressed in these cells (Bohnsack et al., 2004; Breier et al., 1992; Farrington et al., 1997; Yamaguchi et al., 1993). Other proteins promoting yolk sac morphogenesis signal within the extraembryonic mesoderm, as is the case of TGFβ1 (Dickson et al., 1995; Larsson et al., 2001; Oshima et al., 1996). To test whether expression of any of these factors or their receptors is regulated by ZFP568, we quantified their levels of

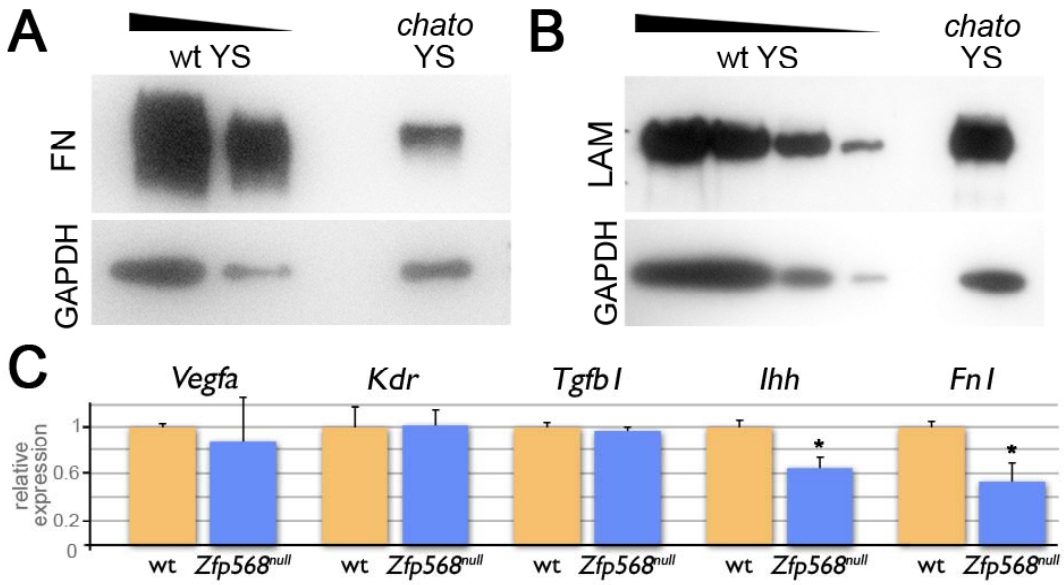

Figure 2.16. Yolk sac signaling is affected in *chato* mutants. (A-B) Western blots of yolk sac extracts from *chato* and littermate wild type embryos using anti-Fibronectin (A) and anti-Laminin (B) antibodies. GAPDH was used as a loading control. Fibronectin levels were reduced 32.2% (as quantified from 3 different experiments), while Laminin levels were comparable between wild type and *chato* mutant extracts (2 experiments) **(C)** Expression of *Vegfa, Kdr, Tgfb1, Ihh and Fn1* in *chato* (blue) yolk sacs relative to wt (orange) was assessed by qRT-PCR. Error bars represent s.d. between two independent pools of yolk sacs. * indicates $p<0.05$.

expression in yolk sac tissues of wild type and *Zfp568* mutant embryos using qRT-PCR. We found that expression of *Vegfa*, its receptor *Kdr,* and *Tgfβ1* were not significantly different between wild type and *Zfp568* mutant samples (Figure 2.16C). However, *Zfp568* yolk sac tissues had on average reduced levels of *Ihh* (64%) and *Fn1* transcripts (54%) as compared to wild type littermate controls (Figure 2.16C). The fact that only some of the factors we tested showed abnormal expression in *chato* mutants excludes the possibility that the *chato* mutation has a general effect on transcription and, hence, attests of the specificity of these results. Together with the experiments above, these results provide strong evidence that ZFP568 controls the production of specific secreted factors required to promote morphogenesis of extraembryonic tissues.

DISCUSSION

The characterization of *chato* extraembryonic defects demonstrates a role of the KRAB domain Zinc finger protein ZFP568 in the morphogenesis of both yolk sac and placental tissues. In the yolk sac, ZFP568 is required for extraembryonic mesoderm morphogenesis, vasculogenesis, allantois extension and proper organization of the VE layer. ZFP568 loss of function also affects the development of the placenta. In *chato* mutants the allantois fails to extend, disrupting choriallantoic attachment. Furthermore, loss of *Zfp568* causes expansion of chorionic ectoderm and failure of the ectoplacental cavity to collapse, a process required for proper labyrinth formation. Analysis of molecular markers failed to reveal abnormalities in the specification of extraembryonic lineages in *chato* mutants (Figures 2.1, 2.2, 2.6, 2.9). Therefore, our data supports that extraembryonic defects in *chato* embryos arise from abnormalities

in the morphogenetic processes that shape these tissues, rather than an imbalance in different extraembryonic cell types.

ZFP568 is expressed ubiquitously throughout embryonic and extraembryonic tissues (Garcia-Garcia et al., 2008). However, the analysis of *chato* chimeric embryos established that ZFP568 is required exclusively in embryonic-derived tissues for early embryo morphogenesis (Figures 2.11-2.12). Because extraembryonic mesoderm originates from embryonic lineages during gastrulation (Lu et al., 2001), it is likely that malformations in yolk sac and trophoblast tissues in *chato* mutants arise because of defects in the extraembryonic mesoderm. ZFP568 is also required in embryonic-derived tissues to control morphogenetic processes in the embryo, including convergent extension and axial rotation (Figure 2.11). Analysis of Cre-induced chimeras using a reversible *Zfp568* allele showed that restoring *Zfp568* function in the embryo and extraembryonic mesoderm, in some cases only rescues defects in yolk sac and trophoblast tissues, but not embryonic morphogenesis (Figure 2.12). These results support distinct requirements for *Zfp568* in extraembryonic mesoderm and embryonic cells to control morphogenesis of extraembryonic and embryonic tissues, respectively. Together with observations that the severity of embryonic defects do not correlate with that of the extraembryonic malformations, these results support independent roles of ZFP568 in the morphogenesis of embryonic and extraembryonic tissues.

chato affects the secretion of extracellular cues required for proper morphogenesis of extraembryonic tissues

chato mutants have strong defects in extraembryonic mesoderm-derived structures such as the primitive vascular plexus and the allantois (Figure 2.6). Results from the analysis of chimeric embryos support that vasculogenesis and allantoic malformations

in *chato* mutants primarily arise from defects in the extraembryonic mesoderm. Explant assays designed to test the migratory ability of extraembryonic mesoderm cells in *chato* mutants indicate that loss of *Zfp568* does not disrupt the cell machinery required for cell migration (e.g. the cytoskeleton). However, we found that the expression of key molecules required for extraembryonic mesoderm and yolk sac morphogenesis is reduced in *chato* embryos (Figure 2.16). Fibronectins are well known for their roles in cell adhesion and migration (Glukhova and Thiery, 1993). Specifically, absence of *Fn1* in mouse embryos leads to severe vasculogenesis defects and a separation of the VE from the extraembryonic mesoderm (George et al., 1997). Therefore, the reduced levels of FN1 in *chato* embryos (Figure 2.16C) might be partially responsible for the abnormal vascular plexus, extraembryonic mesoderm migration and VE adhesion defects in *chato* mutants. Noteworthy, *chato* mutant cells migrate properly when explanted onto FN-coated slides, but their migration is reduced when FN is not provided exogenously (Figure 2.14, Figure 2.15).

qRT-PCR experiments also revealed downregulation of *Ihh* levels in *chato* mutants (Figure 2.16C). *Ihh* is required to sustain yolk sac vasculogenesis (Byrd et al., 2002; Dyer et al., 2001). Hence, lower levels of *Ihh* expression in *chato* embryos may also contribute to the vascular plexus abnormalities in *chato* mutants. Interestingly, *Ihh* is secreted by VE cells (Becker et al., 1997). Since *chato* is required in embryonic-derived tissues, *Ihh* downregulation in *chato* embryos suggests that loss of ZFP568 in the extraembryonic mesoderm indirectly causes malfunctions in the adjacent VE layer. Signaling between the VE and extraembryonic mesoderm is known to be required for proper yolk sac morphogenesis and a number of molecules, including FN1, have been described to mediate these reciprocal interactions (Bohnsack et al., 2004). Therefore, we propose that ZFP568 functions in embryonic-derived tissues to produce factors that signal to adjacent tissues and generate an environment appropriate for extraembryonic

mesoderm migration and yolk sac morphogenesis. Comparision of the *chato* phenotype with that of mutants in *Fn1* (George et al., 1997) and *Ihh* (Byrd et al., 2002; Dyer et al., 2001) suggests that the complexity of extraembryonic defects in *chato* embryos is unlikely due to the downregulation of just these factors. We presume that expression of additional molecules required for extraembryonic mesoderm migration and yolk sac morphogenesis might be compromised in *chato* mutants.

chato disrupts morphogenesis of the yolk sac and placenta

chato embryos show severe malformations in non-embryonic-derived tissues, including the yolk sac VE and the chorionic ectoderm. Since *chato* tetraploid chimeras recapitulate the VE ruffling and chorion abnormalities of *chato* mutants, it is likely that these phenotypes are caused by extraembryonic mesoderm defects. It is possible that downregulation of *Fn1*, *Ihh* and/or additional factors in *chato* mutants affects morphogenesis of the VE and chorion. Another possibility is that abnormal morphogenesis of extraembryonic mesoderm in *chato* mutants physically restricts the development of the adjacent VE and TE lineages. Defective genesis (from the primitive streak), migration and/or proliferation of extraembryonic mesoderm might affect the distribution and/or number of cells lining the exocoelomic cavity, which could impair the ability of the VE to extend and in turn cause loss of adhesiveness between these two adjacent layers, originating yolk sac ruffling such as that observed in *chato* embryos.

chato defects in extraembryonic mesoderm also prevent placental morphogenesis. Mouse mutants in which chorioallantoic fusion is blocked retain a flat chorion and display disrupted labyrinth formation (Gurtner et al., 1995; Hunter et al., 1999; Kwee et al., 1995; Yang et al., 1995). Therefore, failure of the allantois to

extend and reach the chorion likely prevents labyrinth formation in *chato* mutants (Figure 2.7F). Additionally, defects in extraembryonic mesoderm migration in *chato* embryos prevent the rising of the chorion and closure of the ectoplacental cavity, processes required for labyrinth formation. Rising of the chorion and closure of the ectoplacental cavity have been described to influence proliferation within the chorionic ectoderm (Uy et al., 2002). Therefore, we hypothesize that delayed or impaired rising of the chorion in *chato* mutants could lead to a subtle increase in chorionic ectoderm proliferation undetectable by phospho-histone H3 analysis, but sustained over time during development. This sustained proliferation could originate the chorionic phenotypes we observed in class II and class III *chato* embryos.

While these observations support that extraembryonic mesoderm defects in *chato* embryos impose a physical constraint in other extraembryonic tissues, mutants that affect extraembryonic mesoderm morphogenesis, such as *T* or *Bmp4* have not been described to cause such severe defects in extraembryonic tissues as *chato* embryos (Rashbass et al., 1991; Winnier et al., 1995). Therefore, we favor the hypothesis that extraembryonic mesoderm in *chato* mutants both fails to secrete factors that promote morphogenesis and exerts a physical constraint on adjacent tissues.

ZFP568 has overlapping and divergent roles with factors previously described to regulate morphogenesis of extraembryonic tissues

A number of mutants have been identified that affect morphogenesis of extraembryonic tissues. However, *chato* mutants present a unique combination of extraembryonic malformations. As previously indicated, mouse mutants that affect extraembryonic mesoderm morphogenesis (Rashbass et al., 1991; Winnier et al.,

1995), allantoic extension (Chawengsaksophak et al., 2004; Lechleider et al., 2001) or chorioallantoic attachment (Mahlapuu et al., 2001; Solloway and Robertson, 1999; Xu et al., 1998), have not been described to cause chorion expansion, failure to close the ectoplacental cavity or as severe yolk sac ruffling as we have observed in *chato* embryos. Amongst other mutants known to disrupt placental morphogenesis (Inman and Downs, 2007; Rossant and Cross, 2001; Watson and Cross, 2005), only mutants in the transcription factors *Hand1* (Firulli et al., 1998; Riley et al., 1998; Scott et al., 1999) and *Erf* (Papadaki et al., 2007) resembled some of the characteristic features of *chato* mutants.

Similar to *chato* embryos, *Hand1* mutants have yolk sac ruffling and vasculogenesis defects, but *Hand1* embryos have an imbalance in the differentiation of TE-derived lineages that causes a reduction in *Pl1*-positive trophoblast giant cells with a concomitant expansion of the spongiotrophoblast population expressing *Acsl2* (Riley et al., 1998), a phenotype that we have not observed in *chato* embryos (Figure 2.9). Mutants in the ets transcriptional repressor *Erf* also show defects remarkably similar to *chato*, including abnormal vasculogenesis, defective chorioallantoic attachment, failure to close the ectoplacental cavity and an expanded chorion layer (Papadaki et al., 2007). However, *Erf* mutants do not show yolk sac ruffles and, unlike *chato* embryos, loss of *Erf* affects the differentiation of trophoblast stem cells causing a reduction in the number of cells expressing *Tpbpa* and lack of *Gcm1* expression in the chorion at E8.5 (Papadaki et al., 2007). The phenotypic similarities and differences of *chato* embryos with *Hand1* and *Erf* mutants suggest overlapping, as well as divergent roles for these factors on the morphogenesis of extraembryonic tissues. Future studies will help clarify how ZFP568, HAND1 and ERF coordinately and separately control development of the yolk sac and placenta.

CONCLUSIONS

The biological processes controlled by KRAB Zinc finger proteins have been elusive, mostly due to the lack of mouse models disrupting individual KRAB-domain family members. The study of *chato* mutants described here identifies a role of *Zfp568* in the morphogenesis of extraembryonic tissues and defines a primary requirement for *Zfp568* in the extraembryonic mesoderm. Our data supports a requirement for ZFP568 in the production of factors important for cell migration and tissue morphogenesis. The differences between the phenotype of *chato* embryos with that of mouse mutants previously described to affect yolk sac and placenta development suggest that *Zfp568* controls extraembryonic development through distinct molecular mechanisms. Future systems biology approaches will be able to identify the precise targets of ZFP568 ultimately responsible for the morphogenesis of extraembryonic tissues.

ACKNOWLEDGEMENTS

We thank Kathryn Anderson, Joaquim Culi, Juan Modolell, Mark Roberson, John Schimenti, Sol Sotillos, members of the laboratory and anonymous reviewers for helpful discussions and comments on the manuscript; Drs. Ruth Arkell, Kathleen McGrath, Deborah Chapman, James Cross, Kat Hadjantonakis, Janet Rossant and Leif Lundh for mice and reagents; Ke-Yu Deng, personnel at Cornell's Center for Materials Research and CARE for technical help. The conditional genetrap *Zfp568* allele was obtained from the German Gene Trap Consortium (GGTC). This work was supported by Basil O'Connor Starter Scholar Research Award #5-FY06-589 from the March of Dimes Foundation and by NIH grant HD060581.

REFERENCES

Argraves, W. S. and Drake, C. J. (2005). Genes critical to vasculogenesis as defined by systematic analysis of vascular defects in knockout mice. *Anat Rec A Discov Mol Cell Evol Biol* **286**, 875-84.

Baldwin, H. S., Shen, H. M., Yan, H. C., DeLisser, H. M., Chung, A., Mickanin, C., Trask, T., Kirschbaum, N. E., Newman, P. J., Albelda, S. M. et al. (1994). Platelet endothelial cell adhesion molecule-1 (PECAM-1/CD31): alternatively spliced, functionally distinct isoforms expressed during mammalian cardiovascular development. *Development* **120**, 2539-53.

Baron, M. H. (2003). Embryonic origins of mammalian hematopoiesis. *Exp Hematol* **31**, 1160-9.

Barron, M., McAllister, D., Smith, S. M. and Lough, J. (1998). Expression of retinol binding protein and transthyretin during early embryogenesis. *Dev Dyn* **212**, 413-22.

Bartholin, L., Melhuish, T. A., Powers, S. E., Goddard-Leon, S., Treilleux, I., Sutherland, A. E. and Wotton, D. (2008). Maternal Tgif is required for vascularization of the embryonic placenta. *Dev Biol* **319**, 285-97.

Basyuk, E., Cross, J. C., Corbin, J., Nakayama, H., Hunter, P., Nait-Oumesmar, B. and Lazzarini, R. A. (1999). Murine Gcm1 gene is expressed in a subset of placental trophoblast cells. *Dev Dyn* **214**, 303-11.

Becker, S., Wang, Z. J., Massey, H., Arauz, A., Labosky, P., Hammerschmidt, M., St-Jacques, B., Bumcrot, D., McMahon, A. and Grabel, L. (1997). A role for Indian hedgehog in extraembryonic endoderm differentiation in F9 cells and the early mouse embryo. *Dev Biol* **187**, 298-310.

Bohnsack, B. L., Lai, L., Dolle, P. and Hirschi, K. K. (2004). Signaling hierarchy downstream of retinoic acid that independently regulates vascular remodeling and endothelial cell proliferation. *Genes Dev* **18**, 1345-58.

Breier, G., Albrecht, U., Sterrer, S. and Risau, W. (1992). Expression of vascular endothelial growth factor during embryonic angiogenesis and endothelial cell differentiation. *Development* **114**, 521-32.

Burdsal, C. A., Damsky, C. H. and Pedersen, R. A. (1993). The role of E-cadherin and integrins in mesoderm differentiation and migration at the mammalian primitive streak. *Development* **118**, 829-44.

Byrd, N., Becker, S., Maye, P., Narasimhaiah, R., St-Jacques, B., Zhang, X., McMahon, J., McMahon, A. and Grabel, L. (2002). Hedgehog is required for murine yolk sac angiogenesis. *Development* **129**, 361-72.

Chapman, D. L., Garvey, N., Hancock, S., Alexiou, M., Agulnik, S. I., Gibson-Brown, J. J., Cebra-Thomas, J., Bollag, R. J., Silver, L. M. and Papaioannou, V. E. (1996). Expression of the T-box family genes, Tbx1-Tbx5, during early mouse development. *Dev Dyn* **206**, 379-90.

Chawengsaksophak, K., de Graaff, W., Rossant, J., Deschamps, J. and Beck, F. (2004). Cdx2 is essential for axial elongation in mouse development. *Proc Natl Acad Sci U S A* **101**, 7641-5.

Coffinier, C., Thepot, D., Babinet, C., Yaniv, M. and Barra, J. (1999). Essential role for the homeoprotein vHNF1/HNF1beta in visceral endoderm differentiation. *Development* **126**, 4785-94.

Cross, J. C. (2000). Genetic insights into trophoblast differentiation and placental morphogenesis. *Semin Cell Dev Biol* **11**, 105-13.

Damert, A., Miquerol, L., Gertsenstein, M., Risau, W. and Nagy, A. (2002). Insufficient VEGFA activity in yolk sac endoderm compromises haematopoietic and endothelial differentiation. *Development* **129**, 1881-92.

Dickson, M. C., Martin, J. S., Cousins, F. M., Kulkarni, A. B., Karlsson, S. and Akhurst, R. J. (1995). Defective haematopoiesis and vasculogenesis in transforming growth factor-beta 1 knock out mice. *Development* **121**, 1845-54.

Downs, K. M., Hellman, E. R., McHugh, J., Barrickman, K. and Inman, K. E. (2004). Investigation into a role for the primitive streak in development of the murine allantois. *Development* **131**, 37-55.

Dyer, M. A., Farrington, S. M., Mohn, D., Munday, J. R. and Baron, M. H. (2001). Indian hedgehog activates hematopoiesis and vasculogenesis and can respecify prospective neurectodermal cell fate in the mouse embryo. *Development* **128**, 1717-30.

Dziadek, M. A. and Andrews, G. K. (1983). Tissue specificity of alpha-fetoprotein messenger RNA expression during mouse embryogenesis. *EMBO J* **2**, 549-54.

El-Hashash, A. H., Warburton, D. and Kimber, S. J. (2010). Genes and signals regulating murine trophoblast cell development. *Mech Dev* **127**, 1-20.

Farrington, S. M., Belaoussoff, M. and Baron, M. H. (1997). Winged-helix, Hedgehog and Bmp genes are differentially expressed in distinct cell layers of the murine yolk sac. *Mech Dev* **62**, 197-211.

Ferkowicz, M. J. and Yoder, M. C. (2005). Blood island formation: longstanding observations and modern interpretations. *Exp Hematol* **33**, 1041-7.

Firulli, A. B., McFadden, D. G., Lin, Q., Srivastava, D. and Olson, E. N. (1998). Heart and extra-embryonic mesodermal defects in mouse embryos lacking the bHLH transcription factor Hand1. *Nat Genet* **18**, 266-70.

Flamme, I. and Risau, W. (1992). Induction of vasculogenesis and hematopoiesis in vitro. *Development* **116**, 435-9.

Fraser, S. T. and Baron, M. H. (2009). Embryonic fates for extraembryonic lineages: New perspectives. *J Cell Biochem* **107**, 586-91.

Friedrich, G. and Soriano, P. (1991). Promoter traps in embryonic stem cells: a genetic screen to identify and mutate developmental genes in mice. *Genes Dev* **5**, 1513-23.

Garcia-Garcia, M. J. and Anderson, K. V. (2003). Essential role of glycosaminoglycans in Fgf signaling during mouse gastrulation. *Cell* **114**, 727-37.

Garcia-Garcia, M. J., Shibata, M. and Anderson, K. V. (2008). Chato, a KRAB zinc-finger protein, regulates convergent extension in the mouse embryo. *Development* **135**, 3053-62.

George, E. L., Baldwin, H. S. and Hynes, R. O. (1997). Fibronectins are essential for heart and blood vessel morphogenesis but are dispensable for initial specification of precursor cells. *Blood* **90**, 3073-81.

Gladdy, R. A., Nutter, L. M., Kunath, T., Danska, J. S. and Guidos, C. J. (2006). p53-Independent apoptosis disrupts early organogenesis in embryos lacking both ataxia-telangiectasia mutated and Prkdc. *Mol Cancer Res* **4**, 311-8.

Glukhova, M. A. and Thiery, J. P. (1993). Fibronectin and integrins in development. *Semin Cancer Biol* **4**, 241-9.

Goh, K. L., Yang, J. T. and Hynes, R. O. (1997). Mesodermal defects and cranial neural crest apoptosis in alpha5 integrin-null embryos. *Development* **124**, 4309-19.

Goumans, M. J., Zwijsen, A., van Rooijen, M. A., Huylebroeck, D., Roelen, B. A. and Mummery, C. L. (1999). Transforming growth factor-beta signalling in extraembryonic mesoderm is required for yolk sac vasculogenesis in mice. *Development* **126**, 3473-83.

Guillemot, F., Nagy, A., Auerbach, A., Rossant, J. and Joyner, A. L. (1994). Essential role of Mash-2 in extraembryonic development. *Nature* **371**, 333-6.

Gurtner, G. C., Davis, V., Li, H., McCoy, M. J., Sharpe, A. and Cybulsky, M. I. (1995). Targeted disruption of the murine VCAM1 gene: essential role of VCAM-1 in chorioallantoic fusion and placentation. *Genes Dev* **9**, 1-14.

Hashimoto, K., Fujimoto, H. and Nakatsuji, N. (1987). An ECM substratum allows mouse mesodermal cells isolated from the primitive streak to exhibit motility similar to that inside the embryo and reveals a deficiency in the T/T mutant cells. *Development* **100**, 587-98.

Hayashi, S., Lewis, P., Pevny, L. and McMahon, A. P. (2002). Efficient gene modulation in mouse epiblast using a Sox2Cre transgenic mouse strain. *Mech Dev* **119 Suppl 1**, S97-S101.

Hu, D. and Cross, J. C. (2010). Development and function of trophoblast giant cells in the rodent placenta. *Int J Dev Biol* **54**, 341-54.

Hunter, P. J., Swanson, B. J., Haendel, M. A., Lyons, G. E. and Cross, J. C. (1999). Mrj encodes a DnaJ-related co-chaperone that is essential for murine placental development. *Development* **126**, 1247-58.

Inman, K. E. and Downs, K. M. (2006). Brachyury is required for elongation and vasculogenesis in the murine allantois. *Development* **133**, 2947-59.

Inman, K. E. and Downs, K. M. (2007). The murine allantois: emerging paradigms in development of the mammalian umbilical cord and its relation to the fetus. *Genesis* **45**, 237-58.

Jollie, W. P. (1990). Development, morphology, and function of the yolk-sac placenta of laboratory rodents. *Teratology* **41**, 361-81.

Kwee, L., Baldwin, H. S., Shen, H. M., Stewart, C. L., Buck, C., Buck, C. A. and Labow, M. A. (1995). Defective development of the embryonic and extraembryonic circulatory systems in vascular cell adhesion molecule (VCAM-1) deficient mice. *Development* **121**, 489-503.

Larsson, J., Goumans, M. J., Sjostrand, L. J., van Rooijen, M. A., Ward, D., Leveen, P., Xu, X., ten Dijke, P., Mummery, C. L. and Karlsson, S. (2001). Abnormal angiogenesis but intact hematopoietic potential in TGF-beta type I receptor-deficient mice. *EMBO J* **20**, 1663-73.

Lechleider, R. J., Ryan, J. L., Garrett, L., Eng, C., Deng, C., Wynshaw-Boris, A. and Roberts, A. B. (2001). Targeted mutagenesis of Smad1 reveals an essential role in chorioallantoic fusion. *Dev Biol* **240**, 157-67.

Lescisin, K. R., Varmuza, S. and Rossant, J. (1988). Isolation and characterization of a novel trophoblast-specific cDNA in the mouse. *Genes Dev* **2**, 1639-46.

Linzer, D. I. and Fisher, S. J. (1999). The placenta and the prolactin family of hormones: regulation of the physiology of pregnancy. *Mol Endocrinol* **13**, 837-40.

Livak, K. J. and Schmittgen, T. D. (2001). Analysis of relative gene expression data using real-time quantitative PCR and the 2(-Delta Delta C(T)) Method. *Methods* **25**, 402-8.

Lu, C. C., Brennan, J. and Robertson, E. J. (2001). From fertilization to gastrulation: axis formation in the mouse embryo. *Curr Opin Genet Dev* **11**, 384-92.

Luo, J., Sladek, R., Bader, J. A., Matthyssen, A., Rossant, J. and Giguere, V. (1997). Placental abnormalities in mouse embryos lacking the orphan nuclear receptor ERR-beta. *Nature* **388**, 778-82.

Mahlapuu, M., Ormestad, M., Enerback, S. and Carlsson, P. (2001). The forkhead transcription factor Foxf1 is required for differentiation of extra-embryonic and lateral plate mesoderm. *Development* **128**, 155-66.

McGrath, K. E., Koniski, A. D., Malik, J. and Palis, J. (2003). Circulation is established in a stepwise pattern in the mammalian embryo. *Blood* **101**, 1669-76.

Meyers, E. N., Lewandoski, M. and Martin, G. R. (1998). An Fgf8 mutant allelic series generated by Cre- and Flp-mediated recombination. *Nat Genet* **18**, 136-41.

Morikawa, Y. and Cserjesi, P. (2004). Extra-embryonic vasculature development is regulated by the transcription factor HAND1. *Development* **131**, 2195-204.

Nagy, A. (2003). Manipulating the mouse embryo : a laboratory manual. Cold Spring Harbor, N.Y.: Cold Spring Harbor Laboratory Press.

Oshima, M., Oshima, H. and Taketo, M. M. (1996). TGF-beta receptor type II deficiency results in defects of yolk sac hematopoiesis and vasculogenesis. *Dev Biol* **179**, 297-302.

Papadaki, C., Alexiou, M., Cecena, G., Verykokakis, M., Bilitou, A., Cross, J. C., Oshima, R. G. and Mavrothalassitis, G. (2007). Transcriptional repressor erf determines extraembryonic ectoderm differentiation. *Mol Cell Biol* **27**, 5201-13.

Rashbass, P., Cooke, L. A., Herrmann, B. G. and Beddington, R. S. (1991). A cell autonomous function of Brachyury in T/T embryonic stem cell chimaeras. *Nature* **353**, 348-51.

Rhee, J. M., Pirity, M. K., Lackan, C. S., Long, J. Z., Kondoh, G., Takeda, J. and Hadjantonakis, A. K. (2006). In vivo imaging and differential localization of lipid-modified GFP-variant fusions in embryonic stem cells and mice. *Genesis* **44**, 202-18.

Ridley, A. J., Schwartz, M. A., Burridge, K., Firtel, R. A., Ginsberg, M. H., Borisy, G., Parsons, J. T. and Horwitz, A. R. (2003). Cell migration: integrating signals from front to back. *Science* **302**, 1704-9.

Riley, P., Anson-Cartwright, L. and Cross, J. C. (1998). The Hand1 bHLH transcription factor is essential for placentation and cardiac morphogenesis. *Nat Genet* **18**, 271-5.

Rossant, J. and Cross, J. C. (2001). Placental development: lessons from mouse mutants. *Nat Rev Genet* **2**, 538-48.

Rossant, J. and Tam, P. P. (2009). Blastocyst lineage formation, early embryonic asymmetries and axis patterning in the mouse. *Development* **136**, 701-13.

Rossant, J. and Tam, P. P. L. (2002). Mouse development : patterning, morphogenesis, and organogenesis. San Diego, Calif. London: Academic.

Scott, I. C., Anson-Cartwright, L., Riley, P., Reda, D. and Cross, J. C. (1999). The HAND1 basic helix-loop-helix transcription factor regulates trophoblast differentiation via multiple mechanisms. *Mol. Cell. Biol.* **20**, 530-41.

Solloway, M. J. and Robertson, E. J. (1999). Early embryonic lethality in Bmp5;Bmp7 double mutant mice suggests functional redundancy within the 60A subgroup. *Development* **126**, 1753-68.

Schnütgen, F., De-Zolt, S., Sloun, P. V., Hollatz, M., Floss, T., Hansen, J., Altschmied, J., Seisenberger, C., Ghyselinck, N. B., Ruiz, P., et al. (2005). Genomewide production of multipurpose alleles for the functional analysis of the mouse genome. *Proc Natl Acad Sci USA*, **102**, 7221–6.

Tallquist, M. D. and Soriano, P. (2000). Epiblast-restricted Cre expression in MORE mice: a tool to distinguish embryonic vs. extra-embryonic gene function. *Genesis* **26**, 113-5.

Tian, Y., Lei, L., Cammarano, M., Nekrasova, T. and Minden, A. (2009). Essential role for the Pak4 protein kinase in extraembryonic tissue development and vessel formation. *Mech Dev* **126**, 710-20.

Tremblay, K. D., Dunn, N. R. and Robertson, E. J. (2001). Mouse embryos lacking Smad1 signals display defects in extra-embryonic tissues and germ cell formation. *Development* **128**, 3609-21.

Tzu, J. and Marinkovich, M. P. (2008). Bridging structure with function: structural, regulatory, and developmental role of laminins. *Int J Biochem Cell Biol* **40**, 199-214.

Urrutia, R. (2003). KRAB-containing zinc-finger repressor proteins. *Genome Biol* **4**, 231.

Uy, G. D., Downs, K. M. and Gardner, R. L. (2002). Inhibition of trophoblast stem cell potential in chorionic ectoderm coincides with occlusion of the ectoplacental cavity in the mouse. *Development* **129**, 3913-24.

Watson, E. D. and Cross, J. C. (2005). Development of structures and transport functions in the mouse placenta. *Physiology (Bethesda)* **20**, 180-93.

Welsh, I. C. and O'Brien, T. P. (2000). Loss of late primitive streak mesoderm and interruption of left-right morphogenesis in the Ednrb(s-1Acrg) mutant mouse. *Dev Biol* **225**, 151-68.

Winnier, G., Blessing, M., Labosky, P. A. and Hogan, B. L. (1995). Bone morphogenetic protein-4 is required for mesoderm formation and patterning in the mouse. *Genes Dev* **9**, 2105-16.

Xu, X., Weinstein, M., Li, C., Naski, M., Cohen, R. I., Ornitz, D. M., Leder, P. and Deng, C. (1998). Fibroblast growth factor receptor 2 (FGFR2)-mediated reciprocal regulation loop between FGF8 and FGF10 is essential for limb induction. *Development* **125**, 753-65.

Yamaguchi, T. P., Dumont, D. J., Conlon, R. A., Breitman, M. L. and Rossant, J. (1993). flk-1, an flt-related receptor tyrosine kinase is an early marker for endothelial cell precursors. *Development* **118**, 489-98.

Yang, J. T., Rayburn, H. and Hynes, R. O. (1995). Cell adhesion events mediated by alpha 4 integrins are essential in placental and cardiac development. *Development* **121**, 549-60.

CHAPTER 3

A TRIM28 HYPOMORPHIC ALLELE REVEALS DIFFERENTIAL REQUIREMENTS OF KRAB ZINC FINGER PROTEINS DURING MOUSE EMBRYONIC DEVELOPMENT[1]

[1] Reference Shibata and Garcia-Garcia (2010) of this chapter is also Chapter 2.

ABSTRACT

Mammalian genomes contain over 300 Zinc finger family members with Kruppel-associated box (KRAB) domains. It has been proposed that functions of KRAB zinc finger proteins are mediated by TRIM28, a universal corepressor protein that recruits chromatin modifying enzymes. However, the roles of TRIM28 during early mouse embryogenesis are not completely understood. Here I show that *chatwo*, a recessive ENU-induced mutation in the mouse, creates a hypomorphic allele for *Trim28. chatwo* mutants arrest prior to embryonic day 8.5 and display strong morphogenetic defects in both embryonic and extraembryonic tissues, including defective convergent extension and yolk sac ruffling. The phenotype of *chatwo* mutants is similar to that of mouse mutants in the KRAB zinc finger protein ZFP568. Results from genetic interaction studies, and analysis of *Trim28* mosaic embryos suggest that TRIM28 is required as a cofactor of ZFP568 in embryonic tissues to regulate embryo morphogenesis. Additionally, my results provide insight into ZFP568-independent functions for TRIM28 in extraembryonic tissues during early embryonic development.

INTRODUCTION

The Kruppel-associated box (KRAB) zinc finger proteins are a large family of transcriptional repressors found only in tetrapod vertebrates (Urrutia, 2003). This family has undergone a recent expansion, with mouse and human genomes containing over 250 or 300 KRAB zinc finger proteins, respectively (Emerson and Thomas, 2009; Rowe et al., 2010). Recent findings have revealed diverse functions for a handful of individual mouse KRAB zinc finger family members, including the control of sex-dependant gene expression in the liver, regulation of DNA methylation at imprinted loci, and silencing of retroviral DNA sequences in ES cells (Krebs et al., 2003; Li et al., 2008; Wolf and Goff, 2009). The functions of specific KRAB domain

proteins in embryogenesis is still very limited. However, over 250 KRAB zinc finger proteins are expressed in mouse ES cells (Rowe et al., 2010), suggesting that KRAB domain proteins are likely to regulate early embryonic development.

It has been proposed that KRAB zinc finger proteins recognize and bind to specific DNA sequences through their C_2H_2 zinc finger domains, and recruit a transcriptional repressor complex via their KRAB domains to modify chromatin structure (Urrutia, 2003). On the basis of its ability to bind to KRAB domains and mediate transcriptional repression, TRIM28 (also known as TIF1b, KAP1 or KRIP1) has been described as a universal co-repressor for all KRAB domain proteins (Cammas et al., 2000). TRIM28 is a nuclear scaffolding protein containing a N-terminal RBCC (RING finger, B box, coiled coil) domain, a HP1 binding domain, and C-terminal PHD finger and bromodomains. The N-terminal RBCC domains of TRIM28 binds to KRAB domains, whereas the remainder of the protein recruits chromatin-modifying enzymes including Heterochromatin protein 1, histone deacetylases and histone methytransferases (Urrutia, 2003).

Studies of *Trim28* null (*Trim28*$^{-/-}$) embryos have provided evidence for functions of TRIM28 during early postimplantation embryonic development. In *Trim28*$^{-/-}$ mutants, blastocyst formation and implantation at embryonic day (E) 4.5 occur normally, however embryos arrest at approximately E5.5 and fail to gastrulate and form mesoderm (Cammas et al., 2000). *Trim28*$^{-/-}$ embryos also display defects in visceral endoderm (VE) and trophoblast cells, extraembryonic cell types important for supporting embryonic growth and development in utero (Cammas et al., 2000; Tam and Loebel, 2007). As *Trim28* is expressed in multiple cell types throughout development (Cammas et al., 2000), it is unclear whether TRIM28 is required in embryonic tissues, extraembryonic tissues, or both, and tissue specific requirements of TRIM28 during embryonic development have not been studied. Furthermore, the early

lethality of TRIM28 mutants has prevented analysis of functions of TRIM28 during timepoints in embryonic development after E5.5.

Only one KRAB zinc finger protein, ZFP568, has been identified to disrupt embryonic development during mouse gastrulation (Garcia-Garcia et al., 2008). Null mutants for *Zfp568* display morphogenetic defects including mediolateral expansion of somites, neural tube defects and severe abnormalities in yolk sac and placental development (Garcia-Garcia et al., 2008; Shibata and Garcia-Garcia, 2010). The analysis of ZFP568 chimeric embryos created through tetraploid complementation assays have revealed a requirement for ZFP568 in embryonic and embryonic-derived extraembryonic mesoderm cells (Shibata and Garcia-Garcia, 2010). However, it was unknown whether ZFP568 function in these cell types occurred through a TRIM28 mediated complex.

The results presented here show that *chatwo,* an ENU-induced mutation that causes a similar phenotype to *Zfp568* mutants, creates a hypomorphic *Trim28* allele. Characterization of $Trim28^{chatwo}$ mutant phenotypes has revealed requirements of TRIM28 for embryonic and yolk sac morphogenesis. Analysis of TRIM28 tissue specific requirements indicate that *Trim28* is required in both embryonic and extraembryonic cell types. The similarities between the *Zfp568* mutants and *chatwo* suggest that the genes affected by both mutations disrupt the same developmental processes and provide evidence that the ZFP568-TRIM28 interaction is significant for embryonic morphogenesis.

MATERIALS AND METHODS

Mouse strains

chatwo mutants were characterized on FVB and C57BL/6 genetic backgrounds. Genotyping was conducted using polymorphisms between C57BL6/J and FVB strains

using D7Mit178 and D7Mit76 markers. *Sox2Cre* mice were obtained from Jackson Laboratory (Hayashi et al., 2002). *Trim28* knockout and conditional mice were a generous gift from Dr. Florence Cammas (Cammas et al., 2000).

Positional cloning of *chatwo*

The *chatwo* mutation was created on a C57BL6/J genetic background, and outcrossed to FVB as described (Liem et al., 2009). Using a whole genome SNP panel, the *chatwo* mutation was mapped to a 20Mb region on proximal Chromosome 7 (Moran et al., 2006). Further mapping of meiotic recombinants was used to narrow the interval to a 120kb region containing 10 genes, between rs31712695 and rs31644455 SNPs. Primer sequences were CATGTCTATATGAGCATCCCAAGA, GAGTCTACTA-TGCAACAAGTGTCTTT for D7CU11, TGAGCCTACACGAGACACCA, GTC-TAACCTGGGCCACACAG for D7CU14. Sequencing of the *Tripartite motif-containing 28* (*Trim28*) gene using E8.5 *chatwo* cDNA (Superscript One-Step RT-PCR, Invitrogen) revealed mutations in two consecutive base pairs. These mutations created a BslI digest site within a fragment amplified by primers ATGTGTTGTGTGGCCCAGTA and ACCTCTTGGCACCTGCAAC.

Embryo analysis

Embryos were dissected in 4% BSA PBS. In situ hybridizations were conducted as previously described (Shibata and Garcia-Garcia, 2010). The *Trim28* probe was made using primers GTGGAGCCTCATGGTGAGAT, TCCAAGCCTGAGCTGGTACT. Embryos were imaged in methanol, and sectioned with 16 μm cryosections. Immunohistochemistry was performed as described (Nagy, 2003) on 8 μm cryosections. Antibodies were anti-TRIM28 (1:25; amino acids 60-383; MA1-2023, Thermo Scientific), anti-CDH1 (1:500; Sigma-Aldrich), anti-PECAM-1 (1:200; eBioscience) and anti-mouse/rat/rabbit Alexa Fluor 488/568 (1:200; Molecular Probes). Western blots were conducted using antibodies anti-TRIM28 (1:500; 4E6,

Sigma-Aldrich), anti-GAPDH HRP (1:8000; ab9482, Abcam), anti-Myc (1:1000; 9E10, Hybridoma Bank), anti-GFP (1:5000; 632375, Clontech) and anti-mouse HRP (1:10000; Jackson ImmunoResearch) and quantified using Image J. *Sox2Cre; Trim28*$^{fl/-}$ embryos were generated by crossing *Trim28*$^{fl/fl}$, *Trim28*$^{fl/-}$ or *Trim28*$^{fl/+}$ females to *Sox2Cre; Trim28*$^{+/-}$ males. All comparisons of wild type and mutant embryos are at the same magnification unless otherwise noted.

Cell culture

MYC-TRIM28 vector was made using the pCMV-Myc vector (Clontech) using primers TTAGAATTCGTCCGGCTGCTTCCTCAG and TAAGAATTCGTGGT-TCTACCAGCACAGCAG. MYC-CHATWO vector was made by site-directed mutagenesis using primers CCTGGCCCTGTTCTGGAATGAACCATGCCGTC and GACGGCATGGTTCATTCCAGAACAGGGGGAGG. HEK293 or NIH3T3 cells were transfected with FUGENE 6 (Roche) using pAc-GFP vector (Clontech) as a transfection control. GFP-ZFP568 was made using the pAc-GFP vector and primers TCAGATCTCGAGATGGAGCGCTTGTCCCAGATG, ACCGGTGGATCCCGTT-CACTCCTCCGTCCTGTATG.

RESULTS

***chatwo* mutants display embryonic and extraembryonic defects**

chatwo mutants were discovered in an ENU mutagenesis screen for recessive mutations affecting development of the mid-gestation mouse embryo (Liem et al., 2009). Embryos homozygous for the *chatwo* mutation arrest prior to E9 and display severe yolk sac ruffling (Figure 3.1A-C, brackets). Dissections of embryos at E8.5 revealed two categories of *chatwo* mutant phenotypes; class I mutants that arrested at approximately E8.5 (62.3% n=114/183 Figure 3.1B), and class II mutants that arrested at an E7.5 cup-shaped epiblast stage (37.7%, n=69/183 Figure 3.1C). Defects in

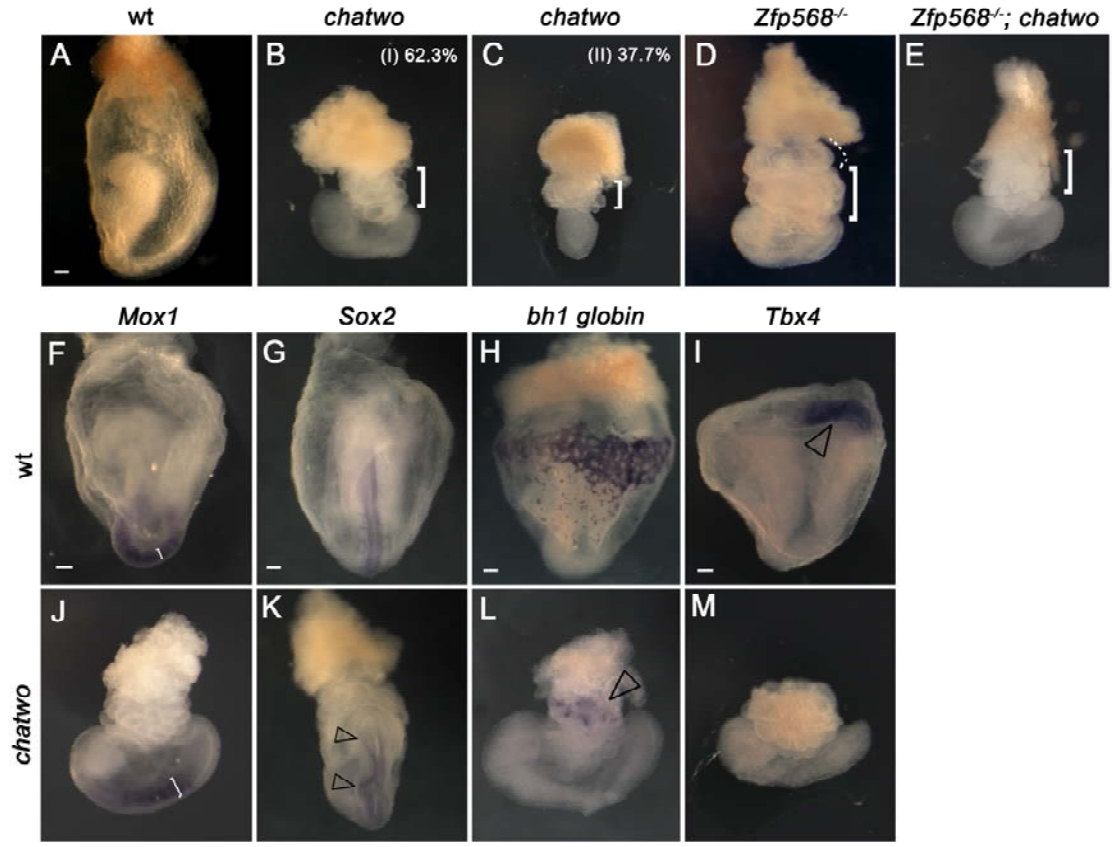

Figure 3.1. Embryonic and extraembryonic defects in *chatwo*. (A-E) Images of whole mount wild type (A,F,G-I), *chatwo* (B-C, J-M), *Zfp568*$^{-/-}$ (D) and *Zfp568*$^{-/-}$; *Trim28*$^{chatwo/chatwo}$ (E) embryos. **(F-M)** In situ hybridizations with *Meox1* (F,J), *Sox2* (G,K), *bh1 globin* (H,L), *Tbx4* (I,M) probes. *chatwo* class I embryos arrest at approximately E8.5, class II embryos arrest at approximately E7.5 (n=183). Brackets in B-E highlight ruffling of the yolk sac. Broken line in D highlights a region of the *Zfp568*$^{-/-}$ yolk sac lacking ruffles. Brackets in F, J highlight mediolateral expansion of *Meox1* expression in *chatwo* mutants. G,K are posterior views. Black arrowheads in K, L point to regions where the neural tube fails to close, and restriction of blood cells in the yolk sac, respectively. Arrowhead in I points to *Tbx4* expression in the wild type allantois. Scale bars represent 100μm.

chatwo mutants were apparent at E7.5, but the two classes of mutants could not be distinguished at this stage. Embryonic and extraembryonic defects in *chatwo* class I mutants, including a failure to form embryonic foregut or hindgut pockets and severe yolk sac ruffling, strongly resemble defects in null mutants for a KRAB zinc finger protein, ZFP568 (Figure 3.1D, Garcia-Garcia et al., 2008, Shibata and Garcia-Garcia, 2010). In order to investigate the similarities between *Zfp568* mutants and *chatwo,* the analysis presented here was focused on *chatwo* class I mutants at E8.5, unless otherwise noted.

To examine whether *chatwo* mutants displayed defects in morphogenesis of embryonic cell types, in situ hybridizations were conducted in whole mount embryos to label specific cell types. *Zfp568* mutant embryos showed irregularities in all embryonic germ layers. Somitic mesoderm showed abnormal mediolateral expansion, and the neuroectoderm failed to neurulate (Garcia-Garcia et al., 2008). In situ hybridizations using a probe for *Meox1*, a marker for somitic mesoderm (Candia et al., 1992), indicated that *Meox1* expressing cells were specified in *chatwo* mutants, but similar to *Zfp568* mutants, expression of *Meox1* was mediolaterally expanded (Figure 3.1F,J Garcia-Garcia et al., 2008). Additional analysis of mesoderm cells with *Twist* and *Foxf1*, markers for somitic and/or lateral plate mesoderm (Quertermous et al., 1994; Mahlapuu et al., 2001) also confirmed the mediolateral expansion of mesenchymal cell types in *chatwo* embryos (data not shown). In addition to defects in morphogenesis of mesoderm cells, *chatwo* mutants also displayed neural tube defects, with wavy neural tubes that failed to close completely, as shown by expression of a neural marker, *Sox2* Figure 3.1G,K, Collignon et al., 1996). Altogether, the embryonic defects in *chatwo* strongly resemble defects in *Zfp568* mutants.

Marker analysis of extraembryonic tissues highlighted similarities in the extraembryonic phenotypes of *chatwo* and *Zfp568* mutants. In wild type embryos, the

yolk sac, which is formed by VE and embryonic-derived extraembryonic mesoderm cells, is an extraembyonic tissue that serves as the site of initial hematopoiesis and vascular network formation (Rossant and Cross, 2001). In *chatwo* mutants, *bh1 globin*-expressing embryonic blood cells (McGrath et al., 2003) remained at their sites of origin at the blood islands, and were not distributed throughout the yolk sac (Figure 3.1H,L). *Zfp568* embryos with severe phenotypes fail to develop an allantois, a structure that gives rise to the future umbilical cord (Rossant and Cross, 2001Shibata and Garcia-Garcia, 2010, Rossant and Cross, 2001). Similarly, *Tbx4* positive allantois cells (Chapman et al., 1996) were not detected in *chatwo* mutants (Figure 3.1I,M). Specification of extraembryonic mesoderm and VE cells was not affected in *chatwo* mutants (Figure 3.2A-D), as evidenced from analysis of *Hand1* (Firulli et al., 1998) and *Afp* expression (Law and Dugaiczyk, 1981). However, detachment of the VE from the extraembryonic mesoderm was observed in some regions of *chatwo* yolk sacs, in a manner indistinguishable from defects previously reported for *Zfp568* mutants (Figure 3.2A-D, Shibata and Garcia-Garcia, 2010).

Despite similarities between *chatwo* and *Zfp568* embryos, the phenotypes of the mutants were not identical. In contrast to *Zfp568* mutants, where yolk sac ruffles are often clustered in a region proximal to the embryo, ruffling of the yolk sac extended throughout the entire yolk sac in all *chatwo* embryos (Figure 3.1B-D, brackets; Shibata and Garcia-Garcia, 2010). Since the severity of yolk sac ruffling was correlated with chorionic defects in *Zfp568* mutants (Shibata and Garcia-Garcia, 2010), sections of *chatwo* embryos were examined for chorionic abnormalities. The chorion is a layer of extraembryonic ectoderm cells lined by extraembryonic mesoderm cells, which normally unites with the ectoplacental cone by E8.5 to form part of the developing placenta (Rossant and Cross, 2001). Analysis of *Esrrb* expression (Luo et al., 1997) in sagittal sections revealed strong abnormalities in the

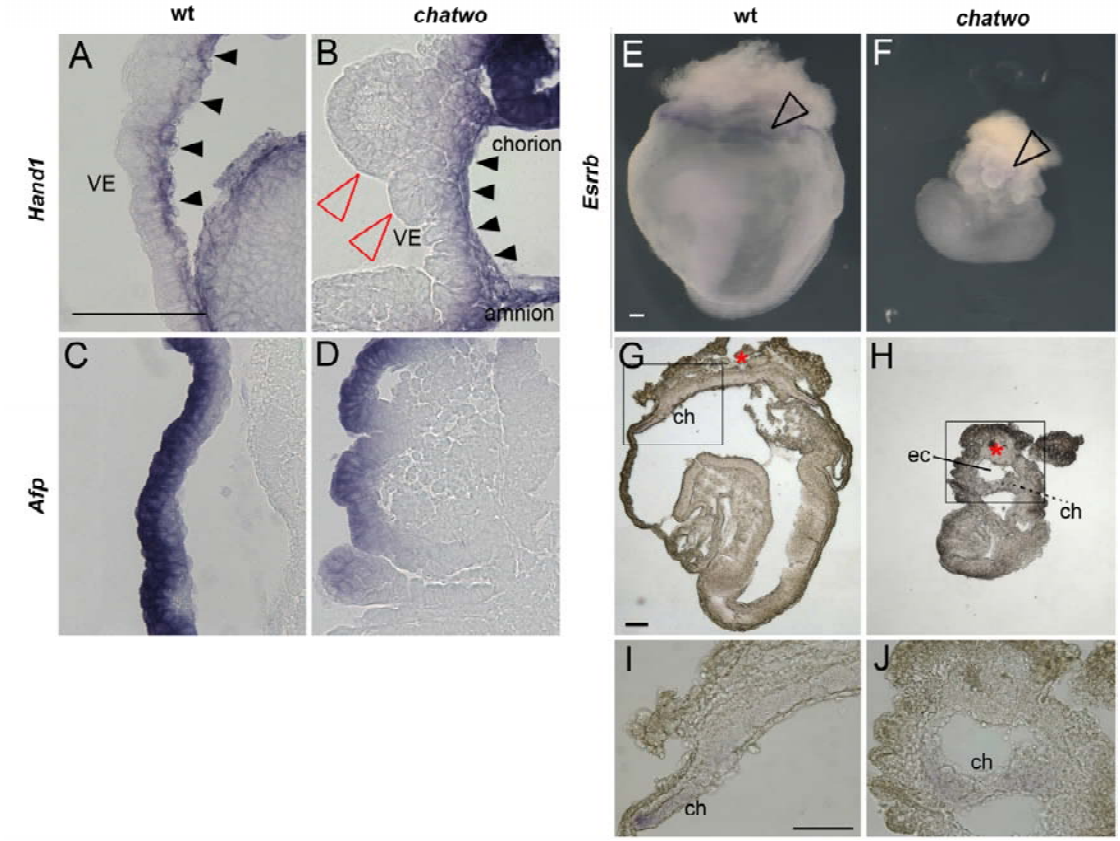

Figure 3.2. Characterization of yolk sac and chorion defects in *chatwo.* (A-D) Yolk sac sections of wild type (A,C) and *chatwo* (B,D) embryos after whole mount in situ hybridizations for *Hand1* (A-B) and *Afp* (C-D). **(E-F)** Whole mount in situ hybridizations for *Esrrb* on wild type (E) and *chatwo* (F) embryos. **(G-H)** Sections of embryos in E,F. **(I-J)** Higher magnification images of boxed areas from G,H. Black arrowheads in A,B point to extraembryonic mesoderm cells. Red arrowheads in B point to regions where the visceral endoderm (VE) is ruffled and detached from the extraembryonic mesoderm in *chatwo.* Arrowheads in E,F point to the chorion (ch). Red asterisks in G,H mark the ectoplacental cone. ec, ectoplacental cavity. Scale bars represent 100μm.

chorion of *chatwo* embryos. In most *chatwo* mutants, the closure of the ectoplacental cavity and rising of the chorion, events necessary for proper placental development, were not observed (Figure 3.2 E-J). The severity of the yolk sac and chorionic defects suggest that *chatwo* may disrupt additional morphogenetic processes to those regulated by *Zfp568*.

The *chatwo* mutation disrupts *Trim28* function

Using positional cloning techniques, the *chatwo* mutation was mapped to a genetic interval on mouse Chromosome 7 containing 10 genes (Figure 3.3A, see Materials and Methods). Sequencing of the *Trim28* gene in the interval revealed that the *chatwo* mutation affects two adjacent DNA bases in *Trim28*, causing a C to G transition and a C to A transversion (Figure 3.3B). Linkage of these mutations to the *chatwo* phenotype was confirmed in more than 6 *chatwo* carriers (*chatwo/+*) and over 10 mutant embryos using a BslI restriction site created by the *chatwo* allele (Figure 3.3C). The *chatwo* mutations caused Cys713 to Trp, and His714 to Asn missense mutations in TRIM28's C-terminal Bromodomain (Figure 3.3D). These mutations likely disrupt the structural conformation of the α_z helix region of the Bromodomain.

The *chatwo* mutation affects TRIM28 protein levels in the embryo

To determine whether the amino acid changes caused by the *chatwo* mutation affect stability of the TRIM28 protein, transverse sections of *chatwo* embryos at E7.5 were stained with an antibody against the N-terminus of TRIM28 and counterstained with DAPI and anti-CDH1 (Cadherin 1, also know as E-cadherin) antibody. As reported previously, nuclear TRIM28 protein was detected in cells of wild type embryos (Figure 3.4A-D, Cammas et al., 2000). However, TRIM28 staining in nuclei of *chatwo*

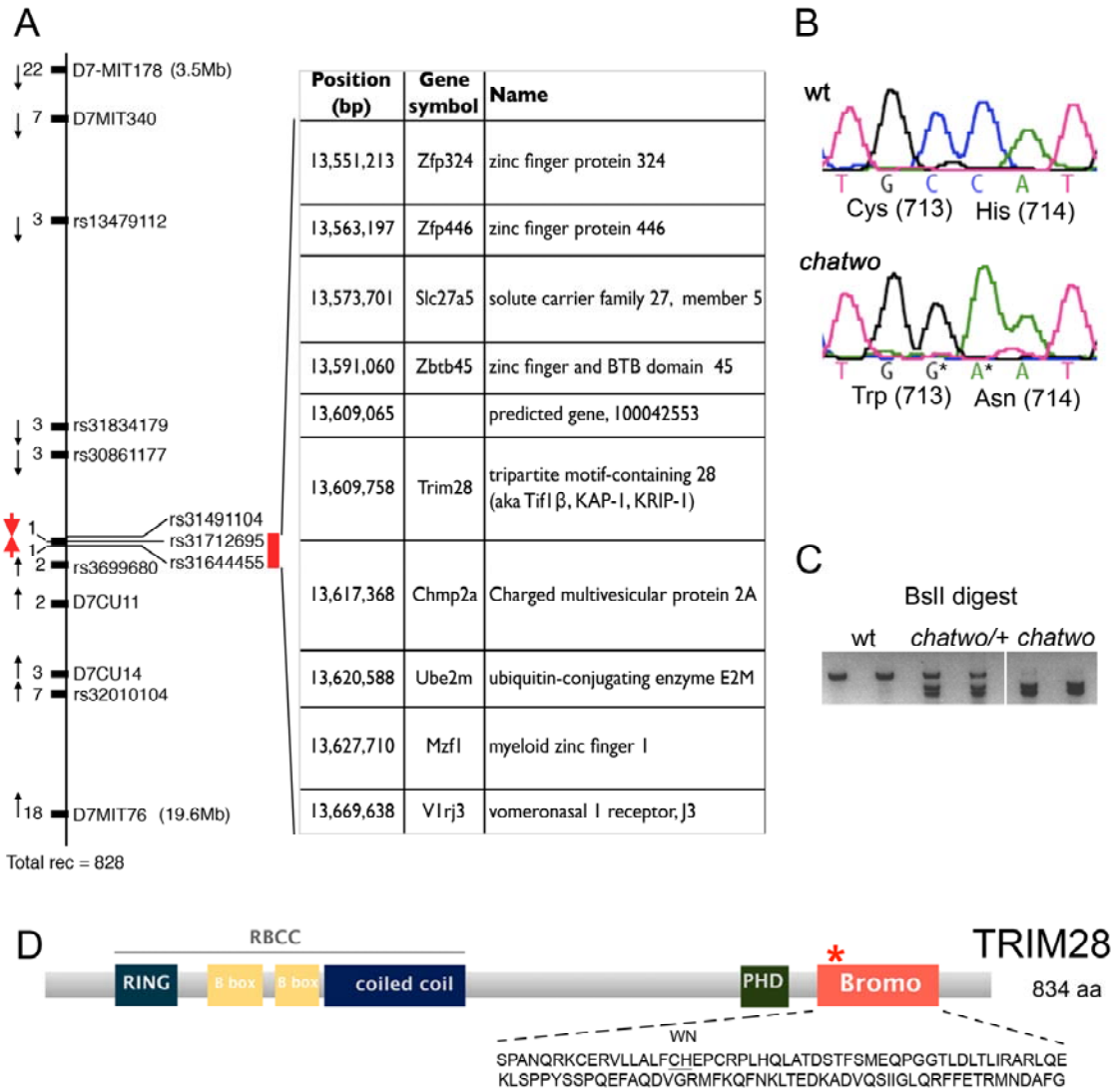

Figure 3.3. The *chatwo* mutation affects *Trim28*. **(A)** Through analysis of naturally occurring recombination events, the *chatwo* mutation was mapped to an interval containing 10 genes, between rs31491104 and rs31644455 SNPs. Numbers on the left side of the panel represent the number of independent recombination events (rec) obtained. Positions are from NCBI build 37. **(B)** Chromatogram obtained from sequencing cDNA from wild type and *chatwo* mutants. *chatwo* creates changes in two DNA base pairs (asterisks), which result in substitutions in amino acids 713 and 714 in TRIM28. **(C)** The *chatwo* mutations create a BslI restriction site. No digestion of PCR fragments using DNA extracted from wt mice, partial digestion in DNA from *chatwo* carriers (*chatwo*/+), and complete digestion in DNA from *chatwo* mutant embryos was observed. **(D)** TRIM28 contains an N-terminal RBCC (RING finger, B box, coiled coil) domain and C-terminal PHD finger and Bromo domains. The amino acids affected by *chatwo* are within the Bromo domain of TRIM28 (asterisk).

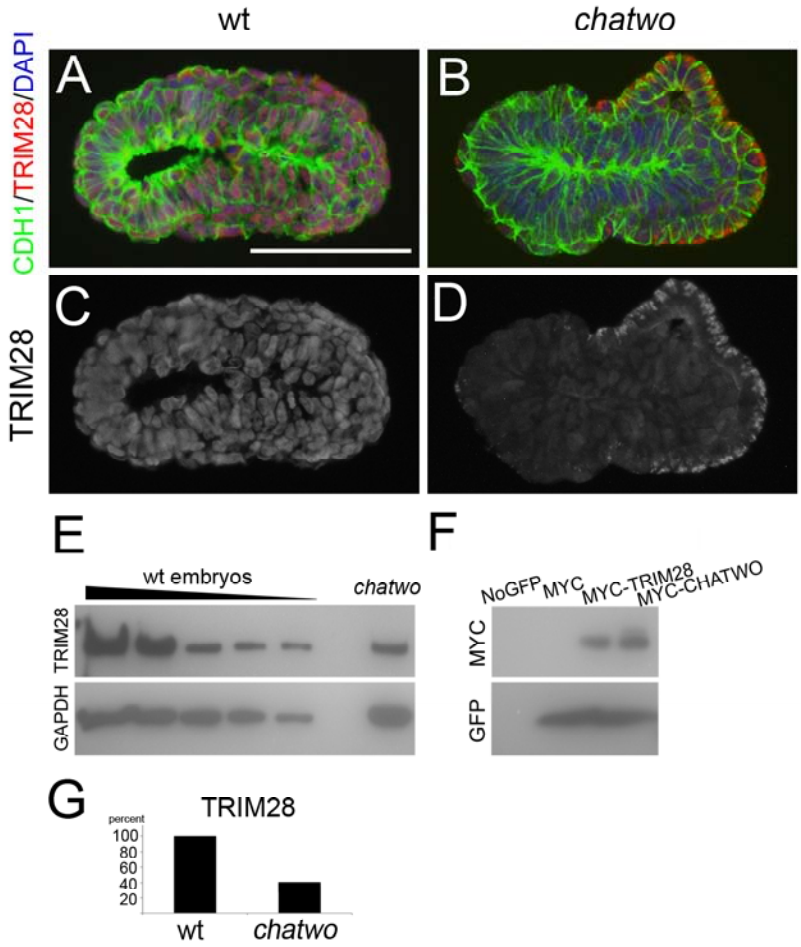

Figure 3.4. TRIM28 protein levels in *chatwo*. (A-D) Antibody staining on transverse sections of E7.5 wild type (A) and *chatwo* (B) embryos with anti-TRIM28 antibody (red). Sections were counterstained with anti-CDH1 antibody (green) and DAPI staining (blue). C,D are sections from A,B showing only anti-TRIM28 staining. Strong non-nuclear staining in *chatwo* mutants (D) is nonspecific staining from the secondary anti-mouse antibody. Scale bar in A represents 100μm. **(E)** Representative western blot using anti-TRIM28 antibody and lysates from a gradient of wild type and *chatwo* embryos. Anti-GAPDH antibody was used as a loading control. **(F)** Representative western blot using lysates from HEK293 cells that were untransfected (No-GFP), transfected with MYC and GFP vectors (MYC), MYC-TRIM28 and GFP vectors (MYC-TRIM28) or MYC-CHATWO and GFP vectors (MYC-CHATWO). **(G)** Quantification of intensity of bands in E.

mutants was much weaker, indicating that protein levels of TRIM28 may be reduced in *chatwo*.

To quantify the overall TRIM28 protein levels, western blots were conducted on *chatwo* mutants. TRIM28 protein levels in E7.5 *chatwo* embryos were compared to wild type littermates using a monoclonal antibody raised against a TRIM28 peptide containing amino acids 379 to 524 (Figure 3.4E). A reduction of TRIM28 protein levels was detected in *chatwo* mutants, with levels of TRIM28 at approximately 40% of levels detected in wild type littermates (Figure 3.4E,G). Because the sequence recognized by TRIM28 antibodies lies far away from the Bromodomain missense mutations in *chatwo*, it is unlikely that the reduction in TRIM28 levels observed in these experiments corresponds to the inability of the antibodies to recognize the CHATWO mutant protein. Similar results were also obtained using a α-TRIM28 polyclonal antibody raised against amino acids 536 to 835 (data not shown). Therefore, these results suggest that the *chatwo* mutation affects the stability of TRIM28 protein within the embryo.

To assess whether the reduction of TRIM28 within the embryo was due to a direct effect of the *chatwo* mutation on the stability of TRIM28, I assessed whether the mutations would create an unstable TRIM28 protein in cultured cells. Either Myc-tagged *chatwo* or Myc-tagged *Trim28* constructs were transiently transfected into HEK293 cells, using GFP vector as a co-transfection control. Western blots on lysates from transfected cells using anti-MYC antibody showed that in contrast to observations in E7.5 embryos, both MYC-TRIM28 and MYC-CHATWO were detected at similar levels (Figure 3.4F). One possibility is that the MYC-CHATWO protein is stable when overexpressed in cell culture, and that the *chatwo* mutation does not affect intrinsic stability of TRIM28. Alternatively, it is also possible that

oligomerization of MYC-CHATWO with endogenous TRIM28 (Peng et al., 2000) stabilizes the MYC-CHATWO protein in HEK293 cells.

chatwo creates a hypomorphic allele for *Trim28*

Previous studies have revealed that embryos homozygous for a *Trim28* knockout allele (*Trim28*$^{-/-}$) implant normally, but arrest at approximately E5.5 (Cammas et al., 2000). *Trim28*$^{-/-}$ embryos fail to gastrulate, and lack expression of *Brachyury*, a marker of the primitive streak (Wilkinson et al., 1990; Cammas et al., 2000). Since *chatwo* creates missense mutations in *Trim28,* and since *chatwo* embryos arrest after E7.5 (Figure 3.1B-C, n=183), I hypothesized that the *chatwo* mutation created a hypomorphic *Trim28* allele.

To obtain genetic evidence that the *chatwo* mutation disrupts *Trim28,* I conducted genetic complementation analysis. Animals heterozygous for *chatwo* (*Trim28*$^{chatwo/+}$) were crossed to *Trim28*$^{+/-}$ animals. Resulting embryos from the cross were either wild type in appearance, or indistinguishable from *chatwo* mutants. Genotyping of the embryos confirmed that all *Trim28*$^{chatwo/-}$ embryos arrested between E7.5 and E8.5 (Figure 3.5E-F). Similarly to *chatwo* embryos, some of the *Trim28*$^{chatwo/-}$ embryos arrested at E7.5 (class II, 63.6% n=7/11, Figure 3.5F) whereas other *Trim28*$^{chatwo/-}$ embryos arrested at E8.5 (class I, 36.4% n=4/11, Figure 3.5E). *Brachyury* expressing mesoderm cells were detected in all *chatwo/-* embryos examined, regardless of their phenotypic class, indicating that phenotypes of *Trim28*$^{chatwo/-}$ embryos are milder than those of *Trim28*$^{-/-}$ mutants (Figure 3.5D-F). These results support the hypothesis that the *chatwo* allele creates a hypomorphic allele for *Trim28*.

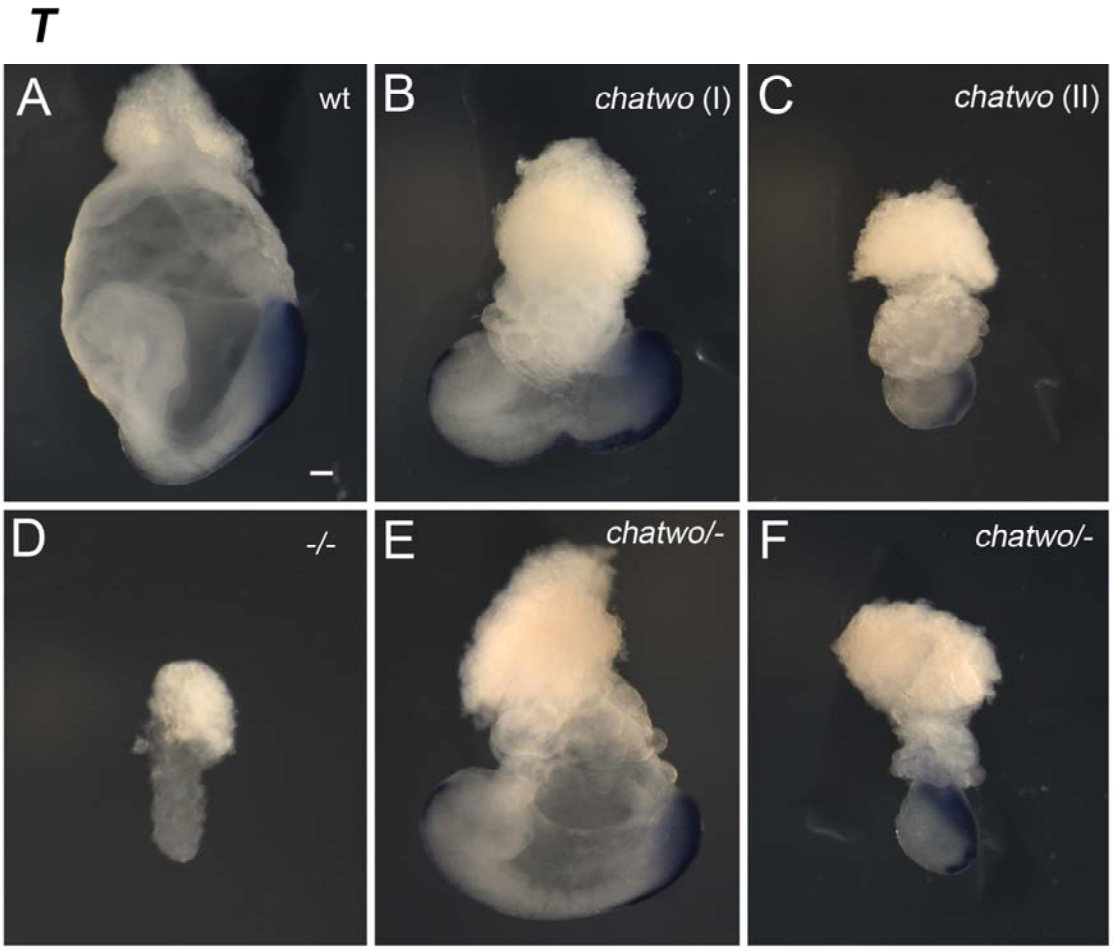

Figure 3.5. *chatwo* creates a hypomorphic *Trim28* allele. (A-F) Whole mount in situ hybridizations on wild type (A), *chatwo* (B,C), *Trim28* null (-/-) (D) and *chatwo/-* embryos using a probe for *brachyury* (*T*). (E,F) *chatwo/-* embryos (n=11) arrested either at E8.5 (class I, 36.4%) or E7.5 (class II, 63.6%), expressed *T* and were indistinguishable form *chatwo* mutants. Scale bar in A represents 100μm.

chatwo and *Zfp568* do not genetically interact

To determine whether the *chatwo* mutation genetically interacts with *Zfp568, chatwo* heterozygotes were crossed to animals heterozygous for a null allele of *Zfp568* (Garcia-Garcia et al., 2008). Viable $Zfp568^{+/-}$; $Trim28^{chatwo/+}$ progeny were obtained at Mendelian frequencies. As these $Zfp568^{+/-}$; $Trim28^{chatwo/+}$ progeny were fertile, I analyzed phenotypes of $Zfp568^{-/-}$; $Trim28^{chatwo/+}$, $Zfp568^{+/-}$; $Trim28^{chatwo/chatwo}$ and $Zfp568^{-/-}$; $Trim28^{chatwo/chatwo}$ embryos, but did not detect any genetic interactions. Whereas $Zfp568^{-/-}$; $Trim28^{chatwo/+}$ embryos resembled *Zfp568* mutant embryos, $Zfp568^{+/-}$; $Trim28^{chatwo/chatwo}$ and $Zfp568^{-/-}$; $Trim28^{chatwo/chatwo}$ embryos were indistinguishable from *chatwo* embryos, arresting either at E8.5 or E7.5 (Figure 3.1A-E, data not shown). These results indicate that *chatwo* and $Zfp568^{-/-}$ do not have additive affects and that *chatwo* is epistatic to *Zfp568*.

Trim28 is required in both embryonic and extraembryonic cells

Although *chatwo* mutants arrest later in development than $Trim28^{-/-}$ embryos, both *chatwo* and $Trim28^{-/-}$ mutants disrupt embryonic and extraembryonic development. *Trim28* is expressed in most cell types prior to gastrulation (Cammas et al., 2000), and tissue specific requirements for *Trim28* have not been determined. Therefore, it is not clear whether *Trim28* is required in both embryonic and extraembryonic tissues, or whether defects in one of these tissues arise secondarily due to a requirement for *Trim28* in a specific cell type. At E7.5, *Trim28* is expressed in extraembryonic cells including the ectoplacental cone and chorionic ectoderm, in embryonic derived extraembryonic mesoderm cells, and at high levels in the embryo (Figure 3.6, Cammas et al., 2000).

Based on the facts that *Zfp568* and *chatwo* mutants have similar embryonic phenotypes and that *Zfp568* is required in embryonic tissues (Shibata and Garcia-

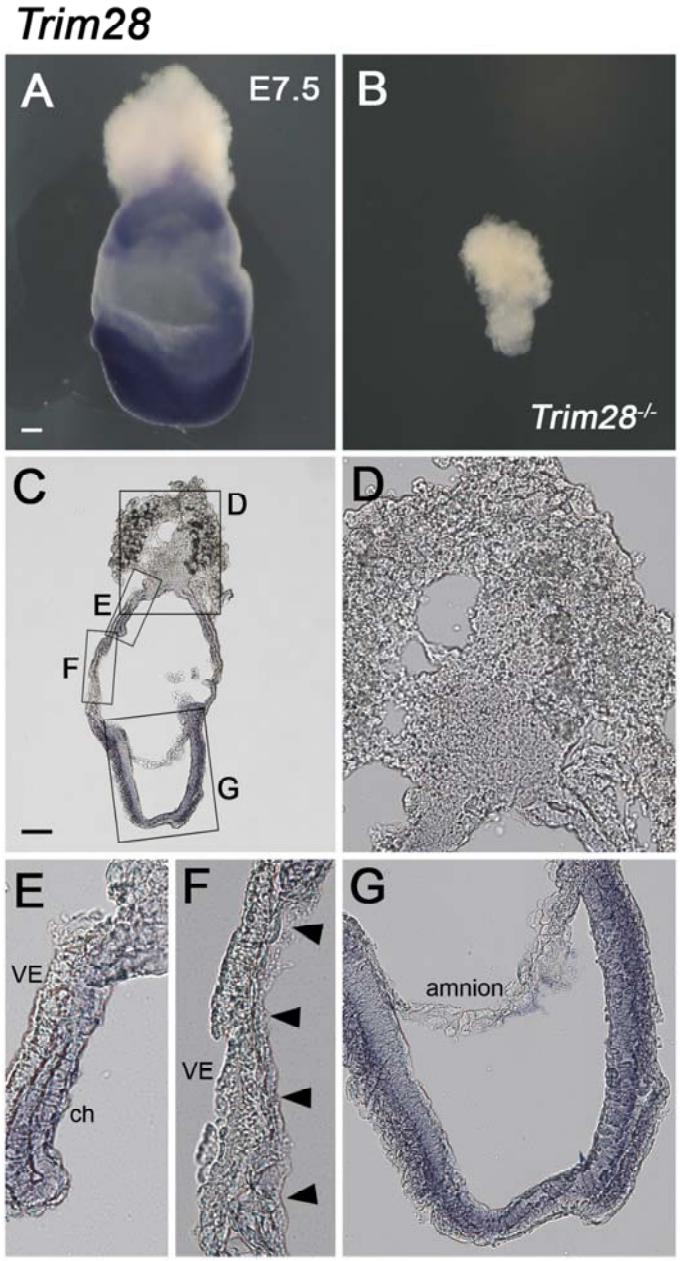

Figure 3.6. *Trim28* is expressed in multiple cell types. Whole mount in situ hybridizations using a *Trim28* probe on wild type **(A)** and control *Trim28*$^{-/-}$ **(B)** embryos. **(C)** Sagittal section of wild type embryo in A. **(D-G)** Higher magnification images of trophoblast (D), chorion (ch) (E), yolk sac (F) and embryo (G) from boxed regions in C. VE, visceral endoderm. Arrowheads in F point to extraembryonic mesoderm cells. Scale bars represent 100μm.

Garcia, 2010), I predicted that *Trim28* was likely to be required in embryonic cells. However, the earlier lethality of *Trim28*$^{-/-}$ mutants in comparison to *Zfp568* mutant phenotypes suggests that TRIM28 has additional, ZFP568-independent functions during gastrulation. To assess whether *Trim28* in extraembryonic VE and trophoblast cells was sufficient to rescue the early lethality of *Trim28*$^{-/-}$ mutants, I created mosaic embryos through inactivation of a floxed conditional allele of *Trim28* (*Trim28*^{fl}) using the *Sox2Cre* transgene (Cammas et al., 2000; Hayashi et al., 2002).

Tissue specific inactivation of *Trim28* in the embryo and embryonic-derived tissues (*Sox2Cre; Trim28*$^{fl/-}$ embryos) caused developmental arrest at approximately E8.5, and embryonic phenotypes that strongly resembled *Zfp568* and *Trim28*^{chatwo} mutant embryos (Figure 3.7). *Sox2Cre; Trim28*$^{fl/-}$ embryos did not properly form foregut and hindgut pockets, and embryos failed to turn. In addition, *Sox2Cre; Trim28*$^{fl/-}$ embryos displayed neural tube defects such as wavy neural tube (Figure 3.7C-D). Embryos with a similar phenotype were also obtained using a *Meox2Cre* allele in which Cre recombinase was expressed in the same cell types as *Sox2Cre* (data not shown, Tallquist and Soriano, 2000).

Surprisingly, yolk sacs of *Sox2Cre; Trim28*$^{fl/-}$ embryos were smooth in appearance, lacking the severely ruffled yolk sac phenotype displayed by *Zfp568* and *chatwo* mutants. To assess whether maternal TRIM28 could be partially rescuing the defects of *Sox2Cre; Trim28*$^{fl/-}$ embryos, I compared the phenotypes of *Sox2Cre; Trim28*$^{fl/-}$ embryos originated from *Trim28*$^{fl/fl}$, *Trim28*$^{fl/+}$ and *Trim28*$^{fl/-}$ mothers. Phenotypes of resulting *Sox2Cre; Trim28*$^{fl/-}$ mutants were indistinguishable (data not shown), indicating that maternal TRIM28 protein or *Trim28* transcripts did not influence the phenotype of mosaic embryos.

Despite the smooth appearance of the yolk sacs of *Sox2Cre; Trim28*$^{fl/-}$ mutants, further characterization revealed defects in yolk sac vasculogenesis. Although

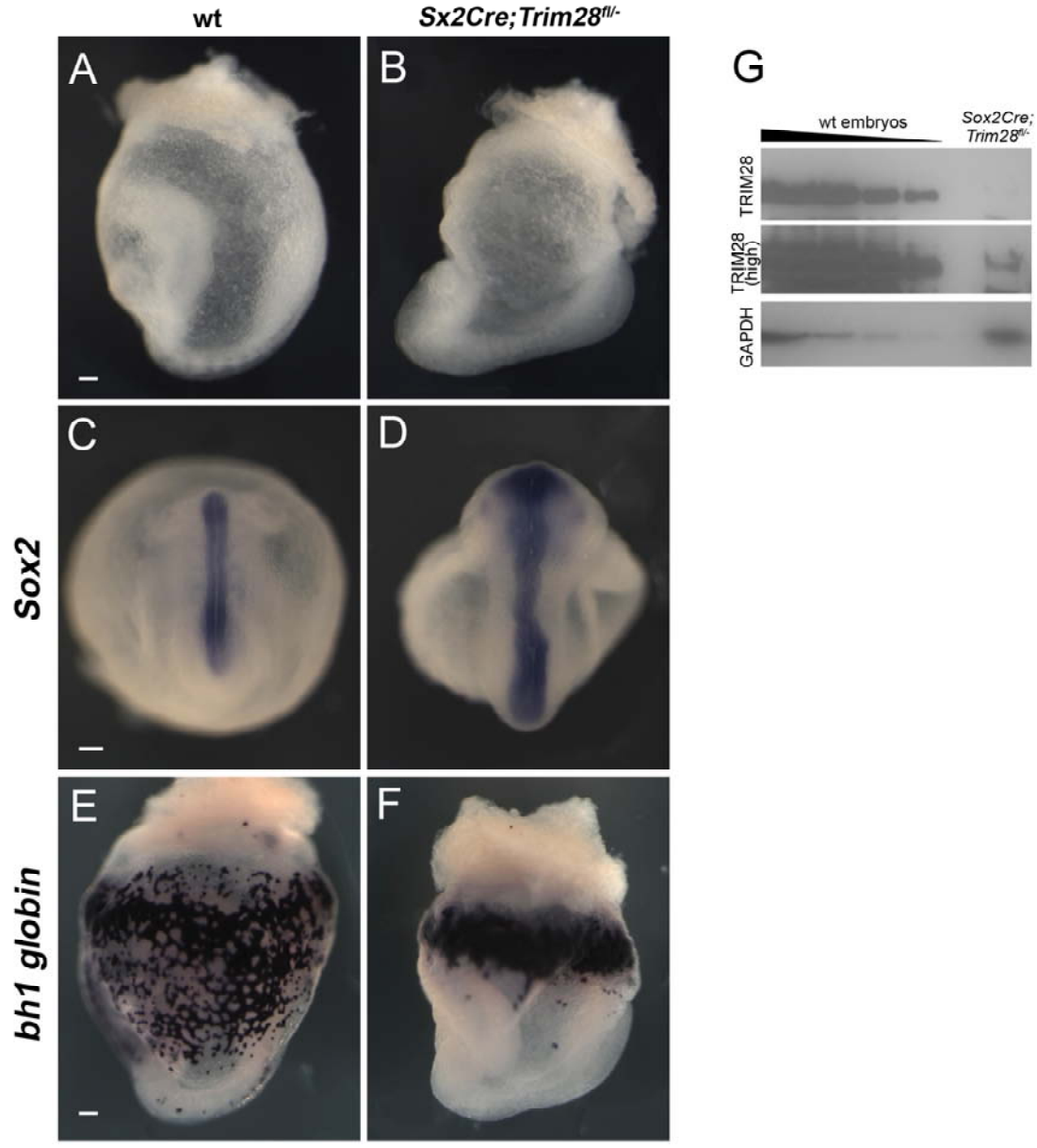

Figure 3.7. *Trim28* is required in embryonic cells for embryonic morphogenesis. (A-F) Whole mount images of wild type (A,C,E) and *Sox2Cre; Trim28*$^{f/-}$ (B,D,F) embryos in which *Trim28* is removed only in the embryo and embryonic derived extraembryonic mesoderm. In situ hybridizations with *Sox2* (C-D, ventral views) and *bh1 globin* (E-F) probes. **(G)** Western blot using lysates of wild type or *Sox2Cre; Trim28*$^{f/-}$ embryos with yolk sacs removed. A small amount of TRIM28 was detected in *Sox2Cre; Trim28*$^{f/-}$ embryos upon a long exposure of the blot (TRIM28 high). GAPDH was used as a loading control. Scale bars in A,C,E represent 100μm.

PECAM positive endothelial cells were specified, the primitive vascular network failed to remodel in *Sox2Cre; Trim28*$^{fl/-}$ yolk sacs (Figure 3.8). Defects in vasculogenesis were slightly milder in *Sox2Cre; Trim28*$^{fl/-}$ yolk sacs as compared to *chatwo* embryos (Figure 3.8C-E), but were significant enough to prevent the circulation of blood cells through the yolk sac, and embryonic blood cells were constricted to the blood islands in most *Sox2Cre; Trim28*$^{fl/-}$ embryos (Figure 3.7E-F). This indicates that TRIM28 is required in embryonic and embryonic derived extraembryonic mesoderm cells for proper yolk sac vasculogenesis.

Western blotting confirmed that conditional inactivation of *Trim28* with *Sox2Cre* was effective in *Sox2Cre; Trim28*$^{fl/-}$ embryos (Figure 3.7G). However, a higher exposure of the blot revealed that a small amount of TRIM28 could be detected in the embryo. Thus, it is possible that the small amount of TRIM28 protein remaining may contribute to the milder yolk sac phenotype of *Sox2Cre; Trim28*$^{fl/-}$ mutants. Altogether, the results of the conditional TRIM28 inactivation experiments indicate that TRIM28 is required in the embryo and extraembryonic mesoderm, as embryos lacking TRIM28 in these tissues (*Sox2Cre; Trim28*$^{fl/-}$) arrest at E8.5 with multiple embryonic defects and yolk sac vasculogenesis abnormalities (Figures 3.7, 3.8). The resemblance of *Sox2Cre; Trim28*$^{fl/-}$ embryos to *Zfp568* mutant embryos also suggests that ZFP568 is a predominant KRAB zinc finger protein requiring functions of TRIM28 within the embryo and extraembryonic mesoderm. In addition, the differences between the E8.5 arrest of *Sox2Cre; Trim28*$^{fl/-}$ embryos and the E5.5 arrest of *Trim28*$^{-/-}$ mutants indicate that TRIM28 is necessary in trophoblast and/or VE cells, but not in embryonic cells during early postimplantation stages of development.

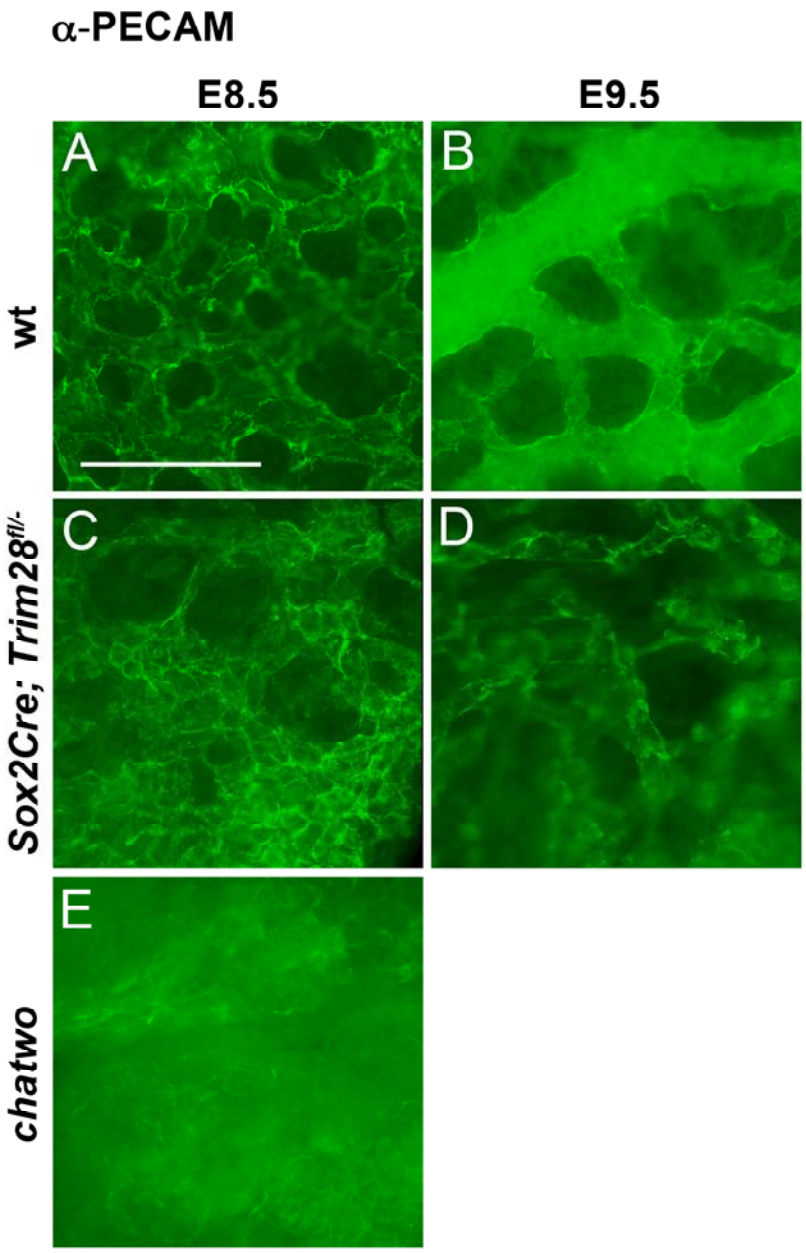

Figure 3.8. PECAM expression in yolk sacs. **(A-E)** Yolk sacs from wild type (A-B), *Sox2Cre; Trim28*$^{f/-}$ (C-D) and *chatwo* (E) were staining using α-PECAM antibody at E8.5 (A,C,E) or E9.5 (B,D). Remodeling of the vascular plexus is disrupted in *Sox2Cre; Trim28*$^{f/-}$ yolk sacs. Scale bar represents 100μm.

TRIM28 co-localizes with ZFP568 in cultured cells

To assess whether TRIM28 and ZFP568 may be functioning as a transcriptional complex, I looked for co-localization of endogenous TRIM28 with ZFP568. NIH3T3 mouse fibroblast cells were transiently transfected with GFP tagged ZFP568, and stained for TRIM28 (Figure 3.9). Control transfections using a GFP vector showed nonspecific cytoplasmic and nuclear localization of the GFP vector (Figure 3.9A,C). In contrast, GFP-ZFP568 was found in nuclear puncta (Figure 3.9B,D). TRIM28 antibody staining revealed co-localization of TRIM28 at the ZFP568 nuclear foci (Figure 3.9B,D,F). Yeast two-hybrid assays and co-immunoprecipitation experiments have confirmed an interaction between ZFP568 and TRIM28 (K. Blauvelt, unpublished). These results provide evidence that ZFP568 and TRIM28 may function as part of a protein complex in vivo.

DISCUSSION

Trim28^{chatwo} mutants arrest prior to E8.5 with embryonic and extraembryonic defects resembling those of mutants in the KRAB zinc finger gene *Zfp568*. The C713W and H714N mutations caused by *chatwo* affect the bromodomain of TRIM28, reducing TRIM28 levels in the embryo and creating a hypomorphic allele. Our findings suggest that high levels of TRIM28 are required for proper embryonic morphogenesis, and that TRIM28 is important for mediating functions of KRAB zinc finger protein ZFP568. Our analysis of embryos mosaic for *Trim28* has also revealed differential tissue specific requirements for TRIM28, highlighting TRIM28 functions in both extraembryonic and embryonic cells.

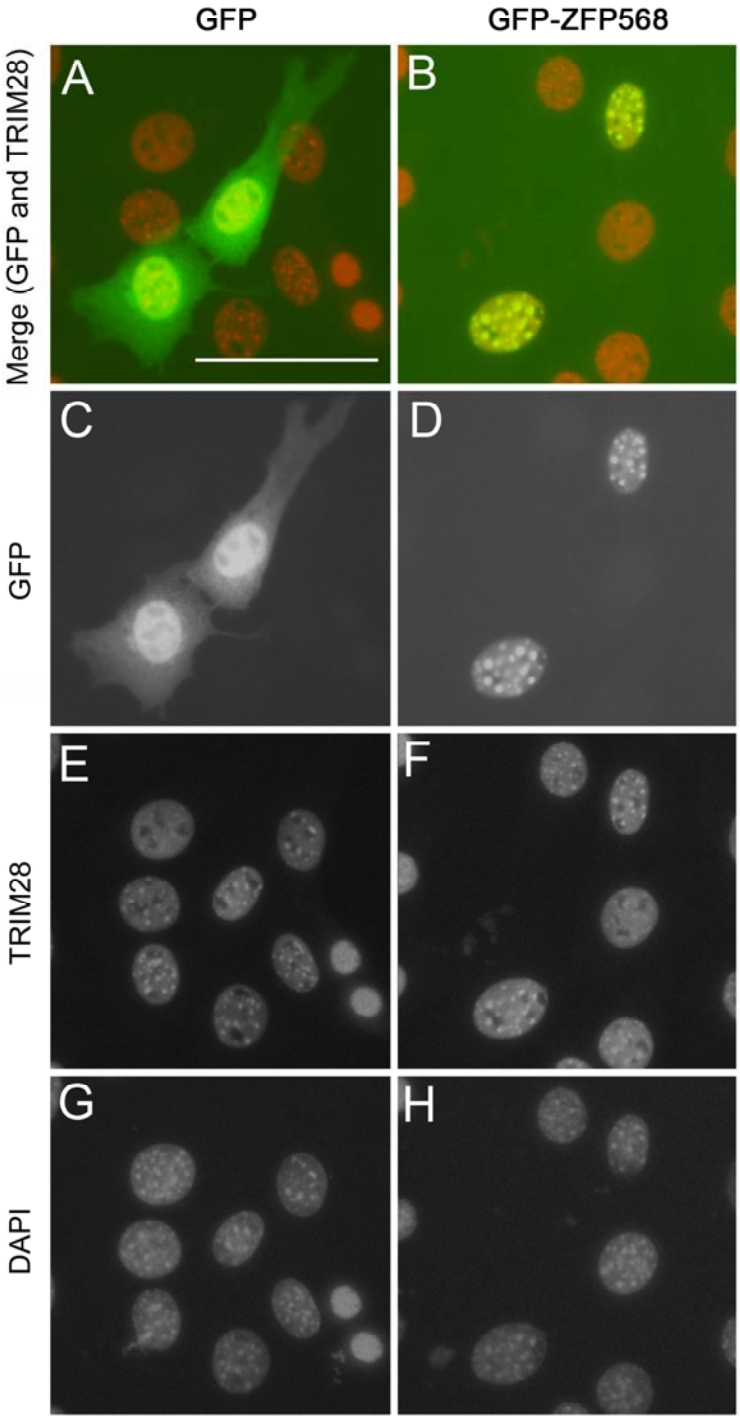

Figure 3.9. Subcellular localization of TRIM28 and ZFP568. (A-B) Overlays of NIH3T3 cells transfected with control GFP vector (A) or GFP-ZFP568 (B) stained with anti-TRIM28 antibody (red). **(C-H)** Images from A,B showing only GFP (C,D), TRIM28 (E,F) or DAPI staining (G,H). Note the co-localization between GFP tagged ZFP568 and endogenous TRIM28 (B,D,F). Scale bar in A represents 50μm.

Effects of *chatwo* on TRIM28

The C713W and H714N mutations in *chatwo* affect amino acids in the α_z helix of the Bromodomain of TRIM28. These two amino acid residues are conserved in the TIF1 family members most similar to TRIM28, TRIM24 (TIF1α) and TRIM 33 (TIF1γ) (Schultz et al., 2001). Furthermore, H714 is conserved in the α_z helix of bromodomains of other proteins including BAZ1A (Bromodomain adjacent to zinc finger domain 1A or WCRF180), KAT2A (Lysine acetyltransferase 2A or GCN5) and KAT2B (Lysine acetyltransferase 2B or pCAF) (Schultz et al., 2001). This suggests that the mutations caused by *chatwo* may affect critical bromodomain residues required for TRIM28 activity.

Although the *chatwo* mutation does not affect stability of the MYC-CHATWO protein when overexpressed in cells, levels of TRIM28 protein were reduced in *chatwo* mutant embryos, even at E7.5 (Figure 3.4). One hypothesis for explaining this discrepancy is that the *chatwo* mutation may affect interactions that stabilize TRIM28 in the embryo. The PHD and bromodomains of TRIM28 function together in mediating transcriptional repression through recruitment of chromatin modifying proteins including CHD3, a subunit of the NuRD histone deacetylase complex, and the histone methyltransferase SETDB1 (Schultz et al., 2001; Zeng et al., 2008). Recent evidence has also indicated that the recruitment of proteins to form a large repression complex may be dependant on SUMOylation of TRIM28 (Zeng et al., 2008). It is possible that *chatwo* may affect binding of chromatin modifying proteins to the PHD and bromo domains, SUMOylation of TRIM28, or interactions with other binding partners.

High levels of TRIM28 are required for embryo morphogenesis

The phenotypic differences between *Trim28*$^{-/-}$ and *Trim28*^{chatwo} mutants, the reduction of TRIM28 protein levels in *Trim28*^{chatwo}, and the phenotypes of *Trim28*$^{chatwo/-}$ mutants all suggest that the *Trim28*^{chatwo} mutation creates a hypomorphic *Trim28* allele. Although the early arrest of *Trim28*$^{-/-}$ embryos at E5.5 indicates that TRIM28 plays an essential role in postimplantion development (Cammas et al., 2000), the viability of *Trim28*^{chatwo} mutants up until E8.5 suggests that reduced function of TRIM28 is sufficient for early postimplantation development and mesoderm formation. However, higher levels of TRIM28 are likely required for embryonic morphogenesis and proper yolk sac and placental development to proceed, as *Trim28*^{chatwo} mutants arrest by E8.5 with defects resembling *Zfp568* mutants.

It is possible that KRAB zinc finger proteins mediating TRIM28 functions prior to E8.5 require only low levels of TRIM28, as *Trim28*^{chatwo} mutants are viable up to E8.5 with reduced TRIM28 protein levels. Alternatively, TRIM28 could have roles independent of KRAB zinc finger proteins prior to E8.5 that do not require high TRIM28 levels. Regardless, the similarity between the *Trim28*^{chatwo} and *Zfp568* mutant phenotypes indicates that ZFP568 is a KRAB zinc finger protein requiring relatively high levels of functional TRIM28.

TRIM28 is required to mediate functions of ZFP568

The results presented here provide genetic evidence that functions of KRAB zinc finger protein ZFP568 are mediated by TRIM28 during embryonic morphogenesis. The similarities between the phenotypes of *Trim28*^{chatwo} and *Zfp568* mutant embryos and the results of genetic interactions studies between *Trim28*^{chatwo} and *Zfp568* suggest that defects in both *Trim28*^{chatwo} and *Zfp568* mutants arise due to a disruption of TRIM28-ZFP568 protein complex activity.

Functions of at least one KRAB zinc finger protein other than ZFP568 are affected in *chatwo* mutants, but are not the primary cause of lethality in *chatwo*. In addition to ZFP568, *chatwo* affects the ability of TRIM28 to function as a partner of at least one additional KRAB zinc finger protein, ZFP57. Embryos lacking ZFP57 disrupt imprinting at several imprinted clusters including the *Dlk1-Dio3* imprinted region (Li et al., 2008). I have found that expression of *Dlk1* is also affected in *Trim28*^{chatwo}, but not in *Zfp568* mutants (Appendix D). However, this imprinting defect is likely not responsible for the phenotypes of *chatwo* mutants, as embryos lacking ZFP57 survive until later in embryonic development.

Given that over 250 KRAB zinc finger proteins are expressed in ES cells (Rowe et al., 2010), the strong resemblance between *Trim28*^{chatwo} and *Zfp568* mutants is somewhat surprising. My findings indicate that ZFP568 is a major mediator of TRIM28 functions, in processes such as embryonic morphogenesis, neural tube closure, vasculogenesis and allantois formation.

Tissue specific requirements of TRIM28

Previous studies have identified multiple requirements of TRIM28, including roles in early post-implantation development (Cammas et al., 2000), maintenance of spermatogenesis (Weber et al., 2002), and in the forebrain to control behavioral stress responses (Jakobsson et al., 2008). TRIM28 is also required for maintenance of pluripotency of embryonic stem cells (Hu et al., 2009) and has been found to be upregulated in metastatic breast tumors (Ho et al., 2009).

My analysis of tissue specific requirements for *Trim28* during embryonic development have revealed functions for *Trim28* in both embryonic and extraembryonic cell types. The early lethality of *Trim28*$^{-/-}$ embryos is rescued in *Sox2Cre; Trim28*$^{fl/-}$ embryos by wild type *Trim28* in VE and trophoblast cells,

indicating that the E5.5 arrest of *Trim28*$^{-/-}$ embryos is due to defects in these cell lineages. However, *Sox2Cre; Trim28*$^{fl/-}$ embryos display embryonic morphogenetic defects and resemble *Zfp568*^{chato} and *Trim28*^{chatwo} mutants, suggesting that *Trim28* is required in embryonic cells to mediate functions of *Zfp568*. In the yolk sac VE and/or trophoblast, TRIM28 likely has functions independent of ZFP568, but in the embryo and extraembryonic mesoderm, functions of TRIM28 are mediated by ZFP568.

The fact that conditional inactivation of *Trim28* in embryonic tissues (*Sox2Cre; Trim28*$^{fl/-}$ embryos) caused defects similar to those of *Zfp568* mutants suggests that *Zfp568* is a predominant KRAB zinc finger protein required for embryo morphogenesis during this stage of development. However, the smooth yolk sac phenotype of *Sox2Cre; Trim28*$^{fl/-}$ embryos in contrast to the ruffled yolk sacs of *Zfp568* embryos indicates that removal of TRIM28 was not complete, and that small amounts of TRIM28 were sufficient to restore yolk sac defects (Figure 3.7). Unfortunately, a complete removal of TRIM28 through tetraploid complementation analysis by aggregating tetraploid embryos with ES cells mutant for *Trim28* (Tam and Rossant, 2003) cannot be tested, as TRIM28 is required to maintain pluripotency of ES cells (Hu et al., 2009).

Interestingly, removal of *Smad4*, an effector of *TGFβ* signaling, from embryonic cell types through tetraploid complementation experiments or with the use of a conditional allele causes embryonic arrest at E8.5 and failure of foregut and hindgut pocket formation, similar to phenotypes in *Sox2Cre; Trim28*$^{fl/-}$ embryos (Sirard et al., 1998; Chu et al., 2004). However, *Smad4* chimeras are not identical to *Sox2Cre; Trim28*$^{fl/-}$ embryos. For instance, defects such as fusion of somites across the midline are seen in *Smad4* chimeras but not in *Sox2Cre; Trim28*$^{fl/-}$ embryos. One hypothesis is that within embryonic cells, SMAD4 and ZFP568-TRIM28 may share some, though not all downstream targets.

Although TRIM28 has been found to bind to over 3000 genes in ES cells (Hu et al., 2009), targets for TRIM28 within embryonic cells during development remain unknown. Future studies aimed at the identifying targets of TRIM28 and ZFP568 in the embryo will be informative for understanding how TRIM28 and ZFP568 control embryonic morphogenesis (see Appendix C). Identification of KRAB zinc finger proteins that may mediate functions of TRIM28 in tissues such as the trophoblast cells could also shed light on functions of individual KRAB zinc finger proteins.

CONCLUSIONS

My analysis of the *Trim28*^{chatwo} mutation and tissue specific requirements of *Trim28* show that TRIM28 is required in embryonic cells to mediate functions of KRAB zinc finger protein ZFP568. Despite the abundance of KRAB zinc finger proteins in higher vertebrates, functions of TRIM28 during embryonic morphogenesis appear to be mediated predominantly by ZFP568. My findings also indicate a requirement for TRIM28 in extraembryonic tissues. Although reasons for the expansion of KRAB zinc finger proteins in tetrapod vertebrates remain unknown, it is possible that some KRAB zinc finger proteins may have evolved specialized functions for the control of early embryonic development in mammals.

ACKNOWLEDGEMENTS

We thank Drs. Ken Kemphues, Paul Soloway, and Garcia lab members for helpful discussions and comments; Drs. Kathryn Anderson and Karel Liem for the *chatwo* mice, and CARE for technical help; Drs. Ruth Arkell, Debbie Chapman, Vincent Giguère and Kathleen McGrath for reagents. This work was supported by NSF (IOS-1020878) and NIH (HD060581) grants to Maria Garcia-Garcia.

REFERENCES

Cammas, F., Mark, M., Dolle, P., Dierich. A., Chambon, P., and Losson, R. (2000). Mice lacking the transcriptional corepressor TIF1beta are defective in early postimplantation development. *Development*, **127**, 2955-2963.

Candia, A. F., Hu, J., Crosby, J., Lalley, P. A., Noden, D., Nadeau, J. H., and Wright, C. V. (1992). Mox-1 and Mox-2 define a novel homeobox gene subfamily and are differentially expressed during early mesodermal patterning in mouse embryos. *Development*, **116**, 1123-1136.

Chapman, D. L., Garvey, N., Hancock, S., Alexiou, M., Agulnik, S. I., Gibson-Brown, J. J., Cebra-Thomas, J., Bollag, R. J., Silver, L. M., and Papaioannou, V. E. (1996). Expression of the T-box family genes, Tbx1-Tbx5, during early mouse development. *Dev Dyn*, **206**, 379–90.

Chu, G. C., Dunn, N. R., Anderson, D. C., Oxburgh, L., and Robertson, E. J. (2004). Differential requirements for Smad4 in TGFβ-dependent patterning of the early mouse embryo. *Development*, **131**, 3501 -3512.

Collignon, J., Sockanathan, S., Hacker, A., Cohen-Tannoudji, M., Norris, D., Rastan, S., Stevanovic, M., Goodfellow, P. N., and Lovell-Badge, R. (1996). A comparison of the properties of Sox-3 with Sry and two related genes, Sox-1 and Sox-2. *Development*, **122**, 509-520.

Emerson, R. and Thomas, J. (2009). Adaptive Evolution in Zinc Finger Transcription Factors. *PLoS Genetics*.

Firulli, A. B., McFadden, D. G., Lin, Q., Srivastava, D., and Olson, E. N. (1998). Heart and extra-embryonic mesodermal defects in mouse embryos lacking the bHLH transcription factor Hand1. *Nature genetics*, **18**, 266–70.

Garcia-Garcia, M. J., Shibata, M., and Anderson, K. V. (2008). Chato, a KRAB zinc-finger protein, regulates convergent extension in the mouse embryo. *Development*, **135**, 3053–3062.

Hayashi, S., Lewis, P., Pevny, L., and McMahon, A. P. (2002). Efficient gene modulation in mouse epiblast using a Sox2Cre transgenic mouse strain. *Mechanisms of development*, **119 Suppl 1**, S97-S101.

Ho, J., Kong, J., Choong, L., Loh, M., Toy, W., Chong, P., Wong, C., Wong, C., Shah, N., and Lim, Y. (2009). Novel Breast Cancer Metastasis-Associated Proteins. *Journal of Proteome Research*, **8**, 583-594.

Hu, G., Kim, J., Xu, Q., Leng, Y., Orkin, S. H., and Elledge, S. J. (2009). A

genome-wide RNAi screen identifies a new transcriptional module required for self-renewal. *Genes & Development*, **23**, 837–48.

Jakobsson, J., Cordero, M. I., Bisaz, R., Groner, A. C., Busskamp, V., Bensadoun, J., Cammas, F., Losson, R., Mansuy, I. M., Sandi, C., et al. (2008). KAP1-mediated epigenetic repression in the forebrain modulates behavioral vulnerability to stress. *Neuron*, **60**, 818–31.

Krebs, C. J., Larkins, L. K., Price, R., Tullis, K. M., Miller, R. D., and Robins, D. M. (2003). Regulator of sex-limitation (Rsl) encodes a pair of KRAB zinc-finger genes that control sexually dimorphic liver gene expression. *Genes & Development*, **17**, 2664-2674.

Law, S. W. and Dugaiczyk, A. (1981). Homology between the primary structure of [alpha]-fetoprotein, deduced from a complete cDNA sequence, and serum albumin. *Nature*, **291**, 201-205.

Li, X., Ito, M., Zhou, F., Youngson, N., Zuo, X., Leder, P., and Ferguson-Smith, A. C. (2008). A maternal-zygotic effect gene, Zfp57, maintains both maternal and paternal imprints. *Developmental cell*, **15**, 547-557.

Liem, K. F., He, M., Ocbina, P. J. R., and Anderson, K. V. (2009). Mouse Kif7/Costal2 is a cilia-associated protein that regulates Sonic hedgehog signaling. *Proceedings of the National Academy of Sciences*.

Luo, J., Sladek, R., Bader, J. A., Matthyssen, A., Rossant, J., and Giguère, V. (1997). Placental abnormalities in mouse embryos lacking the orphan nuclear receptor ERR-beta. *Nature*, **388**, 778–82.

Mahlapuu, M., Ormestad, M., Enerbäck, S., and Carlsson, P. (2001). The forkhead transcription factor Foxf1 is required for differentiation of extra-embryonic and lateral plate mesoderm. *Development*, **128**, 155–66.

McGrath, K. E., Koniski, A. D., Malik, J., and Palis, J. (2003). Circulation is established in a stepwise pattern in the mammalian embryo. *Blood*, **101**, 1669-1676.

Moran, J. L., Bolton, A. D., Tran, P. V., Brown, A., Dwyer, N. D., Manning, D. K., Bjork, B. C., Li, C., Montgomery, K., Siepka, S. M., et al. (2006). Utilization of a whole genome SNP panel for efficient genetic mapping in the mouse. *Genome Research*, **16**, 436-440.

Peng, H., Begg, G. E., Schultz, D. C., Friedman, J. R., Jensen, D. E., Speicher, D. W., and Rauscher III, F. J. (2000). Reconstitution of the KRAB-KAP-1 repressor complex: a model system for defining the molecular anatomy of

RING-B box-coiled-coil domain-mediated protein-protein interactions. *Journal of Molecular Biology*, **295**, 1139-1162.

Quertermous, E. E., Hidai, H., Blanar, M. A., and Quertermous, T. (1994). Cloning and characterization of a basic helix-loop-helix protein expressed in early mesoderm and the developing somites. *Proc. Natl. Acad. Sci. U.S.A*, **91**, 7066-7070.

Rossant, J. and Cross, J. C. (2001). Placental development: Lessons from mouse mutants. *Nat Rev Genet*, **2**, 538-548.

Rowe, H. M., Jakobsson, J., Mesnard, D., Rougemont, J., Reynard, S., Aktas, T., Maillard, P. V., Layard-Liesching, H., Verp, S., Marquis, J., et al. (2010). KAP1 controls endogenous retroviruses in embryonic stem cells. *Nature*, **463**, 237–240.

Schultz, D. C., Friedman, J. R., and Rauscher, F. J. (2001). Targeting histone deacetylase complexes via KRAB-zinc finger proteins: the PHD and bromodomains of KAP-1 form a cooperative unit that recruits a novel isoform of the Mi-2α subunit of NuRD. *Genes & Development*, **15**, 428-443.

Shibata, M. and Garcia-Garcia, M. (2010). The mouse KRAB Zinc-Finger protein CHATO is required in embryonic-derived tissues to control yolk sac and placenta morphogenesis. *Dev. Biol*.

Sirard, C., de la Pompa, J. L., Elia, A., Itie, A., Mirtsos, C., Cheung, A., Hahn, S., Wakeham, A., Schwartz, L., Kern, S. E., et al. (1998). The tumor suppressor gene Smad4/Dpc4 is required for gastrulation and later for anterior development of the mouse embryo. *Genes & Development*, **12**, 107-119.

Tallquist, M. and Soriano, P. (2000). Epiblast-restricted Cre expression in MORE mice: a tool to distinguish embryonic vs. extra-embryonic gene function. *Genesis*.

Tam, P. P. L. and Loebel, D. A. F. (2007). Gene function in mouse embryogenesis: get set for gastrulation. *Nat Rev Genet*, **8**, 368-381.

Tam, P. P. L. and Rossant, J. (2003). Mouse embryonic chimeras: tools for studying mammalian development. *Development*, **130**, 6155 -6163.

Urrutia, R. (2003). KRAB-containing zinc-finger repressor proteins. *Genome biology*, **4**, 231.

Weber, P., Cammas, F., Gerard, C., Metzger, D., Chambon, P., Losson, R., and Mark, M. (2002). Germ cell expression of the transcriptional co-repressor

TIF1beta is required for the maintenance of spermatogenesis in the mouse. *Development*, **129**, 2329–37.

Wilkinson, D. G., Bhatt, S., and Herrmann, B. G. (1990). Expression pattern of the mouse T gene and its role in mesoderm formation. *Nature*, **343**, 657-659.

Wolf, D. and Goff, S. P. (2009). Embryonic stem cells use ZFP809 to silence retroviral DNAs. *Nature*, **458**, 1201–1204.

Zeng, L., Yap, K., Ivanov, A., Wang, X., and Mujtaba, S. (2008). Structural insights into human KAP1 PHD finger–bromodomain and its role in gene silencing. *Nature Structural & Molecular Biology*.

CHAPTER 4

CONCLUSIONS AND FUTURE DIRECTIONS[1]

[1] Reference Shibata and Garcia-Garcia (2010) of this chapter is also Chapter 2.

Tetrapod vertebrates have evolved a large family of Zinc finger proteins containing Kruppel Associated Box (KRAB) domains (Urrutia, 2003). Although it has been proposed that these proteins may have functions specific to higher vertebrates, reasons for the evolutionary expansion of this family are not well understood. The goal of this dissertation was to study the role of a specific KRAB zinc finger protein, ZFP568, and its partner TRIM28 in mouse embryonic development. In this chapter, I present overall conclusions from my work and provide ideas for future studies.

Control of extraembryonic development in the mouse by ZFP568

Prior studies on *chato,* a recessive embryonic lethal mouse mutation affecting the KRAB zinc finger protein ZFP568, revealed a role of this protein in embryonic axis elongation (Garcia-Garcia et al., 2008). The *chato* mutation creates a leucine to proline amino acid change in the KRAB domain of ZFP568, completely disrupting ZFP568 function (Garcia-Garcia et al., 2008).

In Chapter 2 of this thesis, I presented results indicating that *Zfp568*^{chato} mutants display severe abnormalities in the development of extraembryonic tissues. Defects in *Zfp568*^{chato} embryos include bubble-like protrusions in the yolk sac, a detachment of the visceral endoderm from the underlying extraembryonic mesoderm, defective extraembryonic mesoderm migration, and failure of placental development (Shibata and Garcia-Garcia, 2010). In order to identify the tissue requirements of *Zfp568* during embryogenesis, I assayed the phenotype of embryonic chimeras. Tetraploid chimeras formed of wild type extraembryonic cell types (visceral endoderm and trophectoderm) and mutant embryonic-derived tissues (including extraembryonic mesoderm) displayed identical defects to *Zfp568*^{chato} mutant embryos, indicating that wild type *Zfp568* function in extraembryonic lineages is not sufficient to rescue defects in *Zfp568*^{chato} mutants. However, reverse chimeras obtained through a

conditional *Zfp568* genetrap allele showed that *Zfp568* mutant defects in both embryonic and extraembryonic tissues were rescued by the endogenous expression of *Zfp568* in embryonic tissues and extraembryonic mesoderm. Altogether, these results revealed requirements for ZFP568 in embryonic-derived tissues to control embryonic and extraembryonic morphogenesis.

It is not clear whether a functional ortholog for mouse ZFP568 exists in other tetrapod vertebrates. Comparisons of human, chimpanzee, mouse and dog genomes have revealed a list of 103 conserved KRAB zinc finger genes (Huntley et al., 2006). However, establishing the evolutionary and functional relationships between KRAB zinc finger sequences across genomes can be difficult, due to the large number and recent expansion of KRAB zinc finger genes in tetrapod vertebrate genomes. Further studies will be needed to determine whether *Zfp568* functions are conserved in other organisms.

Whether ZFP568 may be involved in the control of morphogenesis during other developmental events at later stages of embryogenesis in the mouse also remains to be investigated. *Zfp568* expression is ubiquitous during early embryonic development (M. Harden, personal communication, Garcia-Garcia et al., 2008; Shibata and Garcia-Garcia), suggesting possible functions in additional developmental processes. Initial attempts to create a conditional allele for removal of *Zfp568* from specific cell types using the *Zfp568* genetrap allele are described in Appendix A. Because *Zfp568* mutant embryos are embryonic lethal at E9.5, the creation of viable mice carrying a conditional *Zfp568* allele will be necessary to assess ZFP568 function at later timepoints in development.

ZFP568 functions are mediated by TRIM28

Two lines of evidence suggest that TRIM28, the proposed universal co-repressor of all KRAB zinc finger proteins (Urrutia, 2003) is a co-factor of ZFP568. First, TRIM28 has been identified as a binding partner of ZFP568 in yeast two hybrid assays (Kristin Blauvelt, personal communication). Second, I have found that *Trim28*^{chatwo} mutants display defects in convergent extension and yolk sac morphogenesis similar to those of *Zfp568*^{chato} mutants (Chapter 3). The ENU-induced *Trim28*^{chatwo} mutation is a hypormophic allele, creating novel missense mutations in two adjacent amino acids in the bromodomain of TRIM28 (Chapter 3). Moreover, epistasis analysis showed that the phenotype of *Zfp568*^{chato}*; Trim28*^{chatwo} double mutants is most similar to that of *Trim28*^{chatwo} embryos, suggesting that the genes affected by both mutations disrupt the same molecular processes. Altogether, these results provide molecular and genetic evidence that the ZFP568-TRIM28 interaction is important for embryonic morphogenesis. These findings are significant, as they show that TRIM28 is required to mediate functions of KRAB zinc finger proteins during embryonic development.

Requirements for TRIM28 and additional KRAB zinc finger proteins during embryonic development

Through phenotypic characterization, quantification of TRIM28 protein levels and complementation analysis with the *Trim28* null allele, I have shown that *Trim28*^{chatwo} generates a hypomorphic allele unable to mediate ZFP568 functions (Chapter 3). However, the severity of the *Trim28* null (*Trim28*$^{-/-}$) mutants, which fail to gastrulate and arrest shortly after implantation (Cammas et al., 2000), as compared to *Trim28*^{chatwo} indicates that TRIM28 has ZFP568-independent functions at early developmental stages which may be mediated by other yet unidentified KRAB zinc finger proteins.

My analysis of *Trim28* chimeric (*Sox2Cre; Trim28*$^{fl/-}$) embryos presented in Chapter 3 suggested ZFP568-independent requirements for TRIM28 in visceral endoderm, trophoblast cells, or both, during early postimplantation development. As high levels of *Trim28* expression are not detected in the visceral endoderm (Chapter 3, Cammas et al., 2000), TRIM28 is likely to be required specifically in the trophoblast. It is possible that additional KRAB zinc finger proteins mediating functions of TRIM28 are important for trophoblast development. To fully understand requirements for TRIM28 during embryonic development, further studies in identifying functions of other KRAB zinc finger proteins will be necessary.

Determining targets of ZFP568 and TRIM28

Although KRAB zinc finger proteins have been proposed to direct a TRIM28 associated transcriptional repression complex to specific regions of the genome, it has been difficult to identify the binding sites and genes regulated by specific KRAB zinc finger proteins. In Chapter 2, I presented results indicating that expression levels of *Fibronectin* and *Indian Hedgehog* were reduced in *Zfp568*^{null} yolk sacs. Further studies are needed to understand whether these genes are direct targets of *Zfp568.*

Fibronectin and *Indian Hedgehog* are likely not the only genes affected in *Zfp568* mutants, therefore, the identification of additional molecules regulated by *Zfp568* will be important for understanding how ZFP568 and its partner TRIM28 control embryonic and extraembryonic development. To this end, I have conducted a preliminary microarray analysis to identify genes misregulated in *Zfp568*^{null} and *Trim28*^{chatwo} embryos at E7.75 (Appendix C). It is likely that some of the genes identified from the analysis will be direct targets of ZFP568 and TRIM28.

As KRAB zinc finger proteins are proposed to bind DNA (Urrutia, 2003), identification of DNA binding sites for ZFP568 through ChIP-sequencing would

expand the understanding of the molecular mechanisms through which ZFP568 controls embryonic morphogenesis. Unfortunately, several attempts in the Garcia lab to create ZFP568 specific antibodies have been unsuccessful. The creation of a knock-in allele for *Zfp568* by homologous recombination to create a ZFP568 protein with a tag sequence such as a tandem affinity purification (TAP) tag would allow for the identification of targets for endogenously expressed ZFP568 during embryonic development. Such experiments would be useful to evaluate whether ZFP568 binds to promoters of genes such as *Hand1* and *Yap1*, which are essential for extraembryonic development, and cause similar defects to $Zfp568^{chato}$ and $Trim28^{chatwo}$ when mutated (Morin-Kensicki et al., 2006; Riley et al., 1998).

Analysis of the subcellular localization of a tagged ZFP568 protein during embryonic development would be useful for determining whether ZFP568 localizes exclusively in the nucleus. Although the similarities between the *Zfp568* and $Trim28^{chatwo}$ mutant phenotypes suggest that many functions of ZFP568 are mediated by TRIM28, studies of subcellular localization of tagged ZFP568 proteins in cell culture have revealed both nuclear and cytoplasmic ZFP568 localization (Chapter 3, Appendix B), suggesting that ZFP568 may also have functions independent of TRIM28.

In summary, the characterization of $Zfp568^{chato}$ and $Trim28^{chatwo}$ mutant phenotypes and analysis of tissue specific requirements of *Zfp568* and *Trim28* presented in this thesis have expanded our knowledge of the biological functions of KRAB zinc finger proteins and their binding partners during mouse embryonic development. Future studies should be directed at understanding the downstream molecular functions and targets of these proteins.

REFERENCES

Cammas, F., Mark, M., Dollé, P., Dierich, A., Chambon, P., and Losson, R. (2000). Mice lacking the transcriptional corepressor TIF1beta are defective in early postimplantation development. *Development*, **127**, 2955-2963.

Garcia-Garcia, M. J., Shibata, M., and Anderson, K. V. (2008). Chato, a KRAB zinc-finger protein, regulates convergent extension in the mouse embryo. *Development*, **135**, 3053–3062.

Huntley, S., Baggott, D. M., Hamilton, A. T., Tran-Gyamfi, M., Yang, S., Kim, J., Gordon, L., Branscomb, E., and Stubbs, L. (2006). A comprehensive catalog of human KRAB-associated zinc finger genes: insights into the evolutionary history of a large family of transcriptional repressors. *Genome Res*, **16**, 669–77.

Morin-Kensicki, E. M., Boone, B. N., Howell, M., Stonebraker, J. R., Teed, J., Alb, J. G., Magnuson, T. R., O'Neal, W., and Milgram, S. L. (2006). Defects in yolk sac vasculogenesis, chorioallantoic fusion, and embryonic axis elongation in mice with targeted disruption of Yap65. *Mol Cell Biol*, **26**, 77–87.

Riley, P., Anson-Cartwright, L., and Cross, J. C. (1998). The Hand1 bHLH transcription factor is essential for placentation and cardiac morphogenesis. *Nature genetics*, **18**, 271–275.

Shibata, M. and Garcia-Garcia, M. (2010). The mouse KRAB Zinc-Finger protein CHATO is required in embryonic-derived tissues to control yolk sac and placenta morphogenesis. *Dev. Biol*.

Urrutia, R. (2003). KRAB-containing zinc-finger repressor proteins. *Genome biology*, **4**, 231.

APPENDIX A

CHARACTERIZATION OF A HYPOMORPHIC ALLELE FOR ZFP568

INTRODUCTION

In Chapter 2, I showed that ZFP568, a Kruppel-Associated-Box (KRAB) domain zinc finger protein, is required in embryonic and embryonic derived extraembryonic mesoderm cells for proper development of embryonic and extraembryonic tissues in the mouse. One of the *Zfp568* alleles described in Chapter 2, *Zfp568*$^{rGT\text{-}restored}$, created a hypomorphic allele of *Zfp568,* with *Zfp568*$^{rGT\text{-}restored/null}$ embryos only expressing 10% of wild type *Zfp568* transcript levels (Shibata and Garcia-Garcia, 2010). Surprisingly, 54% of *Zfp568*$^{rGT\text{-}restored/null}$ embryos looked wild type at embryonic day (E) 9.5, suggesting that a small amount of *Zfp568* was sufficient for development until that developmental stage (Shibata and Garcia-Garcia, 2010). Here I present results from characterization of phenotypes of *Zfp568*$^{rGT\text{-}restored/null}$ embryos at E8.5 and E9.5. My findings indicate that high levels of *Zfp568* are required for embryonic viability after E9.5. In addition, I report results from analysis of *Sox2Cre; Zfp568*$^{rGT\text{-}restored/null}$ embryos, in which *Zfp568* was removed from embryonic cell types. Additional studies to understand requirements for *Zfp568* after E9.5 will require the creation of a conditional allele that, unlike *Zfp568*$^{rGT\text{-}restored,}$ does not disrupt *Zfp568* function in its wild type configuration.

MATERIALS AND METHODS

The *Zfp568*$^{rGT\text{-}mutant}$ reversible allele was generated as previously described (Shibata and Garcia-Garcia, 2010). The *Zfp568*$^{rGT\text{-}restored}$ allele was created by breeding *Zfp568*$^{rGT\text{-}mutant/+}$ mice to FLPe (B6.Cg-Tg(ACTFLPe)9205Dym/J) mice from Jackson

Laboratories. *Sox2Cre; Zfp568*$^{rGT\text{-}restored/null}$ chimeras were generated by crossing *Sox2Cre; Zfp568*$^{+/null}$ males to *Zfp568*$^{rGT\text{-}resotred/+}$ females.

RESULTS AND DISCUSSION

Characterization of *Zfp568*$^{rGT\text{-}restored/null}$ embryos

Despite only expressing around 10% of wild type levels of *Zfp568,* 54% of *Zfp568*$^{rGT\text{-}restored/null}$ embryos lacked yolk sac and embryonic defects of *Zfp568*^{chato} embryos at E9.5 (Figure A.1A-B, Shibata and Garcia-Garcia, 2010). To assess whether a small amount of *Zfp568* is sufficient for normal embryonic development past E9.5, I characterized the embryonic and extraembryonic phenotypes of *Zfp568*$^{rGT\text{-}restored/null}$ embryos. Removal of extraembryonic tissues from *Zfp568*$^{rGT\text{-}restored/null}$ embryos revealed severe neurulation defects in many *Zfp568*$^{rGT\text{-}restored/null}$ embryos. Whereas neural tube closure is initiated around E8.5 in wild type embryos (Copp et al., 2003), unfused neural folds were detected in *Zfp568*$^{rGT\text{-}restored/null}$ embryos at E9.5 (Figure A1.D-E, arrowheads). Since defects in neural tube closure can be caused secondarily by other defects, including a delay in development or a failure to establish proper maternal-embryonic connections (Copp et al., 2003), I sectioned *Zfp568*$^{rGT\text{-}restored/null}$ embryos at E8.5 to assess whether other defects could be detected. Whereas all wild type littermates sectioned had established a chorio-allantoic connection (Figure A.1F), 4/4 *Zfp568*$^{rGT\text{-}restored/null}$ embryos displayed an irregular shaped allantois that had failed to unite with the chorion (Figure A.1G-H, arrowheads). Although *Zfp568*$^{rGT\text{-}restored/null}$ embryos did not contain as severe chorionic defects as those characteristic of *Zfp568*^{chato} and *Zfp568*^{null} embryos (Shibata and Garcia-Garcia, 2010), the allantois defects of *Zfp568*$^{rGT\text{-}restored/null}$ likely prevent the formation of a placenta and contribute to embryonic lethality.

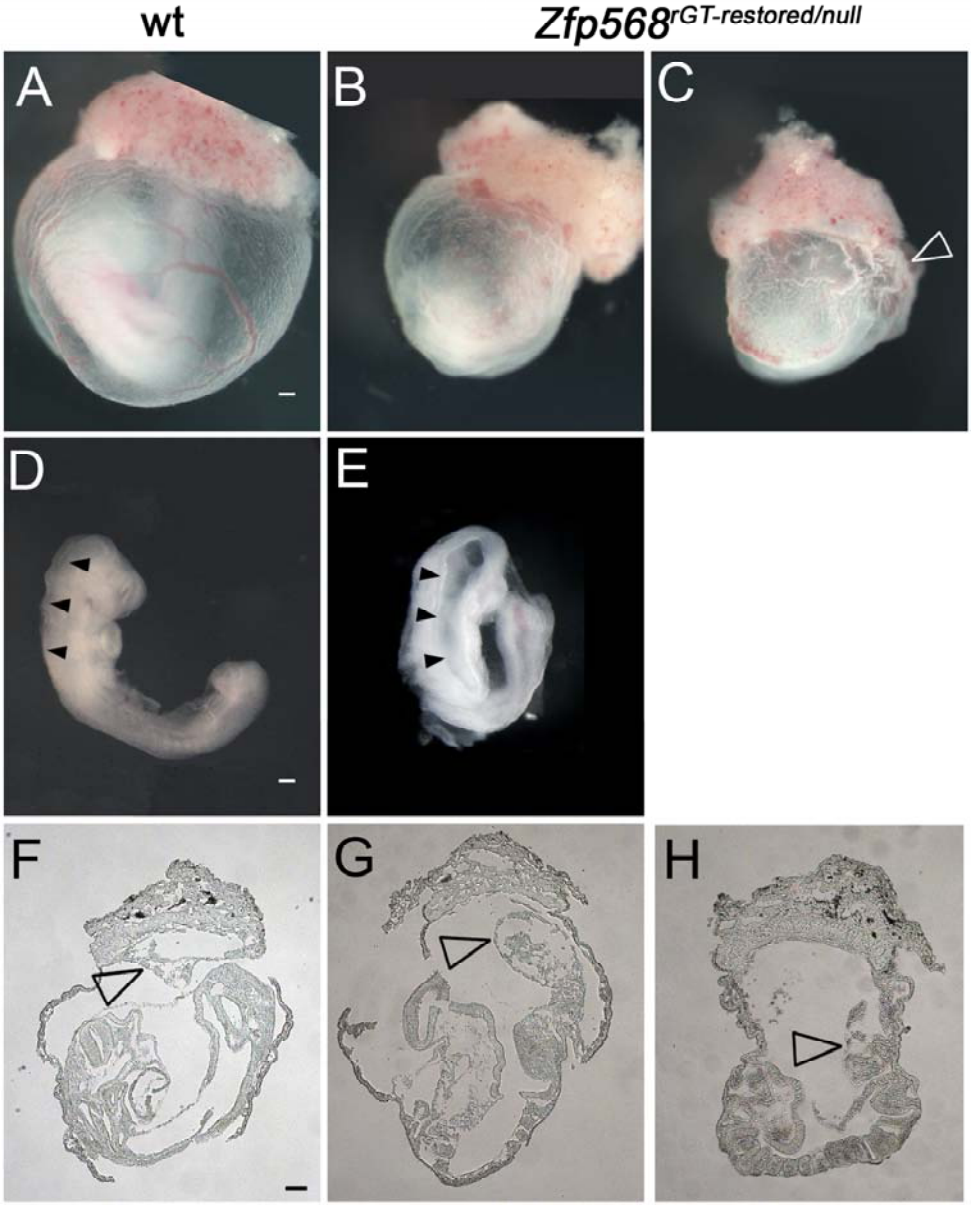

Figure A.1. *Zfp568*$^{rGT\text{-}restored/null}$ embryos display neuronal and allantois defects. **(A-C)** At E9.5, some *Zfp568*$^{rGT\text{-}restored/null}$ embryos displayed a smooth yolk sac (B) whereas other *Zfp568*$^{rGT\text{-}restored/null}$ embryos displayed a ruffled yolk sac (C, arrowhead). Wild type littermate embryos display a smooth yolk sac and have completed embryonic turning (A). **(D-E)** Wild type (D) and *Zfp568*$^{rGT\text{-}restored/null}$ (E) embryos with yolk sacs removed. Note the open neural tube in the *Zfp568*$^{rGT\text{-}restored/null}$ embryo in E compared to D (arrowheads). **(F-H)** Sagittal sections of wild type (F) and *Zfp568*$^{rGT\text{-}restored/null}$ (G,H) embryos. Arrowheads point to allantois. Scale bars represent 100μm.

Zfp568$^{rGT\text{-}restored}$ animals arrest prior to E10.5

To establish whether homozygous *Zfp568*$^{rGT\text{-}restored}$ animals, predicted to have 20% of wild type levels of *Zfp568* were viable, *Zfp568*$^{rGT\text{-}restored/+}$ females were bred with *Zfp568*$^{rGT\text{-}restored/+}$ males and resulting pups were genotyped. Out of 36 total pups from 5 litters, 24 pups were *Zfp568*$^{rGT\text{-}restored/+}$, and 14 pups were homozygous wild type. According to Mendelian ratios, 12 homozygous *Zfp568*$^{rGT\text{-}restored}$ pups were expected, yet none were obtained. This suggested that *Zfp568*$^{rGT\text{-}restored}$ embryos were embryonic lethal, and that low levels of *Zfp568* were not sufficient for embryos to complete gestation.

Homozygous *Zfp568*$^{rGT\text{-}restored}$ embryos from two litters were examined between the ages of E9.5 and E10.5 (n=4). One *Zfp568*$^{rGT\text{-}restored}$ embryo that looked wild type in appearance was obtained at E9.5. Another *Zfp568*$^{rGT\text{-}restored}$ embryo from the same litter contained a bulbous allantois that was not connected to the chorion, similar to defects observed in *Zfp568*$^{rGT\text{-}restored/null}$ embryos (Figure A.1G). Two embryos dissected at E10.5 displayed yolk sac hemorrhages and had failed to complete embryonic turning, an event that normally occurs around E8.5. From these preliminary results, it appears that the majority of homozygous *Zfp568*$^{rGT\text{-}restored}$ embryos arrest prior to E10.5, displaying defects similar to *Zfp568*$^{rGT\text{-}restored/null}$ embryos in the yolk sac, allantois, or in embryonic turning.

Altogether, these results suggest that a small amount (~10% expression) of *Zfp568* is sufficient for embryos to initiate embryonic turning and for restoration of normal chorionic development. However, neural tube closure, yolk sac vascular network formation and proper placental development require higher levels of *Zfp568* expression.

Removal of *Zfp568* from embryonic cell types of *Zfp568*$^{rGT\text{-}restored/null}$ embryos

The orientation of the gene trap insertion in the mutant *Zfp568* reversible allele (*Zfp568*$^{rGT\text{-}mutant}$) described in Chapter 2 can be reversed with either Flippase recombination enzyme (FLP) or Cre recombinase, as the gene trap insertion is flanked by FRT and loxP recombination sites (Figure A.2A, Schnütgen et al., 2005, Shibata and Garcia-Garcia, in press). Using a ubiquitously expressed FLP recombinase, I generated a *Zfp568*$^{rGT\text{-}restored}$ allele that could be used to remove *Zfp568* from specific cell types with Cre recombinase, as the loxP sites remained intact (Figure A.2A). An embryonic and extraembryonic mesoderm specific *Sox2-Cre* line was then used to generate chimeric embryos containing *Zfp568* mutant embryonic and extraembryonic mesoderm cells and low levels of *Zfp568* in visceral endoderm (VE) and trophoblast cells (*Sox2Cre; Zfp568*$^{GT\text{-}restored/null}$, Figure A.2).

Sox2Cre mediated removal of *Zfp568* from the embryo resulted in surprisingly mild phenotypes compared to results from tetraploid complementation assays, where *Zfp568* was also removed from embryonic and extraembryonic mesoderm cells (Shibata and Garcia-Garcia, 2010). Since the *Zfp568*$^{rGT\text{-}mutant}$ allele (but not the *Zfp568*$^{GT\text{-}restored}$ allele) generates a β-geo fusion protein (Figure A.2A), the effectiveness of the Cre-mediated recombination in *Sox2Cre; Zfp568*$^{GT\text{-}restored/null}$ chimeras was confirmed by X-gal staining. This experiment confirmed that, despite Cre-mediated recombination at the Zfp568 locus in *Sox2Cre; Zfp568*$^{GT\text{-}restored/null}$ chimeras in both the embryo and extraembryonic mesoderm (Figure A.2B-E), severe yolk sac ruffling and embryonic axis elongation defects characteristic of *Zfp568* mutant embryos were not observed (n=7, Figure A.2). The mild phenotype of *Sox2Cre; Zfp568*$^{rGT\text{-}restored/null}$ embryos compared to embryos where *Zfp568* was completely removed from the embryo using tetraploid complementation assays suggests that complete removal of *Zfp568* from embryonic cell types was not obtained

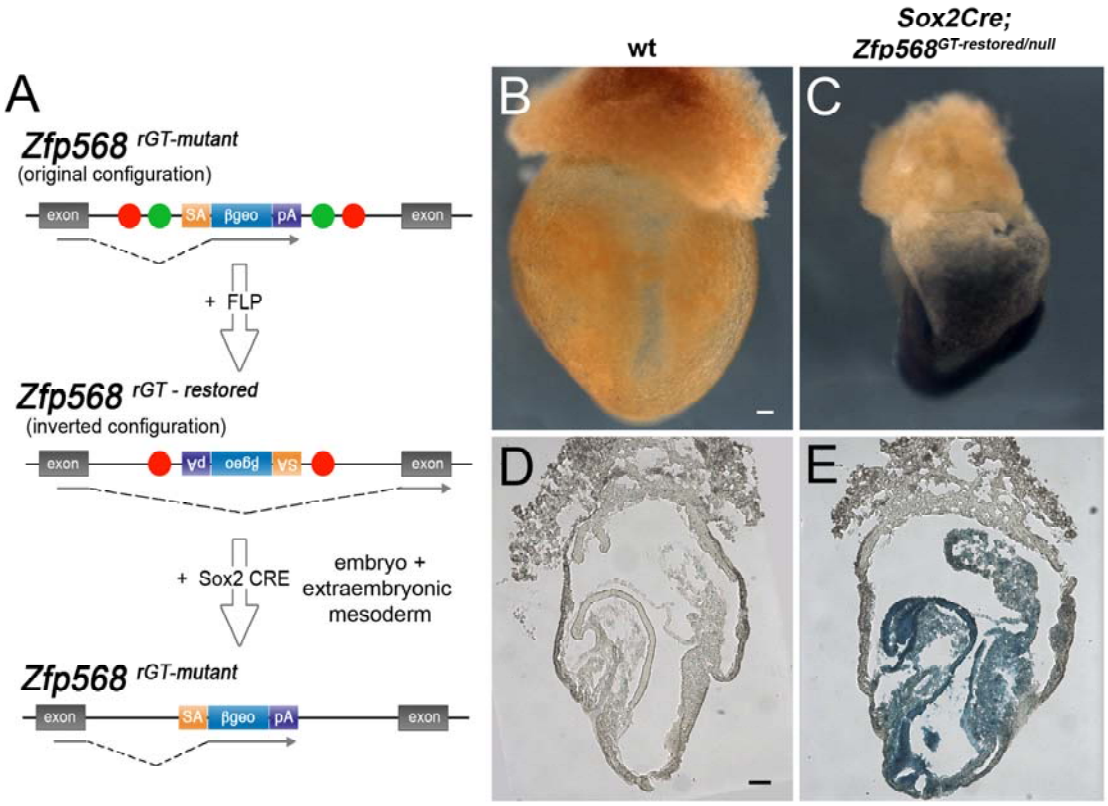

Figure A.2. Characterization of *Sox2Cre; Zfp568*$^{GT\text{-}restored/null}$ embryos. (A) A *Zfp568*$^{GT\text{-}restored}$ allele was generated using FLP, which mediates recombination at *FRT* sites (green circles). *Sox2Cre* was used to remove *Zfp568* specifically from the embryo and extraembryonic mesoderm. Alleles no longer expressing full length *Zfp568* express *β-geo*. Red circles represent loxP sites. Modified from Shibata and Garcia-Garcia, 2010. **(B-E)** Whole mount images of wild type (B) and *Sox2Cre; Zfp568*$^{GT\text{-}restored/null}$ (C) embryos after X-gal staining. Sections of the same embryos are shown in D and E. X-gal positive cells indicate cells from which *Zfp568* has been removed. Scale bars represent 100μm.

in *Sox2Cre; Zfp568*$^{rGT\text{-}restored/null}$ embryos. Although a detailed analysis of *Sox2Cre; Zfp568*$^{rGT\text{-}restored/null}$ embryos was not conducted, these results agree with findings presented in Chapter 2, which suggest that *Zfp568* expression from a few wild type cells in the embryo can rescue yolk sac ruffling and embryonic defects found in *Zfp568* mutant embryos (Shibata and Garcia-Garcia, 2010).

Additional studies to understand requirements for *Zfp568* in neural tube closure, yolk sac vascular network formation and placental development will require the creation of a conditional allele that does not disrupt *Zfp568* function in its wild type configuration.

APPENDIX B

SUBCELLULAR LOCALIZATION OF ZFP568 AND TRIM28

INTRODUCTION

Members of the KRAB zinc finger family have been proposed to act as nuclear transcriptional repressors by binding to DNA and recruiting corepressor proteins (Urrutia, 2003). However, there is also evidence that KRAB zinc proteins modulate activity by interacting with other DNA binding factors. For example, ZFP128 has been identified as a KRAB zinc finger protein that interacts with SMAD proteins to repress TGFβ/BMP targets (Jiao et al., 2002). An interesting possibility is that other KRAB zinc finger family members such as ZFP568 may also bind to SMAD proteins, especially considering that some of the phenotypes observed in *Zfp568*^{chato} mutants are similar to those of TGFβ signaling loss of function mutants. Here I show that GFP tagged ZFP568 is detected both in the nucleus and cytoplasm. Furthermore, I have found that overexpression of MYC tagged TRIM28 can influence the subcellular localization of ZFP568.

MATERIALS AND METHODS

Zfp568 was amplified with primers TCAGATCTCGAGATGGAGCGCTTGTCC-CAGATG and ACCGGTGGATCCCGTTCACTCCTCCGTCCTGTATG from clone E80006K18 (RIKEN) and digested with XhoI and BamHI for ligation into pAcGFP1-C3 and pAcGFP1-N1 vectors. MYC-TRIM28 and MYC-CHATWO expressing vectors are described in Chapter 3. NIH3T3 or HEK293 cells were transiently transfected using Lipofectamine 2000 (Invitogen) or FUGENE 6 (Roche) transfection reagent. Antibodies used were anti-Myc (1:200; 9E10, Hybridoma Bank) and anti-mouse Alexa Fluor 568 (1:200; Molecular Probes).

RESULTS AND DISCUSSION

To study the subcellular localization of ZFP568, vectors expressing wild type ZFP568 fused to a GFP tag were transiently transfected into NIH3T3 mouse fibroblast cells. Whereas a control GFP vector was detected in the nucleus and cytoplasm (Figure A.3A-B), distinct localization patterns were detected for the GFP tagged ZFP568 proteins. In some cells, I detected nuclear localization of GFP tagged ZFP568 (Figure A.3C-F), suggesting that ZFP568 may function as a nuclear transcription factor by binding to DNA and recruiting corepressor proteins, as reported for several other members of the KRAB zinc finger protein family. Interestingly, I also detected localization of GFP tagged ZFP568 in cytoplasmic puncta and fibers, suggesting that ZFP568 may have additional functions outside of the nucleus (Figure A.3E-H). This localization to cytoplasmic fibers was more often observed when GFP was tagged to the N-terminus of ZFP568 (GFP-ZFP568) rather than the C-terminus (ZFP568-GFP) suggesting that the GFP tag may affect the behavior of ZFP568.

Another tagged ZFP568 fusion protein (MYC-ZFP568) transfected into STO fibroblasts (V. Wells, personal communication), and HEK293 cells expressing DsRED tagged ZFP568 (K. Blauvelt, personal communication) showed a subcellular localization similar to GFP-ZFP568, suggesting that ZFP568 is responsible for these localization patterns. The subcellular localization of endogenous ZFP568 in the embryo remains to be determined, as unfortunately, attempts to create ZFP568 specific antibodies have been unsuccessful.

To address whether GFP tagged ZFP568 colocalized with TRIM28, a binding partner for KRAB zinc finger proteins, I created a vector expressing MYC tagged TRIM28. I also created a vector containing the *Trim28*^{chatwo} mutation described in

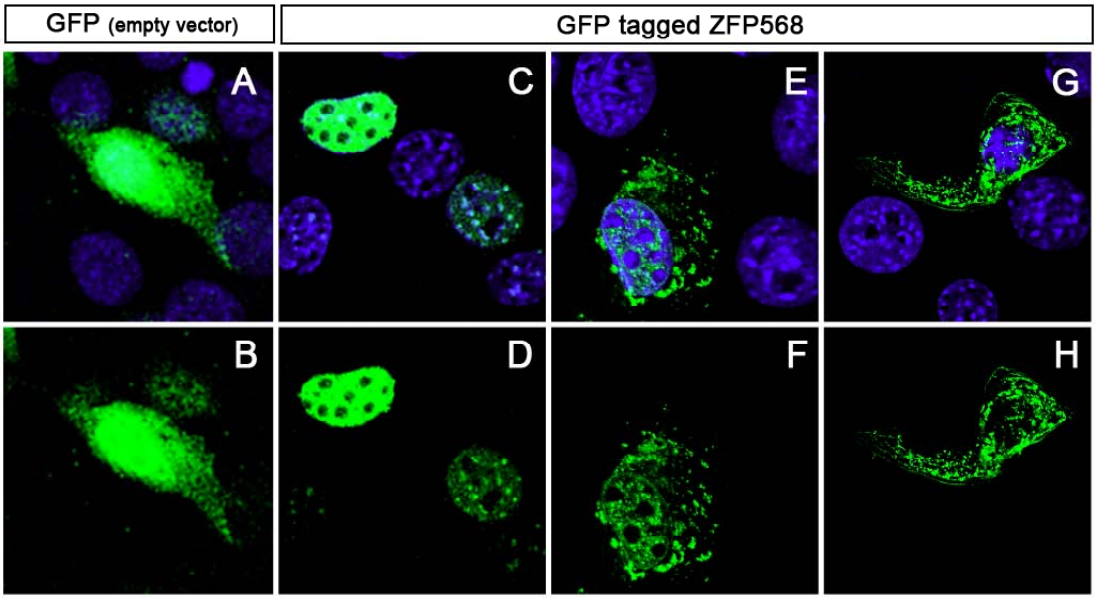

Figure A.3. Subcellular localization of GFP tagged ZFP568. NIH3T3 cells were transiently transfected with empty GFP vector (A-B, green) or GFP tagged ZFP568 (C-H, green) and stained with DAPI (blue). GFP was tagged to both the C-terminus (ZFP568-GFP, C-D) and the N-terminus (GFP-ZFP568, E-H) of ZFP568. Both nuclear and cytoplasmic localization of GFP tagged ZFP568 was observed. Panels B,D,F,H show images from A,C,E,G with DAPI staining overlay removed.

Chapter 3. Transient transfection of Myc tagged *Trim28* or *chatwo* constructs in HEK293 cells revealed similarities and differences in the localization of MYC-CHATWO and MYC-TRIM28 proteins (Figure A.4, A.5). In most transfected cells, both MYC-TRIM28 and MYC-CHATWO localized to the nucleus, although cytoplasmic localization of MYC-TRIM28 and MYC-CHATWO was also detected in some cells. MYC-TRIM28 and MYC-CHATWO often localized to large abnormal regions of chromatin with reduced DAPI staining that appeared as a consequence of MYC-TRIM28 or MYC-CHATWO expression. However, compared to MYC-TRIM28, MYC-CHATWO formed smaller puncta within the nucleus. Although the mechanisms responsible for this altered localization of MYC-CHATWO are unknown, these findings suggest that functions of MYC-TRIM28 are likely altered by the $Trim28^{chatwo}$ mutation.

Co-transfection of ZFP568-GFP with MYC-TRIM28 or MYC-CHATWO did not affect the subcellular localization of MYC-TRIM28 or MYC-CHATWO. However, ZFP568-GFP strongly co-localized with both MYC-TRIM28 and MYC-CHATWO (Figure A.5). These findings support the hypothesis that ZFP568 and TRIM28 form a protein complex in vivo. The $Trim28^{chatwo}$ mutation does not affect the ability of TRIM28 to form a complex with ZFP568, but likely affects other functions of TRIM28.

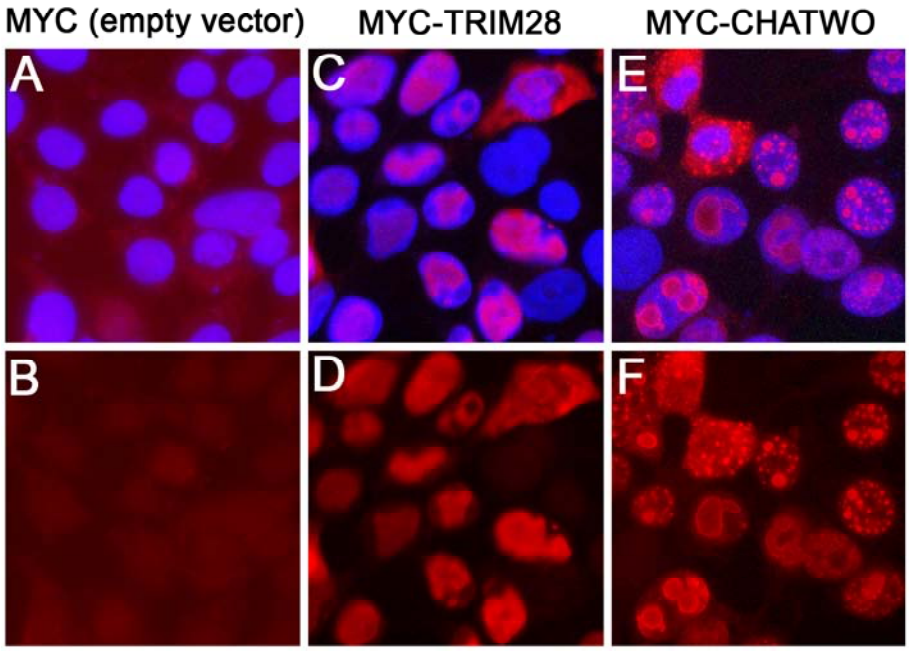

Figure A.4. Subcellular localization of MYC tagged CHATWO. HEK293 cells were transiently transfected with empty MYC vector (A-B, red), MYC-TRIM28 (C-D, red) or MYC-CHATWO (E-F, red) and stained with DAPI (blue). The *Trim28*^{chatwo} mutation affects the subcellular localization of MYC-TRIM28. Panels B,D,F show images from A,C,E with DAPI staining overlay removed.

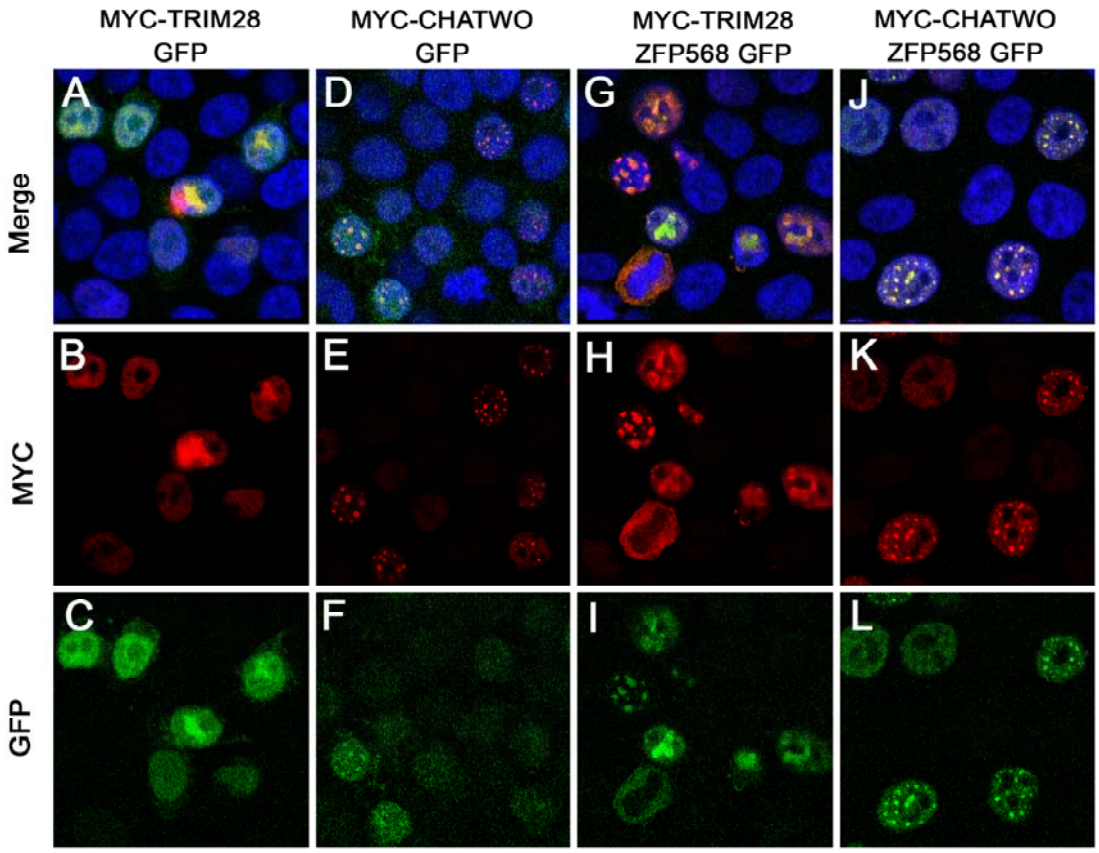

Figure A.5. Colocalization of MYC-TRIM28 and ZFP568-GFP. HEK293 cells were transiently transfected with MYC-TRIM28 (A-C, G-I, red), MYC-CHATWO (D-F, J-L, red), empty GFP vector (A-F, green) or ZFP568-GFP (G-L, green) and DAPI stained (blue). ZFP568-GFP colocalized with both MYC-TRIM28 and MYC-CHATWO. Panels B,E,H,K and C,F,I,J show images from A,D,G,J showing only red (MYC) or green (GFP) channels.

APPENDIX C

MICROARRAY ANALYSIS OF GENE EXPRESSION IN ZFP568, TRIM28 AND HAND1 MUTANTS

INTRODUCTION

The similarity of developmental defects observed in *Zfp568* and *Trim28*^{chatwo} mutants (Chapters 2 and 3, Garcia-Garcia et al., 2008) suggest that ZFP568 and TRIM28 form a protein complex that controls key genes required for embryonic morphogenesis. Mouse mutants for the bHLH transcription factor *Hand1* display defects similar to those of *Zfp568* and *Trim28*^{chatwo} mutants (Firulli et al., 1998; Riley et al., 1998). Although at present a possible relationship between *Hand1*, *Zfp568* and *Trim28* has not been established, it is reasonable to hypothesize that ZFP568-TRIM28 complexes and HAND1 might regulate a common set of genes, ultimately responsible for the morphological abnormalities in these mutants. In order to understand the basis for the phenotypes observed in *Zfp568, Trim28*^{chatwo} and *Hand1* mutants, I conducted a comparative microarray analysis.

MATERIALS AND METHODS

Mouse strains

The *Trim28*^{chatwo} allele used in this study was characterized on the FVB genetic background, as described in Chapter 3. The *Zfp568*^{null} allele was characterized on a CAST/Ei background (Chapter 2, Garcia-Garcia et al., 2008). *Hand1* mutant mice were obtained from Dr. James Cross and genotyped as previously described (Riley et al., 1998).

Microarray analysis

Early headfold to early foregut stage embryos (E7.75) were collected from timed matings and yolk sacs were removed for genotyping. RNA was extracted from pools of 4-6 embryos of the same genotype using the RNeasy Plus Mini RNA purification kit (QIAGEN). For the *Trim28*^{chatwo} sample, RNA was collected from 20 pooled embryos. Independent RNA samples from wild type (3 samples), *Zfp568*^{null} (3 samples), *Hand1*^{null} (3 samples) and *Trim28*^{chatwo}(1 sample) embryos were processed for microarray analysis. aRNA was synthesized using MessageAmp III RNA amplification kit (Ambion) using 200ng of input RNA. Hybridization to Affymetrix Expression Genechip arrays (Mouse genome 430 2.0), processing and statistical analysis was conducted by the Cornell Microarray Facility (Wei Wang and Jacob Kresovich). Gene ontology analysis was conducted using Ingenuity software.

qRT-PCR

qRT-PCR was conducted as previously described using *Gapdh* as a standard (Shibata and Garcia-Garcia, 2010). Primers for analysis of *Hand1* expression were TGAACTCAAAAAGACGGATGG and CTTTAATCCTCTTCTCGCCG.

RESULTS AND DISCUSSION

I carried out microarray analyses to identify genes misregulated in *Zfp568*^{null}, *Trim28*^{chatwo} and *Hand1*^{null} embryos. To maximize the recovery of direct targets of ZFP568, TRIM28 and HAND1, wild type littermates and mutant embryos were collected at early headfold and early foregut stages (E7.75), when morphological defects were not severe. Yolk sacs of embryos were genotyped, and RNA was extracted from pools of 4-6 embryos. The overall yield of RNA obtained from *Zfp568*^{null} and *Hand1*^{null} embryos did not differ from wild type. However, extraction of RNA from *Trim28*^{chatwo} mutants was more challenging, and equivalent amounts of

RNA were obtained only after pooling together 15 mutant embryos. Aside from this exception, samples were processed in parallel and gene expression profiles of *Zfp568*^{null}, *Trim28*^{chatwo} and *Hand1*^{null} embryos were compared to wild type littermates.

In *Zfp568*^{null} mutants compared to wild type embryos, 32 genes were significantly upregulated (Table A.1), whereas 127 genes were downregulated (Figure A.6A). Of the upregulated genes, only one gene, *Hbb-bh1* was upregulated more than 3-fold. On average, the genes that were statistically significantly upregulated in *Zfp568*^{null} embryos were overexpressed 1.7 fold compared to wild type. A slightly larger number of misregulated genes were detected in *Hand1*^{null} mutants, where 174 genes were significantly upregulated, and 264 genes were downregulated (Figure A.6A). Although the results from the *Trim28*^{chatwo} sample are preliminary, as only one sample was analyzed, 107 genes were found to be upregulated more than 3.25 fold, and 197 genes were downregulated more than 3.25 fold (Figure A.6A).

Gene ontology analysis revealed that the genes affected in the mutants are required for diverse molecular and cellular functions (Figure A.7). Genes involved in controlling cell morphology, cellular development, cell-cell signaling and cellular growth and proliferation were overrepresented among the list of misregulated genes.

Interestingly, despite the similarities in the phenotypes of *Zfp568*^{null}, *Trim28*^{chatwo} and *Hand1*^{null} mutants, there was surprisingly little overlap between the genes misregulated in these mutants (Figure A.6B, Table A.2). Only 17 genes, or around 10% of the genes affected in *Zfp568*^{null} embryos were also affected in *Hand1*^{null} embryos. 15 genes, or less than 5% of the genes misregulated in *Trim28*^{chatwo} embryos were also abnormally expressed in *Hand1*^{null} mutants (Figure A.6B).

When only genes misregulated more than 3.25 fold in *Trim28*^{chatwo} mutants were considered, there was only one gene, *Hand1,* commonly misexpressed in all

Table A.1. List of genes upregulated in *Zfp568*^{null} embryos.

Genes upregulated in *Zfp568*^{null} embryos	
Hbb-bh1	hemoglobin Z, beta-like embryonic chain
Mmrn2	multimerin 2
Kdelr3	KDEL (Lys-Asp-Glu-Leu) endoplasmic reticulum protein retention receptor 3
Ldb3	LIM domain binding 3
Aqp3	aquaporin 3
	Gene model 201, (NCBI)
AW550831	Expressed sequence AW550831
2210016H18Rik	RIKEN cDNA 2210016H18 gene
Atp1b1	ATPase, Na+/K+ transporting, beta 1 polypeptide
Rrad	Ras-related associated with diabetes
Cmya1	cardiomyopathy associated 1
Kcnk6	potassium inwardly-rectifying channel, subfamily K, member 6
Socs5	Suppressor of cytokine signaling 5
Mybpc3	myosin binding protein C, cardiac
Sdhc	succinate dehydrogenase complex, subunit C, integral membrane protein
9330161F08Rik	RIKEN cDNA 9330161F08 gene
Tnfsf9	tumor necrosis factor (ligand) superfamily, member 9
2310037P21Rik	RIKEN cDNA 2310037P21 gene
Flrt2	Fibronectin leucine rich transmembrane protein 2
Calr3	calreticulin 3
AW539964	expressed sequence AW539964
1700025B16Rik	RIKEN cDNA 1700025B16 gene
2610528J11Rik	RIKEN cDNA 2610528J11 gene
Uble1a	ubiquitin-like 1 (sentrin) activating enzyme E1A
Adcy9	Adenylate cyclase 9
E130106K10Rik	RIKEN cDNA 130106K10 gene
Tssk4	testis-specific serine kinase 4
Clic5	Chloride intracellular channel 5
2210011C24Rik	RIKEN cDNA 2210011C24 gene
Slc23a1	solute carrier family 23 (nucleobase transporters), member 1
Ttr	transthyretin
9030611O19Rik	RIKEN cDNA 9030611O19 gene

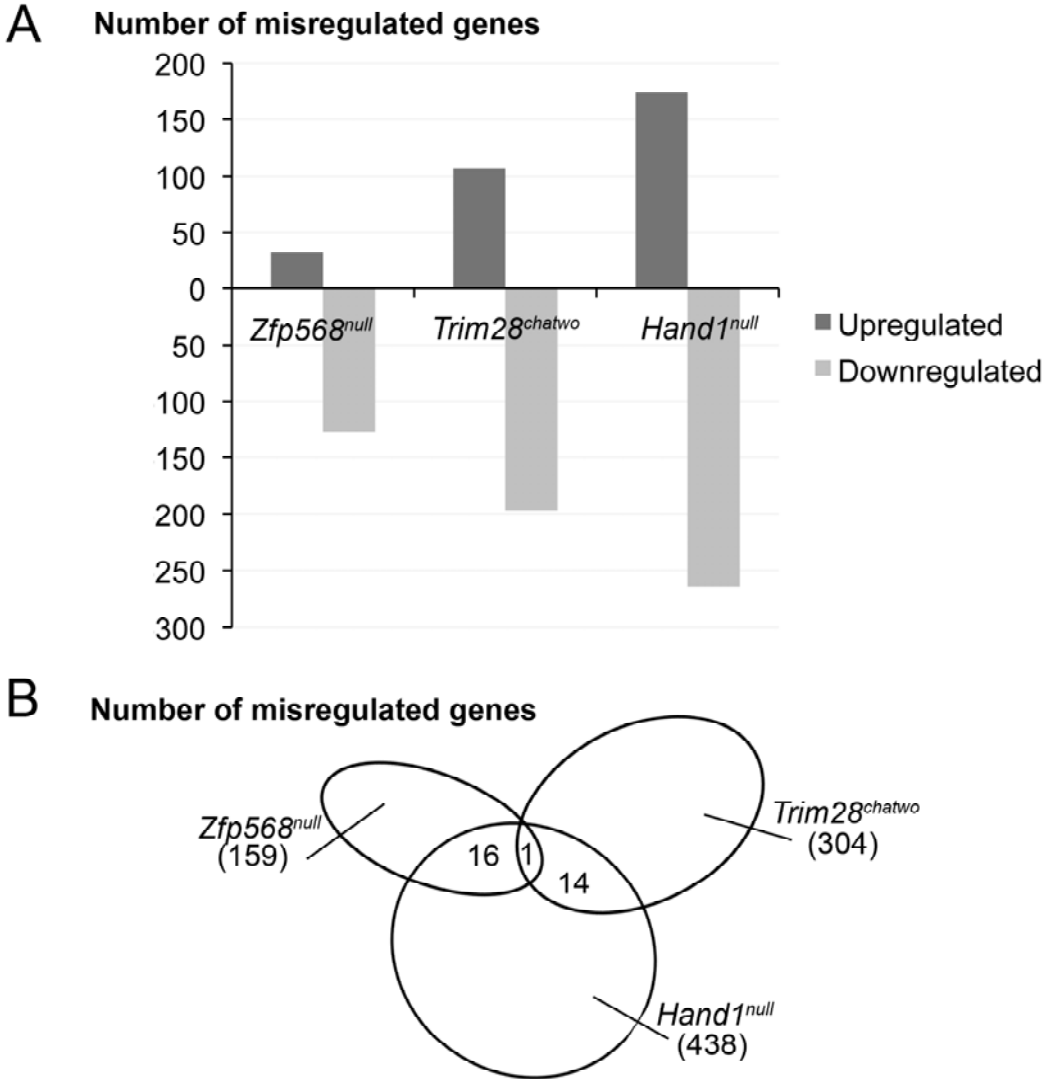

Figure A.6. Misregulated genes in *Zfp568*^{null} *Trim28*^{chatwo} and *Hand1* mutants. (A) Graph showing numbers of misregulated genes identified compared to wild type. In *Zfp568*^{null} mutants, 32 genes were significantly upregulated and 127 genes were downregulated. In *Hand1*^{null} embryos, 174 genes were significantly upregulated, and 264 genes were downregulated. 107 genes were upregulated more than 3.25 fold, and 197 genes were downregulated more than 3.25 fold in *Trim28*^{chatwo} embryos. **(B)** Diagram illustrating overlap between the genes misregulated in *Zfp568*^{null}, *Trim28*^{chatwo} and *Hand1*^{null} mutants. The numbers of misregulated genes included for each mutant are indicated in brackets. Diagram is not drawn to scale.

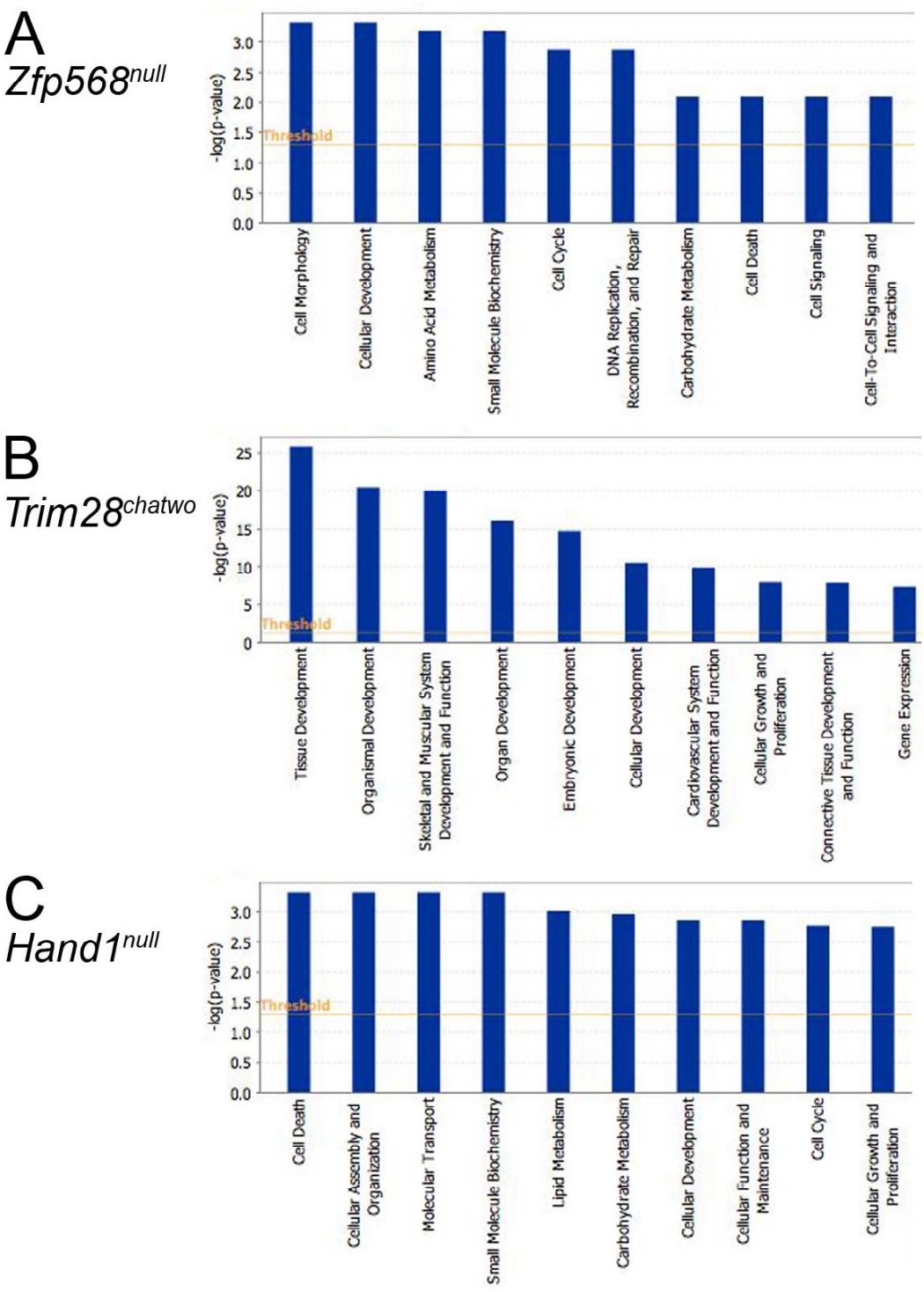

Figure A.7. Molecular and cellular functions of misregulated genes. Ingenuity pathway analysis was conducted to identify functions of genes most significantly misregulated in **(A)** *Zfp568*^{null}, **(B)** *Trim28*^{chatwo} and **(C)** *Hand1*^{null} embryos. Y axis represents –log(p-value) with threshold line drawn at p=0.05.

Table A.2. List of common misregulated genes.

Genes misregulated in both *Zfp568^{null}* and *Hand1^{null}* embryos	
Upregulated genes	
Hbb-bh1	hemoglobin Z, beta-like embryonic chain
Sdhc	succinate dehydrogenase complex, subunit C, integral membrane protein
9330161F08Rik	RIKEN cDNA 9330161F08 gene
Downregulated genes	
Phgdh	3-phosphoglycerate dehydrogenase
1110019K23Rik	RIKEN cDNA 1110019K23 gene
Ccne1	cyclin E1
Hand1	heart and neural crest derivatives expressed transcript 1
B230214O09Rik	RIKEN cDNA B230214O09 gene
Thy1	thymus cell antigen 1, theta
Oprs1	opioid receptor, sigma 1
Gfpt2	glutamine fructose-6-phosphate transaminase 2
Tbc1d20	TBC1 domain family, member 20
Bbs7	Bardet-Biedl syndrome 7
B430119L13Rik	RIKEN cDNA B430119L13 gene
1700045I11Rik	RIKEN cDNA 1700045I11 gene
6720422M22Rik	RIKEN cDNA 6720422M22 gene
Ga17	Dendritic cell protein GA17

Genes misregulated in both *Trim28^{chatwo}* and *Hand1^{null}* embryos	
Upregulated genes	
Fmr1nb	fragile X mental retardation 1 neighbor
Slc15a2	solute carrier family 15 (H+/peptide transporter), member 2
Lefty1	left right determination factor 1
AI662270	expressed sequence AI662270
Nalp5	NACHT, leucine rich repeat and PYD containing 5
Prss12	protease, serine, 12 neurotrypsin (motopsin)
Downregulated genes	
Clec1b	C-type lectin domain family 1, member b
5730593N15Rik	RIKEN cDNA 5730593N15 gene
Zfp503	zinc finger protein 503
AA415817	expressed sequence AA415817
	Transcribed locus
Hand1	heart and neural crest derivatives expressed transcript 1
Wnt6	wingless-related MMTV integration site 6
Sdk2	sidekick homolog 2 (chicken)
Rgs5	regulator of G-protein signaling 5

Genes misregulated in *Zfp568^{null}*, *Trim28^{chatwo}* and *Hand1^{null}* embryos	
Downregulated genes	
Hand1	heart and neural crest derivatives expressed transcript 1

three mutants (Figure A.6B). The downregulation of *Hand1* in RNA from *Zfp568*^{null} and *Trim28*^{chatwo} mutants was confirmed by quantitative RT-PCR (Figure A.8). *Zfp568* expression levels in the mutants could not be evaluated from the arrays, but *Trim28* expression levels were not affected in *Zfp568,* *Trim28*^{chatwo} or *Hand1* mutants. Altogether, this suggests that TRIM28 and ZFP568 are required for proper control of *Hand1* expression.

A genome scale chromatin immunoprecipitation experiment in human Ntera2 testicular carcinoma cells has identified ~7000 binding sites for TRIM28 (O'Geen et al., 2007). Interestingly, one of these sites is in the promoter region of human *Hand1* gene. I attempted a chromatin immunoprecipitation experiment to test whether endogenous TRIM28 binds to the promoter regions of mouse *Hand1* using NIH3T3 cells, a mouse fibroblast cell line, but results were inconclusive. Follow up experiments will be needed to assess whether *Hand1* may be a direct target of TRIM28 and ZFP568.

Hand1 is not likely to be the only gene commonly misregulated in *Zfp568*^{null} and *Trim28*^{chatwo} embryos. One of the major limitations in the comparison of gene expression profiles was that triplicate arrays could not be run for *Trim28*^{chatwo} samples, due to insufficient RNA. It is possible that the difficulties experienced in collecting sufficient quantities of *Trim28*^{chatwo} RNA were caused by a developmental delay, reducing the size of *Trim28*^{chatwo} mutants at E7.75. Another limitation is that changes in gene expression limited to a small number of specific cells could easily have been missed, as RNA was extracted from a mixture of cell types in this analysis.

In summary, these microarray studies have disclosed a list of transcriptional targets that may be regulated by ZFP568, TRIM28 and HAND1. Future studies should focus on confirmation of target genes by quantitative RT-PCR and in situ hybridization analysis in mutant embryos.

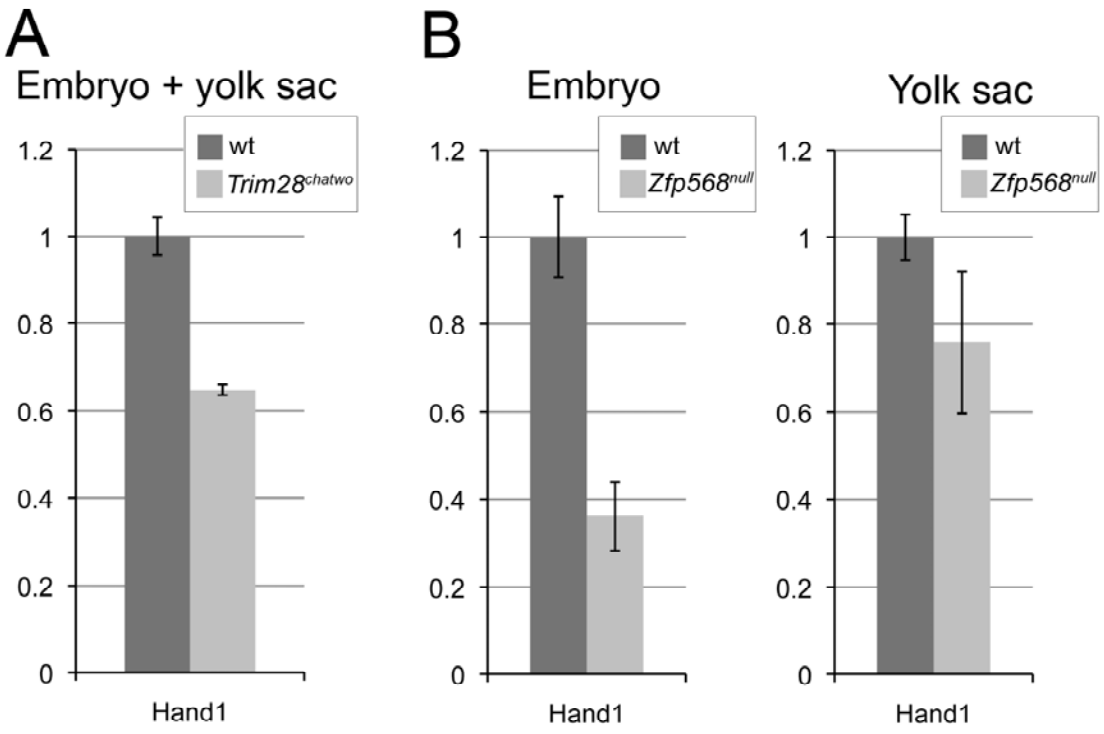

Figure A.8. Expression of *Hand1* in *Zfp568*^{null} and *Trim28*^{chatwo} mutants. Expression of *Hand1* relative to wild type was assessed by qRT-PCR in *Trim28*^{chatwo} (A, light bar) and *Zfp568*^{null} (B, light bars) embryos and/or yolk sacs. Error bars represent s.d. between two independent pools of RNA.

APPENDIX D

IMPRINTING DEFECTS IN CHATWO EMBRYOS

INTRODUCTION

Whereas most mammalian genes are expressed biallelically, from both maternally and paternally inherited alleles, imprinted genes are expressed only from one allele, and both the timing and tissue specificity of their expression is often precisely controlled (Reik, 2007). In KRAB zinc finger *Zfp57* mutants, expression of genes in several imprinted clusters are misregulated (Li et al., 2008). As functions of KRAB zinc finger proteins are mediated by TRIM28, this suggests a requirement for *Trim28* in the control of imprinted gene expression. However, a requirement of *Trim28* in imprinting has not been studied. Here I present results indicating that expression of many imprinted genes is affected in *Trim28*^{chatwo} embryos, suggesting that *Trim28* is required for the regulation of imprinted gene expression.

MATERIALS AND METHODS

Trim28^{chatwo} and *Trim28*^{null} embryos were characterized on the FVB genetic background, as described in Chapter 3. *Zfp568*^{chato} embryos were characterized on a CAST/Ei background (Garcia-Garcia et al., 2008).

Expression analysis of imprinted genes was conducted by SYBR Green real-time PCR as described (Shibata and Garcia-Garcia, 2010) with beta-Actin as the standard. qRT-PCR primer sequences were obtained from Drs. Timothy Bestor and Mathieu Boulard and are listed in Table A.3. For *Trim28*^{chatwo}, cDNA samples were synthesized from RNA from 3 independent pools of 5-6 embryos, which were a mixture of class I and class II mutants (Chapter 3). For *Zfp568*^{chato}, cDNA samples

Table A.3. Sequences of qRT-PCR primers.

qRT-PCR Primers	
Kcnq1ot1	AGGGCCAGGCCCACTAGT ACCTGGACAGCAGCCTGAGT
Cdkn1c	GACGATGGAAGAACTCTGGG AGCGTACTCCTTGCACATGG
Airn	GTGGATTCAGGTTTCATG GGCCCAGATATAGAATGT
Igf2r	TAGTTGCAGCTCTTTGCACG ACAGCTCAAACCTGAAGCG
Gtl2	GGGCGCCCACAGAAGAA GGTGTGAGCCGATGATGTCA
Dlk1	TTACCGGGGTTCCTTAGAGC TGCATTAATAGGGAGGAAGGG
H19	TTGCACTAAGTCGATTGCACT GGAACTGCTTCCAGACTAGGC
Igf2	TTGTGCTGCATCGCTGCTTAC TAGACACGTCCCTCTCGGACTT
beta-Actin	AAGTGACGTTGACATCCG GATCCACATCTGCTGGAAGG

were synthesized from RNA from 2 different pools of embryos. Pooled wild type littermate embryos were used as controls.

For analysis of biallelic expression of *Igf2r*, E8.5 embryos were collected from reciprocal crosses between wild type or *Trim28*$^{chatwo/+}$ mice on FVB and C57BL6 (referred to as BL6) genetic backgrounds. cDNA was synthesized from RNA from 2-6 pooled embryos. *Igf2r* cDNA was amplified with primers TAGGCACCTCTGACATGACC, CCAGAGGACACACAGCTGAA and sequenced or digested with MspA1I. The BL6 allele contains a restriction site (rs6369995, dbSNP Build 128) not present in FVB.

Immunohistochemsitry was conducted as described (Shibata and Garcia-Garcia, 2010) on 8μm cyosections. Antibodies used were anti-H3K9me3 (1:500; Millipore), anti-H3K27me3 (1:500; Millipore) and anti-rabbit Alexa Fluor 488 (1:200; Molecular Probes).

RESULTS AND DISCUSSION

Most imprinted genes are found in clusters that contain a non-coding RNA gene, and a differentially imprinted imprinting control region (ICR) that is methylated on the maternal or paternal allele (Edwards and Ferguson-Smith, 2007).

Methylation marks at the ICR are maternally inherited at *Kcnq1ot/Cdkn1c* and *Airn/Igf2r* imprinted domains, and paternally inherited at *Gtl2/Dlk1* and *H19/Igf2* domains (Edwards and Ferguson-Smith, 2007).

To address whether expression of imprinted genes was altered in *Trim28*^{chatwo} and *Zfp568*^{chato} embryos, qRT-PCR experiments were conducted. Analysis of expression of imprinted genes at E8.5 revealed that regulation of genes at both paternally and maternally imprinted loci was disrupted in *Trim28*^{chatwo} mutants (Figure A.9A). *Kcnq1ot, Airn, Gtl2*, and *H19* noncoding RNAs were overexpressed in

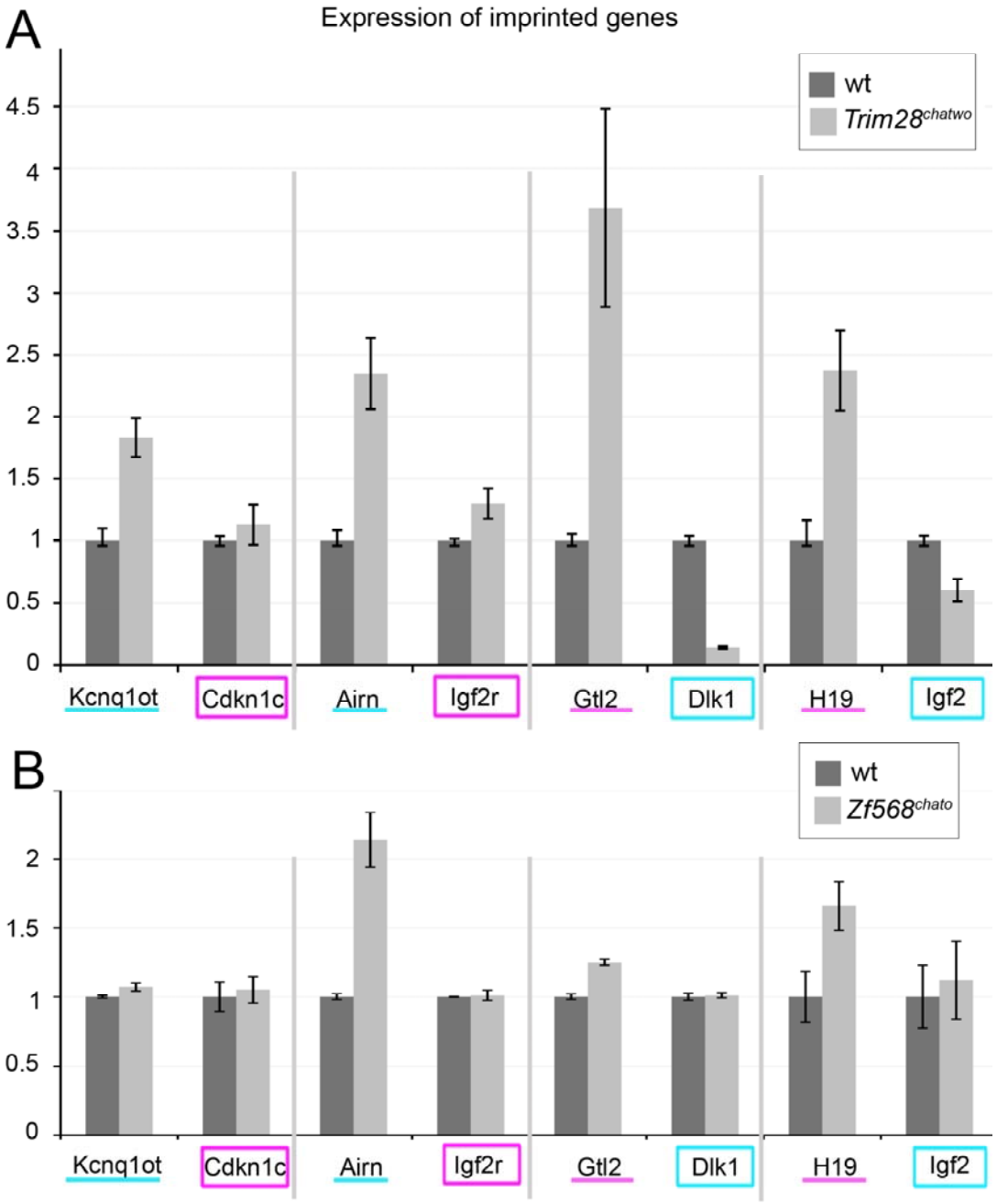

Figure A.9. Expression of imprinted genes in *Trim28*^{chatwo} and *Zfp568*^{chato}. Expression of *Kcnq1ot/Cdkn1c, Airn/Igf2r, Gtl2/Dlk1, H19/Igf2* in *Trim28*^{chatwo} (A, light bars) or *Zfp568*^{chato} (B, light bars) embryos relative to wild type littermates (dark bars) assessed by qRT-PCR. Error bars indicate s.d. between biological replicates. Numbers on y-axis indicate represent relative expression. Genes encoding for non-coding RNA (*Kcnq1ot, Airn, Gtl2, H19)* are underlined, protein coding genes (*Cdkn1c, Igf2r, Dlk1, Igf2)* are boxed. Pink indicates expression from the maternally inherited allele, blue indicates expression from the paternally inherited allele.

Trim28^{chatwo} embryos as compared to wild type littermates. In addition, expression of two imprinted protein coding genes, *Dlk1* and *Igf2*, was reduced in *Trim28*^{chatwo} embryos (Figure A.9A). The misregulation of many of these genes, despite the hypomorphic nature of the *Trim28*^{chatwo} mutation suggests that levels of *Trim28* in *Trim28*^{chatwo} mutants are not sufficient for proper regulation of imprinted genes. Aside from the slight upregulation of *Airn* and *H19* detected in *Zfp568*^{chato} embryos, expression of imprinted genes analyzed was normal in *Zfp568*^{chato} embryos (Figure A.9B).

At the *Airn/Igf2r* imprinted domain, expression of the non-coding *Airn* transcript from the paternally inherited allele represses *Igf2r* expression, and thus *Igf2r* is expressed only from the maternally inherited allele (Edwards and Ferguson-Smith, 2007). To address whether the slight upregulation of *Igf2r* detected in *Trim28*^{chatwo} embryos was due to abnormal biallelic expression from both paternal and maternal alleles, I sequenced cDNA from *Trim28*^{chatwo} embryos obtained from FVB genetic background mice crossed to BL6 background mice. A single-nucleotide polymorphism (SNP) in the *Igf2r* cDNA sequence between FVB and BL6 mouse strains was used to determine whether maternally inherited, paternally inherited, or both *Igf2r* alleles were expressed. I found that in all wild type, wild type littermates of *Trim28*^{chatwo} mutants and *Trim28*^{chatwo} mutants, *Igf2r* was expressed from the maternally inherited allele (Figure A.10A). Expression of the maternally inherited allele was also confirmed by a MspA1I restriction digest on amplified *Igf2r* cDNA (Figure A.10B). These results suggest that reasons other than biallelic *Igf2r* expression are responsible for the upregulation of *Igf2r* expression in *Trim28*^{chatwo} mutants. Experiments to address whether overexpression of *Kcnq1ot, Airn, Gtl2* or *H19* may be due to biallelic expression in *Trim28*^{chatwo} mutants are in progress. The *Trim28*^{chatwo}

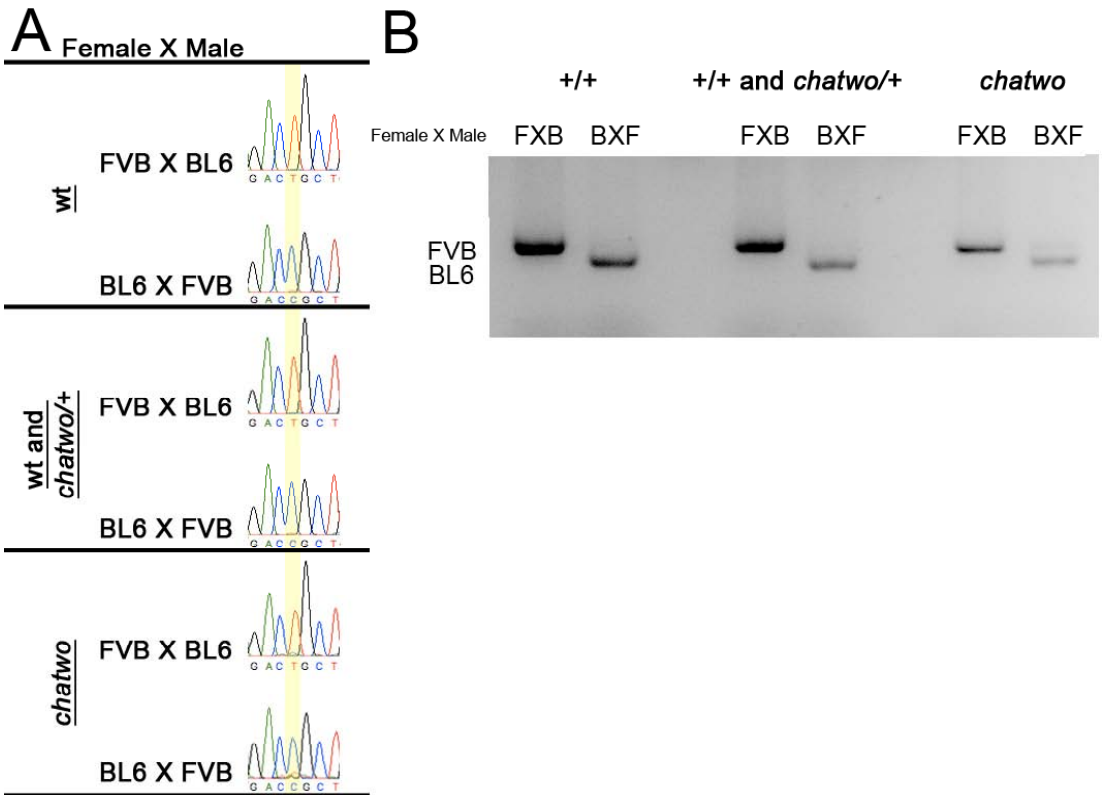

Figure A.10. Analysis of *Igf2r* expression. (A) Sequencing of *Igf2r* cDNA from wild type (top panel), wild type littermates of *Trim28*^{chatwo} (middle panel) or *Trim28*^{chatwo} embryos (bottom panel) from reciprocal FVB X BL6 crosses at E8.5. Allelic expression of *Igf2r* was determined by SNP rs6369995, where T indicated FVB allele expression, C indicated BL6 allele expression. *Igf2r* was expressed from the maternally inherited allele in all cases. **(B)** Restriction digests of amplified *Igf2r* cDNA from wild type (left lanes), wild type littermates of *Trim28*^{chatwo} (middle lanes) or *Trim28*^{chatwo} mutants (right lanes) at E8.5 using MspA1I enzyme. Digestion of the PCR product (BL6 allele) was observed only in embryos from BL6 mothers, indicating expression of *Igf2r* from the maternally inherited allele in all cases.

mutation is being moved to other genetic backgrounds, as SNPs between BL6 and FVB genetic backgrounds could not be identified in these genes.

Preliminary results from bisulfite sequencing have indicated that methylation at *Kcnq1ot/Cdkn1c* and *Airn/Igf2r* ICR are normal in *Trim28*^{chatwo} and *Trim28*$^{-/-}$ embryos, whereas the *H19/Igf2* ICR is demethylated in *Trim28*^{chatwo} and *Trim28*$^{-/-}$ embryos but not *Zfp568*^{chato} mutants (M. Boulard, personal communication). It is likely that *Trim28* is involved in the maintenance of methylation at some but not all ICRs. The upregulation of *Kcnq1ot* and *Airn* noncoding RNAs in *Trim28*^{chatwo} mutants despite normal methylation at the ICR suggests that TRIM28 is required for repression of these methylated promoters.

Histone marks including H3K9me3 and H3K27me3 have been associated with imprinted genes (Koerner et al., 2009). As TRIM28 has been shown to interact with SETDB1, one of three known H3K9 methyltransferases (Urrutia, 2003; Koerner et al., 2009), I used anti-H3K9me3 and anti-H3K27me3 antibodies to determine whether these marks were maintained in *Trim28*^{chatwo} and *Trim28*$^{-/-}$ embryos (Figure A.11, A.12). The overall distribution of H3K9me3 and H3K27me3 stained foci did not appear altered in *Trim28*^{chatwo} and *Trim28*$^{-/-}$ embryos, although additional experiments such as chromatin immunoprecipitation are required to determine whether TRIM28 may be regulating histone marks at specific loci.

Although some imprinted genes are expressed only in specific extraembryonic tissues such as the visceral endoderm (VE) or placenta, *Kcnq1ot, Cdkn1c, Airn, Igf2r, Gtl2, Dlk1, H19* and *Igf2* are expressed in embryonic and extraembryonic tissues (Hudson et al., 2010; Miri and Varmuza, 2009). However, tissue specific and developmental timepoint specific differences in expression levels of these genes have not been studied in detail. Further experiments, such as in situ hybridizations to study

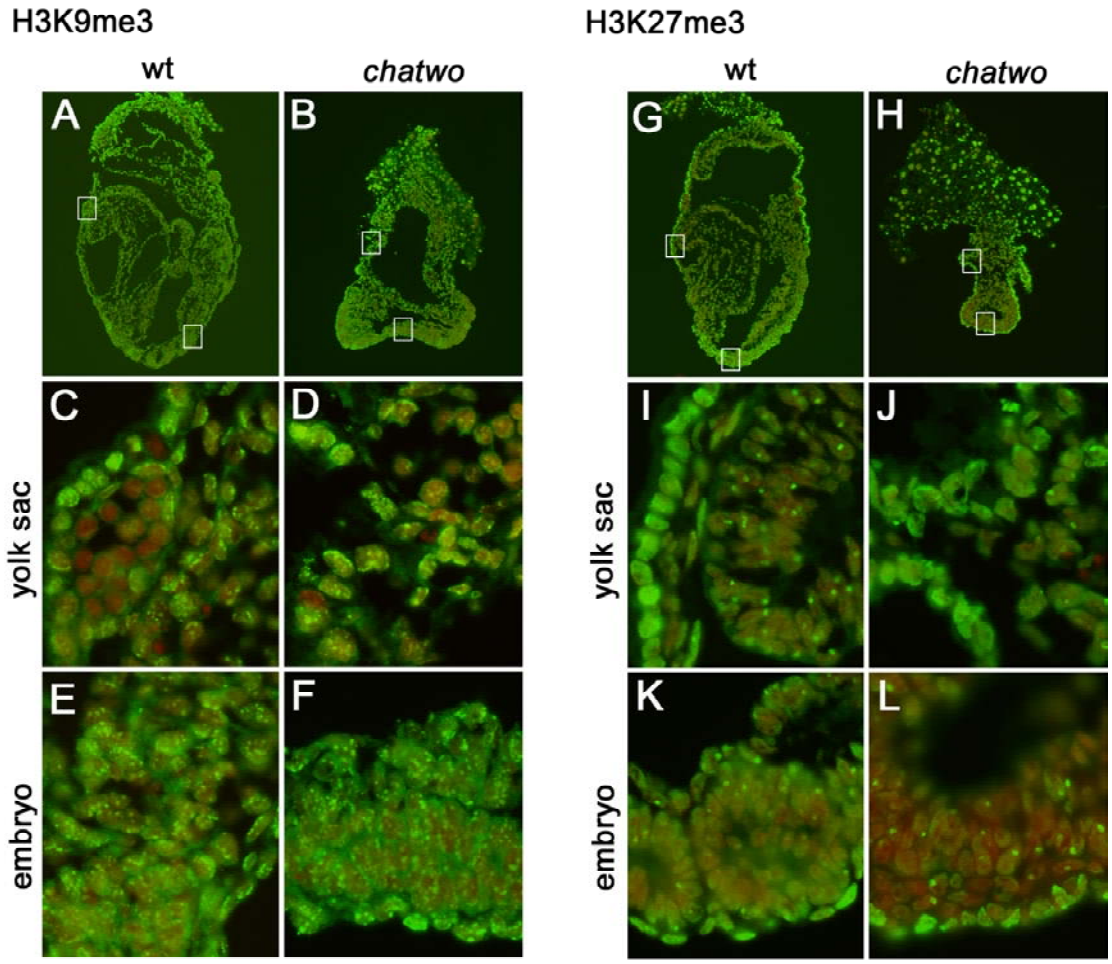

Figure A.11. H3K9me3 and H3K27me3 analysis in *Trim28*^{chatwo} embryos. Sagittal sections of E8.5 wild type (A,G) and *Trim28*^{chatwo} (B,H) embryos stained with anti-H3K9me3 (A,B; green) or anti-H3K27me3 (G,H; green) antibodies and DAPI (red) counterstaining. C-F, I-L are magnified yolk sac or embryo regions of boxes in A,B,G,H.

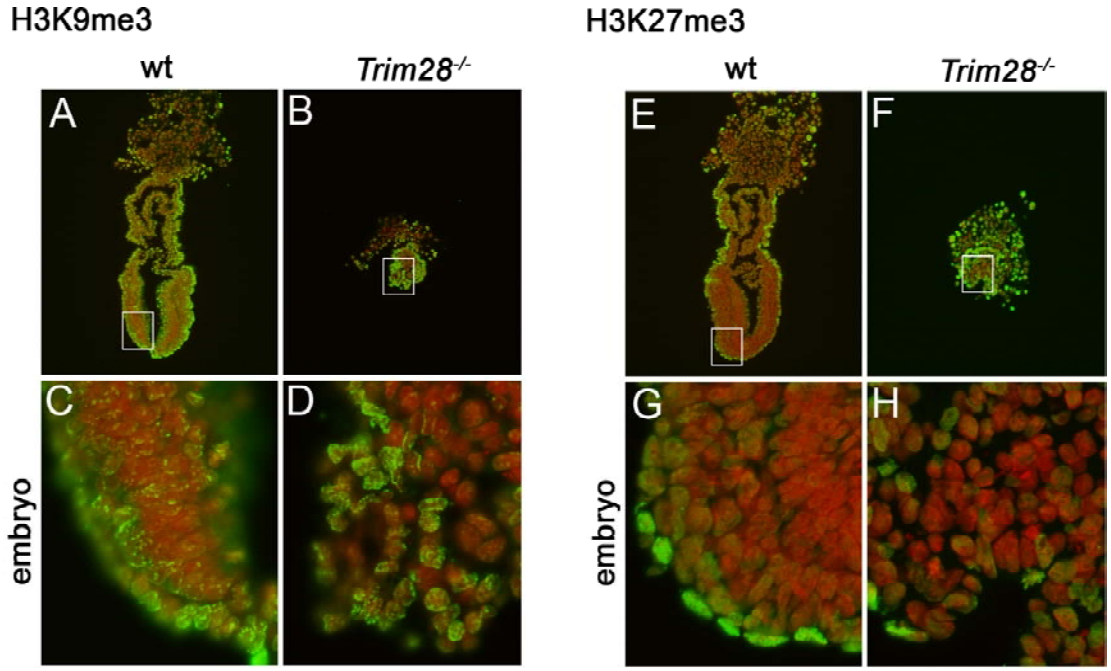

Figure A.12. H3K9me3 and H3K27me3 analysis in *Trim28*$^{-/-}$ embryos. Sagittal sections of E7.5 wild type (A,E) and *Trim28*$^{-/-}$ (B,F) embryos stained with anti-H3K9me3 (A,B; green) or anti-H3K27me3 (E,F; green) antibodies and DAPI (red) counterstaining. C-D, G-H are magnified embryo regions of boxes in A,B,E,F.

the cell types in which these genes are expressed at E8.5, will be useful for determining whether *Trim28* affects expression of imprinted genes in all cell types.

ACKNOWLEDGEMENTS

We thank Drs. Ken Kemphues, Paul Soloway, and Garcia lab members for helpful discussions and comments; Wei Wang and Jacob Kresovich from the Cornell Microarray Facility for help with the microarray analysis in Appendix C; Drs. Tim Bestor and Mathieu Boulard for helpful discussions and suggestions concerning experiments in Appendix D; CARE for technical help. This work was supported by March of Dimes (#5-FY06-589), NSF (IOS-1020878) and NIH (HD060581) grants to Maria Garcia-Garcia.

REFERENCES

Copp, A. J., Greene, N. D. E., and Murdoch, J. N. (2003). The genetic basis of mammalian neurulation. *Nat Rev Genet*, **4**, 784-793.

Edwards, C. A. and Ferguson-Smith, A. C. (2007). Mechanisms regulating imprinted genes in clusters. *Current opinion in cell biology*, **19**, 281–9.

Firulli, A. B., McFadden, D. G., Lin, Q., Srivastava, D., and Olson, E. N. (1998). Heart and extra-embryonic mesodermal defects in mouse embryos lacking the bHLH transcription factor Hand1. *Nature genetics*, **18**, 266–70.

Garcia-Garcia, M. J., Shibata, M., and Anderson, K. V. (2008). Chato, a KRAB zinc-finger protein, regulates convergent extension in the mouse embryo. *Development*, **135**, 3053–3062.

Hudson, Q. J., Kulinski, T. M., Huetter, S. P., and Barlow, D. P. (2010). Genomic imprinting mechanisms in embryonic and extraembryonic mouse tissues. *Heredity*.

Jiao, K., Zhou, Y., and Hogan, B. L. M. (2002). Identification of mZnf8, a mouse Krüppel-like transcriptional repressor, as a novel nuclear interaction partner of Smad1. *Mol Cell Biol*, **22**, 7633–44.

Koerner, M. V., Pauler, F. M., Huang, R., and Barlow, D. P. (2009). The function of non-coding RNAs in genomic imprinting. *Development*, **136**, 1771–1783.

Li, X., Ito, M., Zhou, F., Youngson, N., Zuo, X., Leder, P., and Ferguson-Smith, A. C. (2008). A maternal-zygotic effect gene, Zfp57, maintains both maternal and paternal imprints. *Developmental cell*, **15**, 547-557.

Miri, K. and Varmuza, S. (2009). Chapter 5 - Imprinting and Extraembryonic Tissues-Mom Takes Control. *International Review of Cell and Molecular Biology*, **276**, 215–262.

O'Geen, H., Squazzo, S., Iyengar, S., Blahnik, K., Rinn, J., Chang, H., Green, R., and Farnham, P. (2007). Genome-wide analysis of KAP1 binding suggests autoregulation of KRAB-ZNFs. *PLoS Genet*.

Reik, W. (2007). Stability and flexibility of epigenetic gene regulation in mammalian development. *Nature*, **447**, 425–32.

Riley, P., Anson-Cartwright, L., and Cross, J. C. (1998). The Hand1 bHLH transcription factor is essential for placentation and cardiac morphogenesis. *Nature genetics*, **18**, 271–275.

Schnütgen, F., De-Zolt, S., Sloun, P. V., Hollatz, M., Floss, T., Hansen, J., Altschmied, J., Seisenberger, C., Ghyselinck, N. B., Ruiz, P., et al. (2005). Genomewide production of multipurpose alleles for the functional analysis of the mouse genome. *Proc Natl Acad Sci USA*, **102**, 7221–6.

Shibata, M. and Garcia-Garcia, M. (2010). The mouse KRAB Zinc-Finger protein CHATO is required in embryonic-derived tissues to control yolk sac and placenta morphogenesis. *Dev. Biol*.

Urrutia, R. (2003). KRAB-containing zinc-finger repressor proteins. *Genome biology*, **4**, 231.